

Kneissl Daniel, BSc

**Studies in structural dynamics
in the time and frequency
domain**

MASTER'S THESIS

to achieve the university degree of

Diplom-IngenieurIn

Master's degree programme: Civil Engineering and Structural Engineering

submitted to

Graz University of Technology

Supervisor

Univ.-Prof. Dr.Ing.habil, Thomas-Peter Fries

Dipl.Ing. Dr.techn., Christian Dünser

Institute of Structural Analysis

Graz, August 2021

Affidavit

I declare that I have authored this thesis independently, that I have not used other than the declared sources/resources, and that I have explicitly indicated all material which has been quoted either literally or by content from the sources used. The text document uploaded to TUGRAZonline is identical to the present master's thesis.

Graz, August 2021

Meissl Daniel

Contents





Notation	IV
Acknowledgement	V
Abstract	VI
Zusammenfassung	VII
1 Introduction	1
1.1 Mathematical preliminaries	2
1.2 Fourier theory	4
1.2.1 Fourier series	4
1.2.2 Continuous Fourier transformation	6
1.2.3 Discrete Fourier transformation (DFT)	9
1.2.4 Properties of the Fourier transformation and summary	13
2 Systems with a single degree of freedom (SDOF)	16
2.1 The equation of motion	16
2.2 Analytical solution of the EOM	17
2.2.1 Solving in the time domain	17
2.2.2 Solving in the frequency domain	22
2.2.3 Comparison of calculation methods	29
2.3 Numerical solution of the EOM	30
2.3.1 Numerical solution in the time domain	30
2.3.2 Numerical solution in the frequency domain	33
2.3.3 Comparison of calculation methods	35
2.4 Examples	36
2.4.1 Introduction to example	36
2.4.2 Harmonic excitation	37
2.4.3 Periodic excitation	42
2.4.4 Non-periodic excitation	47
2.4.5 Arbitrary excitation	51
2.4.6 Conclusions	51
3 Systems with multiple degrees of freedom (MDOF)	53
3.1 The equation of motion	53
3.1.1 Systems with discrete masses	53
3.1.2 Systems with distributed properties (FEM-systems)	58
3.2 Numerical solution of the EOM	62
3.2.1 Solving in the time domain	62

3.2.2	Solving in the frequency domain	63
3.3	Example	64
3.3.1	Example 1 - Cantilever beam	64
3.3.2	Example 2 - Multi-story frame	68
4	Modal analysis for systems with multiple degrees of freedom (MDOF)	73
4.1	Decoupling by modal analysis	73
4.2	Model reduction	76
4.3	Solving in the time domain	78
4.4	Solving in the frequency domain	79
4.5	Example	81
4.5.1	Time domain	81
4.5.2	Frequency domain	84
4.6	Comparison of approaches	87
5	Conclusion	88
	List of Figures	89
	List of Tables	90
	Bibliography	92

Notation

a	Scalar
$f(\mathbf{x})$	Scalar function of \mathbf{x}
\mathbf{v}	Vector
$\mathbf{v}(\mathbf{x})$	Vector function of \mathbf{x}
\mathbf{A}, \mathbf{n}	Matrix or tensor
$\mathbf{A}(\mathbf{x})$	Matrix function
$\ \mathbf{v}\ $	Euclidean norm of \mathbf{v}
$\mathbf{v}_{i,j}$	Derivative of v_i in respect to j , i.e., $\frac{\partial v_i}{\partial x_j}$
$\mathbf{a} \cdot \mathbf{b}$	Dot product
$\mathbf{a} : \mathbf{b}$	Contraction of \mathbf{a} and \mathbf{b}
$\nabla \cdot \mathbf{v}$	Divergence of \mathbf{v}
$\nabla \mathbf{v}$	Gradient of \mathbf{v}
$f \circ g$	Composition of the functions f and g , $= f(g(x))$
$\hat{\Omega}$	Reference space
Ω	Real domain
Γ_D	Dirichlet boundary
Γ_N	Neumann boundary
$\ddot{\mathbf{u}}$	Second time derivative of $\mathbf{u} = \frac{\partial^2 \mathbf{u}(t)}{\partial t^2}$
$f * g$	Convolution of function f and g
$F[u]$	Fourier transformed of function $u(t)$
$\Re(a)$	Real part of complex number a
$\Im(a)$	Imaginary part of complex number a

Flow charts

	Decision
	Main step in calculation procedure
	Sub step in calculation procedure, but important enough to show in flow chart
	Optional step in calculation procedure, not essential

Acknowledgement

Alles hat ein Ende, nur die Wurst hat zwei. - Stephan Remmler

Writing this last few lines of my thesis, this song title came to my mind. Probably because this lines mark the end of my educational carrier. Therefore I want to thank some persons which helped me get where I am right now.

I want to thank all teachers and professors for sharing their knowledge and empathy to their subjects. I also want to thank my colleagues for the time spent together. The projects at university but also very fruitful discussions and activities in our free time made my studies a very pleasant experience. Several colleagues deserve special thanks, inter alia, Manuel J. for doing the majority of group projects with me.

I also want to thank my family for emotional and financial support. Thank you, Ilse and Herbert for making my studies, and my educational career, possible. I also want to thank Eva for helping me to overcome difficulties and emotional downs, I love you.

Last but not least I also want to appreciate the excellent supervision of this thesis by Prof. T.-P. Fries and Dr.techn. C. Dünser. I enjoyed and anticipated our weekly video meetings due to COVID-19 restrictions. I also appreciate the thorough revision of the presented thesis by the supervisors.

Daniel Kneissl

Abstract

The goal of this master thesis is to show the similarities and differences of calculations in structural dynamics in the time and frequency domain. In the time domain, results are given as quantities which change over time. Results in the frequency domain are frequency spectra, showing the intensity of harmonics in the sought output, e.g., the sought displacements.

This thesis starts with a short introduction to the Fourier theory in order to calculate the results in the frequency domain. The analytical and numerical procedures for single degree of freedom (SDOF) systems are introduced in both domains. Later on, the context is extended to multi degree of freedom (MDOF) systems. These MDOF systems do not only naturally result for multiple interacting bodies but also in the continuum case when discretized using the Finite Element Method (FEM). In this case, the focus is on the numerical solution as the analytical procedure is hardly possible with reasonable effort.

Huge systems of dynamic equations take a lot of effort to solve, therefore methods are presented to decouple the arising systems of equation. The method used in this thesis is classical *modal analysis* and enables the use of analytical procedures (applied to the decoupled equations) and also the reduction of calculation time by reducing the system. Hence, in the thesis, we do not only compare calculations in the time and frequency domain, but also compare analytical versus numerical techniques and full versus reduced dynamical systems.

Each chapter is supported with examples comparing the results achieved with the different approaches. The SDOF situation is shown by means of a cantilever beam with different loadings. To show examples for the MDOF case, two applications are chosen based on continuous, two-dimensional domains and discretized using the FEM. A two-dimensional extension of the cantilever beam with a single force and a multi-story frame, which is excited harmonically, show the similarities and differences of the calculation. Additionally, the multi-story frame model is reduced based on modal analysis and the comparison to the full system is presented.

In this thesis, it can be clearly seen that equivalent results may be achieved in many different ways: Using the time or frequency domain, employing analytical or numerical methods, using the full or reduced systems of equations in MDOF systems. One has to be careful, though, that the considered boundary value problems, identifying the dynamic structures, may be (slightly) different when performing *numerical* calculations in the time and frequency domain.

Zusammenfassung

Ziel dieser Arbeit ist die Ähnlichkeiten und Unterschiede der Berechnung von Anwendungen in der Strukturmechanik im Zeit- und Frequenzbereich zu zeigen. Im Zeitbereich werden Zustandsgrößen in Abhängigkeit der Zeit angegeben. Resultate im Frequenzbereich sind dagegen Frequenzspektren, zum Beispiel Verschiebungsfrequenzen.

Eine Einführung in die Fouriertheorie bildet den Anfang dieser Arbeit, um eine Basis für die Berechnungen im Frequenzbereich zu schaffen. Analytische und numerische Lösungswege werden dann zunächst für beide Bereiche für den Einmassenschwinger (SDOF) vorgestellt. Anschließend werden Lösungsstrategien für Mehrmassenschwinger (MDOF) eingeführt. Diese Mehrmassenschwinger entstehen nicht nur wenn mehrere Massen und Federn miteinander interagieren, sondern auch durch Diskretisieren eines Kontinuums mit der Finiten Elemente Methode (FEM). Die Angabe einer analytischen Lösung ist in diesem Kontext nur mit erheblichem Aufwand möglich, weshalb hierfür nur die numerische Lösung gezeigt wird.

Riesige Gleichungssysteme von dynamischen Gleichungen erfordern sehr viel Rechenaufwand. Daher werden Methoden der Entkopplung vorgestellt. In dieser Arbeit wird die klassische Methode der *Modalanalyse* verwendet. Sie ermöglicht zum Einen die Nutzung der analytischen Verfahren (angewendet auf die entkoppelten Gleichungen). Zum Anderen lässt sich auch eine Reduktion der Berechnungszeit durch Vernachlässigung von Gleichungen mit wenig Einfluss auf das Gesamtverhalten erzielen, was auch als Modellreduktion bezeichnet wird. Somit wird in dieser Arbeit nicht nur auf den Unterschied zwischen Zeit- und Frequenzbereich eingegangen, sondern auch auf die Vergleiche von analytischer und numerischer Lösung, und von vollständigen und reduzierten dynamischen Systemen.

Beispiele zu jedem Kapitel sollen die theoretischen Aspekte unterstützen und den Vergleich der Bereiche ermöglichen. Der Einmassenschwinger wird durch einen Kragarm veranschaulicht, wobei verschiedene Arten von Belastungen aufgebracht werden. Zwei Beispiele, basierend auf mittels der FEM diskretisierten zweidimensionalen Kontinua, werden als Mehrmassenschwinger interpretiert. Die Ähnlichkeiten bzw. Unterschiede sollen anhand einer zweidimensionalen Erweiterung eines Kragbalkens mit einer Einzellast und eines Mehrgeschossrahmens, welcher harmonisch erregt wird, gezeigt werden. Zusätzlich wird das Modell des Mehrgeschossrahmens mit Hilfe der Modalanalyse reduziert und die Ergebnisse mit jenen des vollständigen Modells verglichen.

Die Schlussfolgerung dieser Arbeit ist, dass ähnliche Ergebnisse auf unterschiedlichen Wegen erzielt werden können: durch die Verwendung des Zeit- oder Frequenzbereiches, durch Anwendung von analytischen oder numerischen Prozeduren oder durch Verwendung des vollen oder reduzierten Gleichungssystems bei Mehrmassenschwingern. Man muss jedoch darauf achten, dass die Anfangswert-

probleme, welche die dynamischen Strukturen beschreiben, (leicht) unterschiedlich sind, wenn *numerische* Berechnungen im Zeit- oder Frequenzbereich durchgeführt werden.

1 Introduction

Structural dynamics is a very broad field of research. The aim of calculations in structural dynamics is to obtain transient physical quantities, for example the displacement over time, or frequency results. Among the various fields of applications are: flight simulations of airplanes, crashtests of cars, the motion of a building according to an earthquake. Many disciplines contribute to the solution of dynamic systems, such as mathematics, mechanics and computer sciences. This work is mainly based on Clough and Penzien [8] and Chopra [7]. The mathematical tools for the calculation in the frequency domain are based on Butz [6].

In structural dynamics, one may classify solution techniques into those working in the time or frequency domain. In the time domain, the sought quantities are obtained by analytically or numerically solving (systems of) differential equations. In the frequency domain, the differential equations are transformed in a way that algebraic equations arise, which is based on *Fourier transformations*.

A further distinction can be done based on the number of degrees of freedom (DOFs). The number of DOFs describe the independent motions in the dynamical system. A single point has six DOFs in a three-dimensional space: three translational and three rotational degrees of freedom. For some applications, it is sufficient to simplify the structure such that only one degree of freedom results. Other applications may require a Finite Element Mesh with a very large number of DOFs ($n_{\text{DOF}} \geq 10000$). In such a setting, analytical solutions are hardly possible and numerical methods are needed. Herein, the *time* discretization is based on *Newmark's Method* and in the *frequency* domain, the *Discrete Fourier Transformation* (DFT/FFT) is used.

Although modern computers can solve a huge amount of equations fast and accurate, calculations with a lot of DOFs are often quite time consuming. Therefore, different ways to reduce the calculation time were introduced over the years. The methods for model reduction range from statical reductions (e.g. Guyan [14]) to dynamic reductions up to defining a subspace in the Krylov setting [3]. Herein, we focus on classical modal analyses for the reduction. Then, an eigenvalue decomposition of the resulting system of dynamic equations is performed to first decouple the equations and then consider only those equations related to significant eigenvalues.

The following work is structured into three main chapters. Chapter 2 deals with single degree of freedom systems, and introduces the most important quantities and equations. In Chapter 3, the context is extended to multi degree of freedom systems. Chapter 4 introduces methods to decouple the system of equations, which enables the use of the methods in Chapter 2 and also to reduce the calculation time by reducing the system. All chapters are supported with calculations in both, the time and frequency domain. The focus is on the similarities and differences and the results are interpreted.

The FEM calculations are done with EduFEM [11] in Matlab (Version R2017b)[1]. The other results are either derived by hand or obtained with Matlab (Version R2017b)[1].

1.1 Mathematical preliminaries

We shortly introduce some standard mathematical operators to be used in this thesis, especially for deriving the equations of motion of systems with distributed properties in Section 3.1.2, see also [2] and [5].

For the definition of the operators, consider an arbitrary scalar function $f(\mathbf{x}) = f(x, y, z)$ and a vector function $\mathbf{v}(\mathbf{x}) = \mathbf{v}(x, y, z)$ with respect to the three Cartesian coordinates. Furthermore, some arbitrary tensors \mathbf{S} and \mathbf{A} are used. Fig. 1.1 shows a clockwise Cartesian coordinate system with three unit-vectors \mathbf{i} , \mathbf{j} and \mathbf{k} .

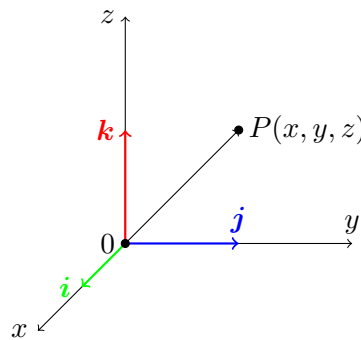


Fig. 1.1: Cartesian coordinate system.

Nabla operator ∇ : The operator is defined in a Cartesian coordinate system as

$$\nabla \equiv \frac{\partial}{\partial x} \mathbf{i} + \frac{\partial}{\partial y} \mathbf{j} + \frac{\partial}{\partial z} \mathbf{k}. \quad (1.1)$$

Gradient: The gradient operator applied to a scalar function f , or a vector function \mathbf{v} , is defined as

$$\text{grad } f = \nabla f = \begin{Bmatrix} \frac{\partial f}{\partial x_1} \\ \vdots \\ \frac{\partial f}{\partial x_n} \end{Bmatrix}, \quad \text{grad } \mathbf{v} = \nabla \mathbf{v} = \begin{bmatrix} \frac{\partial v_1}{\partial x_1} & \cdots & \frac{\partial v_1}{\partial x_n} \\ \vdots & \ddots & \vdots \\ \frac{\partial v_n}{\partial x_1} & \cdots & \frac{\partial v_n}{\partial x_n} \end{bmatrix}. \quad (1.2)$$

Divergence: The divergence of a vector is defined as

$$\text{div } \mathbf{v} = \nabla \cdot \mathbf{v} = \frac{\partial f_x}{\partial x} + \frac{\partial f_y}{\partial y} + \frac{\partial f_z}{\partial z}. \quad (1.3)$$

The divergence of a tensor is defined as

$$\text{div } \mathbf{A} = \nabla \cdot \mathbf{A} = \begin{Bmatrix} \frac{\partial A_{xx}}{\partial x} + \frac{\partial A_{xy}}{\partial y} + \frac{\partial A_{xz}}{\partial z} \\ \frac{\partial A_{yx}}{\partial x} + \frac{\partial A_{yy}}{\partial y} + \frac{\partial A_{yz}}{\partial z} \\ \frac{\partial A_{zx}}{\partial x} + \frac{\partial A_{zy}}{\partial y} + \frac{\partial A_{zz}}{\partial z} \end{Bmatrix}. \quad (1.4)$$

Double dot product (double contraction) : The double dot product of two tensors of second order results in a scalar value [2, p. 34]. It can also be called double-convolution [2, p. 32]. It is defined as

$$\mathbf{S} : \mathbf{A} = c \quad S_{ij}A_{ji} = c. \quad (1.5)$$

Convolution * : The convolution of two scalar functions $f_1(t)$ and $f_2(t)$ is defined as [5, p. 773]

$$f_1(t) * f_2(t) = \int_{-\infty}^{\infty} f_1(\tau)f_2(t - \tau) d\tau. \quad (1.6)$$

The convolution is an integral that expresses the amount of overlap of one function f_1 as it is shifted over another function f_2 . The convolution integral shall later be used to obtain the response in Duhamels integral in Section 2.2.1.

1.2 Fourier theory

This chapter is based on the books [26, pp. 167-238] and [6]. The theory of Fourier is a mathematical tool to disassemble functions into their frequency spectra. A frequency spectrum shows the distribution of the amplitudes (and phases) of each frequency component against the (circular) frequency. This enables the investigation which frequency is most dominant in a signal (or function). The Fourier transformation is an important tool in a lot of disciplines for example physics (optics, acoustics, dynamics, waves...) and mathematics (statistic, probability,...)[6]. In this work the Fourier series, the continuous Fourier transformation and the discrete Fourier transformation are used depending on the application. The three methods are introduced below.

1.2.1 Fourier series

The Fourier series is used to describe a **periodic function** (with period T) as a superposition of sine and cosine-functions. The Fourier series is defined as

$$f(t) = \sum_{k=0}^{+\infty} (A_k \cos(\omega_k t) + B_k \sin(\omega_k t)), \quad (1.7)$$

with $\omega_k = \frac{2k\pi}{T}$ and $B_0 = 0$.

To calculate the coefficients A_k and B_k it is necessary to integrate over a whole period T^1 . The coefficients are calculated as

$$A_0 = \frac{1}{T} \int_{-T/2}^{T/2} f(t) dt, \quad (1.8a)$$

$$A_k = \frac{2}{T} \int_{-T/2}^{T/2} f(t) \cos(\omega_k t) dt \quad \text{for } k \neq 0, \quad (1.8b)$$

$$B_k = \frac{2}{T} \int_{-T/2}^{T/2} f(t) \sin(\omega_k t) dt. \quad (1.8c)$$

The coefficients A_k, B_k can be interpreted as the amplitudes of each cosine or sine wave. A_0 is the mean value of the function $f(t)$ [6, p. 7].

The Fourier series can also be written in complex notation which is more compact and also used herein. Then, the transformation is defined as

$$f(t) = \sum_{k=-\infty}^{+\infty} (C_k e^{i\omega_k t}). \quad (1.9)$$

Note that the summation index ranges from $-\infty$ to ∞ . The conjugated complex coefficients can be calculated with the following equation

$$C_k = \frac{1}{T} \int_{-T/2}^{T/2} f(t) e^{-i\omega_k t} dt \quad \text{for } k = 0, \pm 1, \pm 2, \dots \quad (1.10)$$

¹A period is defined as the shortest interval in which a process is repeated, see Fig. 1.2.

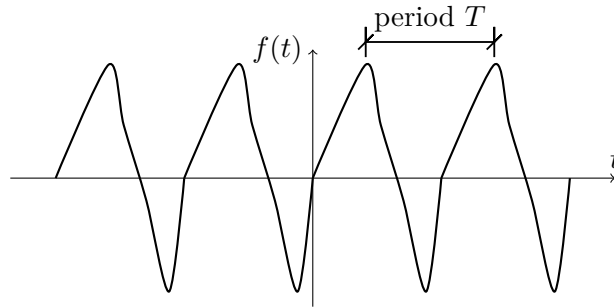


Fig. 1.2: Definition of period T.

The output of Eq. 1.10 (or Eq. 1.8) is, with some reformulation, the desired frequency spectrum. The amplitude spectrum can be calculated as $\text{Ampl}_k = \sqrt{A_k^2 + B_k^2} = \sqrt{\Im(C_k)^2 + \Re(C_k)^2}$, the phase spectrum can be evaluated as $\tan(\phi_k) = A_k/B_k = \Im(C_k)/\Re(C_k)$ [5, p. 474]. The spectrum consists of a sequence of discrete values, e.g., $\{C_k\}$. This series is plotted over the discrete frequency values $\{\omega_k\}$. The unit of the coefficients is the same as the input function. This can be easily understood by looking at the transformation formulas. The trigonometric function as well as the exponential function do not have units thus the coefficients are forced to have the same unit as the input to fulfil the equation.

Many properties of the Fourier series are listed in Section 1.2.4.

As seen in the equation Eq. 1.7, one needs to sum over infinitely many terms in order to reproduce a function exactly. This is, from a practical point of view, impossible. The example below shows the influence of a different number of considered terms.

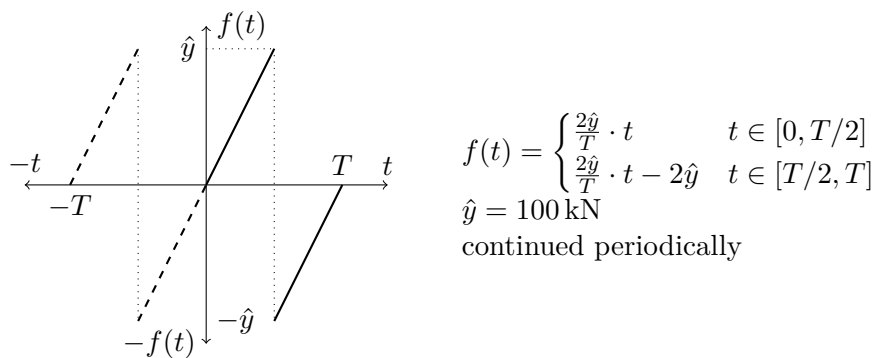


Fig. 1.3: Example of a sawtooth function.

As this function is antimetric, coefficients A_k of Eq. 1.7 are zero [5, p. 476]. Consequently the reduced Fourier series is

$$f(t) = \sum_{k=1}^{+\infty} B_k \sin(k\omega t) \quad \text{with} \quad \omega = \frac{2\pi}{T}, \quad (1.11)$$

with the coefficients

$$\begin{aligned}
 B_k &= \frac{2}{T} \int_T f(t) \sin(k\omega t) dt = \frac{2}{T} \int_{-T/2}^{T/2} \frac{2\hat{y}}{T} t \cdot \sin(k\omega t) dt, \\
 &= \frac{4}{T^2} \hat{y} \left(\frac{T^2(\sin(\pi k) - \pi k \cos(\pi k))}{2\pi^2 k^2} \right), \\
 &= \frac{2\hat{y}}{\pi k} \cdot (-1)^{k+1}.
 \end{aligned} \tag{1.12}$$

Fig. 1.4 shows the sawtooth function with different numbers of considered terms k . The graphic shows that more terms k result in better representations of $f(t)$. Note that the overshoot at discontinuities is typical and is called Gibbs phenomenon². The reason for the deviation to the function and the overshoots is that theoretically infinitely many terms of the Fourier series are needed to represent the function. It is noteworthy that the deviation at discontinuities do not disappear or decrease with increasing number of harmonics [6, p. 25] and the overshoots remain nearly constant in value [6, p. 31]. Fig. 1.5 shows the amplitude spectra of the sawtooth function. Note that the unit of the ordinate is identical to the unit of the original input.

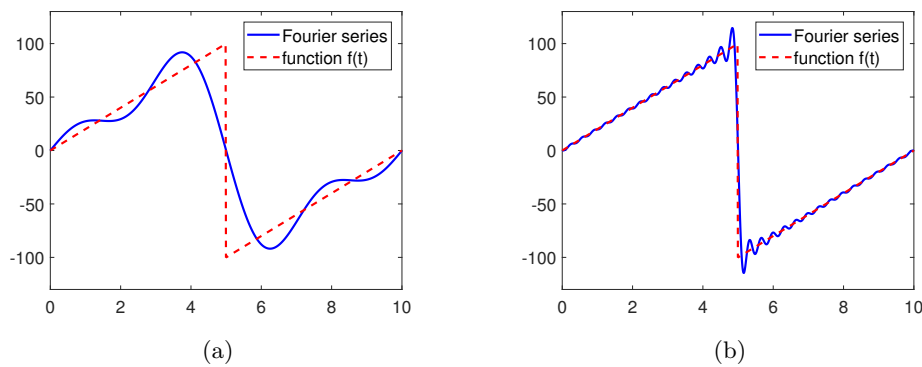


Fig. 1.4: Approximation of sawtooth function with (a) $k = 3$ and (b) $k = 30$ terms.

1.2.2 Continuous Fourier transformation

The continuous Fourier transformation can handle **non-periodic arbitrary functions** $f(t)$. The functions need to be known in closed form and need to be completely integrable³. The transformation can be defined as

$$F[f](\omega) = \int_{-\infty}^{\infty} f(t) e^{-i\omega t} dt. \tag{1.13}$$

²Named after Josiah Willard Gibbs, an American physicist.

³Completely integrable means that the integral exists and is finite everywhere.

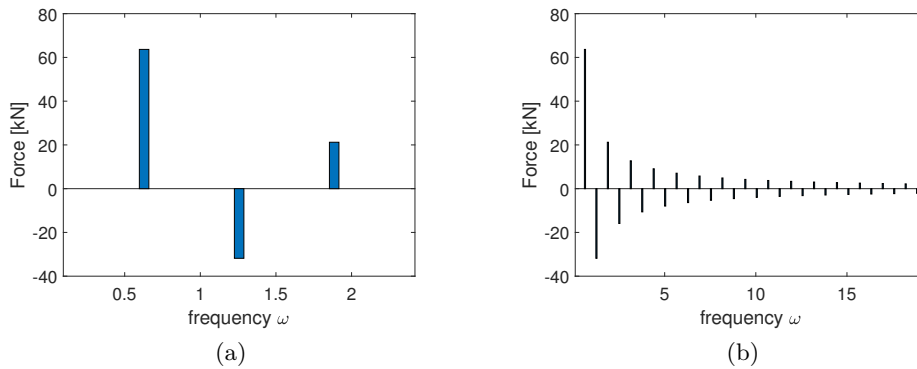


Fig. 1.5: Frequency spectra of approximated sawtooth function with (a) $k = 3$ and (b) $k = 30$ terms.

The inverse (back) transformation is used to back-transform into the time domain and is defined as

$$f(t) = \frac{1}{2\pi} \int_{-\infty}^{\infty} F[f](\omega) e^{+i\omega t} d\omega. \quad (1.14)$$

Note that the constant factor $\frac{1}{2\pi}$ is not uniquely defined [6, p. 35]. Depending on the literature, the constant factor can also be $\frac{1}{\sqrt{2\pi}}$ and is then considered in the transformation as well as back transformation formula. This constant factor makes the transformation formulas *symmetric* [6, p. 36]. Another definition for the transformation, making use of the frequency ν instead of the circular frequency ω , is

$$F[f](\nu) = \int_{-\infty}^{\infty} f(t) e^{-2\pi i \nu t} dt. \quad (1.15)$$

The back transformation is then defined as

$$f(t) = \int_{-\infty}^{\infty} F[f](\nu) e^{+2\pi i \nu t} d\nu. \quad (1.16)$$

This definition makes the formulas symmetric as well. Note that equation (1.13) and (1.15), as well as (1.14) and (1.16) are equivalent.

The integration borders can be altered depending on the input function $f(t)$ to reduce calculation effort. For example if $f(t)$ is zero for $t < 0$ the borders in Eq. 1.13 (or Eq. 1.15) can be defined as $[0, \infty]$. The output of Eq. 1.13 is a complex function which is defined in the whole frequency axis independent of the input function $f(t)$. The unit is due to the integration in Eq. 1.13 the unit of input \times time.

As the Fourier transformed function $F[f](\omega)$ is a complex function as mentioned before, one can display the real part and the imaginary part separately. It can be shown that the real part of the function is always symmetric and the imaginary part antimetric in case of a real valued input [4, p. 230]. This property ensures a real valued output in the back transformation. In this thesis only real valued inputs are investigated.

The most important properties of the continuous transformation are listed in Section 1.2.4.

To demonstrate the continuous Fourier transformation, a rectangular function is considered as an example. The function is defined in Fig. 1.6.

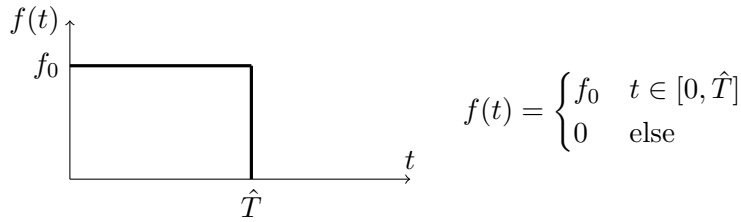


Fig. 1.6: Example of a step function.

This function is neither symmetric ($f(t) \neq -f(t)$) nor antimetric ($f(t) \neq -f(-t)$). To simplify the transformation the function is shifted in the time domain to use the symmetry property Eq. 1.31, solved with Eq. 1.13 and shifted back with Eq. 1.27.

$$\begin{aligned}
 F[f](\omega) &= \underbrace{\int_{-\hat{T}/2}^{\hat{T}/2} f_0 e^{-i\omega t} dt}_{\text{Transformation of symmetric function}} \cdot \underbrace{e^{-i\omega \hat{T}/2}}_{\text{Shift}} = f_0 \int_{-\hat{T}/2}^{\hat{T}/2} \cos(\omega t) \underbrace{-i \sin(\omega t)}_{= 0 \text{ because of sym. input}} dt \cdot e^{-i\omega \hat{T}/2}, \\
 F[f](\omega) &= \hat{T} \cdot f_0 \cdot \frac{\sin(\omega \hat{T}/2)}{\omega \hat{T}/2} \cdot e^{-i\omega \hat{T}/2}.
 \end{aligned} \tag{1.17}$$

Fig. 1.7 and Fig. 1.8 show the frequency spectra for the function Eq. 1.17.

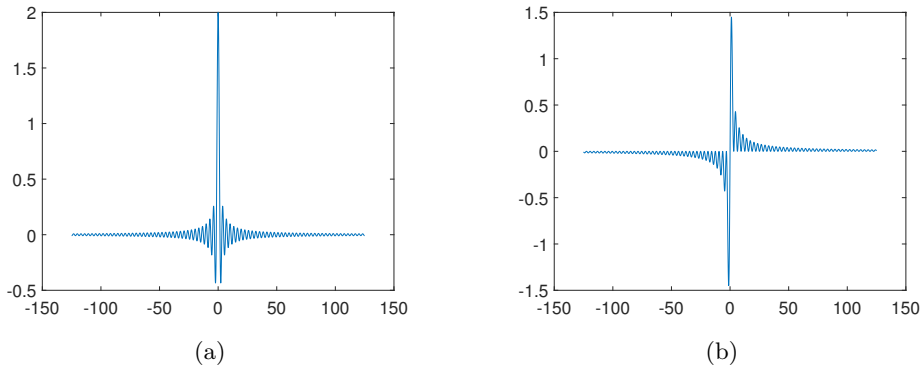


Fig. 1.7: Frequency spectra of step function (a) $\Re(F[f](\omega))$ and (b) $\Im(F[f](\omega))$.

In many applications, only the amplitude spectrum $\text{Abs}(F[f](\omega)) = \sqrt{\Re(F[f](\omega))^2 + \Im(F[f](\omega))^2}$ is of interest. Depending on the literature, only the half-sided amplitude spectrum with the positive frequencies is shown, e.g. in [13], where the values on the ordinate are doubled (compare [6, pp. 11-12], Fig. 1.6. and 1.7. and [6, p. 45]). In this work, the full amplitude spectra are shown. The phase spectrum ($\phi(F[f](\omega)) = \tan(\Im(F[f](\omega))/\Re(F[f](\omega)))$) is needed to transform the data back in the

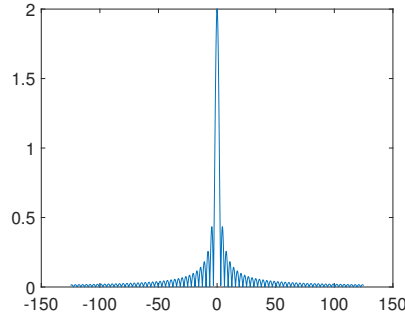


Fig. 1.8: Amplitude spectrum of step function $\text{Abs}(F(\omega))$.

time domain. Fig. 1.7 is shown to confirm that the real part of F is symmetric and the imaginary part of F is antimetric.

1.2.3 Discrete Fourier transformation (DFT)

Most of the time $f(t)$ is **not available in closed form** but with values at discrete time steps as, e.g., signal data coming from sensors and measurements. In this case, the discrete Fourier transformation is used. The discretized function $f(t)$ can be of any form and does not need to be periodic.

The discrete Fourier transformation is defined by

$$F_j = \frac{1}{N} \sum_{k=0}^{N-1} (f_k W_N^{-kj}) \quad \text{with} \quad W_N = e^{2\pi i/N}. \quad (1.18)$$

The inverse discrete Fourier transformation is used to transform the series back into the time domain and is defined as

$$f_k = \sum_{j=0}^{N-1} (F_j W_N^{kj}) \quad \text{with} \quad W_N = e^{2\pi i/N}. \quad (1.19)$$

A similar difference in notation as observed for the continuous transformation can be found for the DFT. Depending on the literature one can find $1/N$ in front of the inverse or normal transformation. The output of Eq. 1.18 is, similar to the Fourier series, a sequence of discrete values $\{F_j\}$. The desired frequency spectrum is obtained by plotting the values over discrete frequency values. The unit of the input and output are identical which means that, for example a load function gives discrete values with Newton as unit. The discrete frequency values are obtained by

$$\{\omega_k\} = \pm\{0, \dots, N/2\}/(t_{\max} - t_{\min}), \quad (1.20)$$

where t_{\min} denotes the beginning of the calculation and t_{\max} the end of the considered period of time. The most important properties of the discrete Fourier transformation are listed in Section 1.2.4.

An important consequence of this transformation is that periodicity is implied by the algorithm and needs to be kept in mind [6, p. 93]. For a graphical explanation of implied periodicity, see Fig. 1.9. The solid line represents the input series. The dashed lines show the periodic continuation of the input.

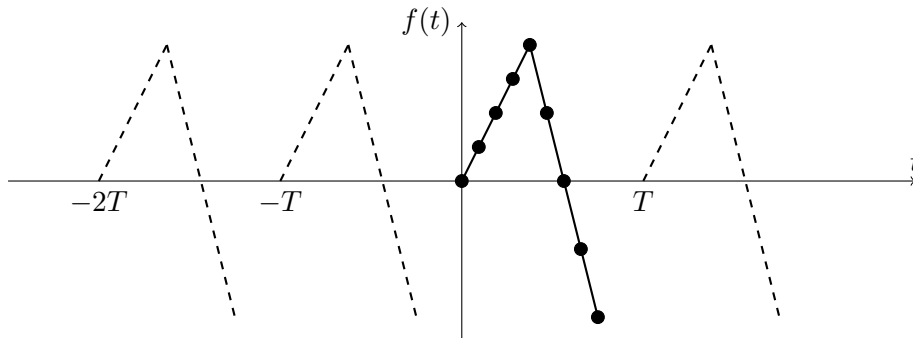


Fig. 1.9: Implied periodicity of the DFT.

To circumvent this restriction it is recommended to either *zero-pad* or *window* the input. Zero-padding means to add a large number of zeros at the end of the time series [6, pp. 118-124]. This helps reducing the implied periodicity because the distance between two data sets increases. Windowing the input means to multiply the input with a window function, which has small function values at the borders of the interval. Good window functions do have small derivatives on the borders as well. Detailed explanations of window functions can be found in [6] or [15].

Another important aspect is that the Fourier coefficients, which are obtained by Eq. 1.18, are sorted in an unintuitive way shown in Fig. 1.10, which is a modified version of [6, p. 99]. The coefficients for the positive frequencies can be found from $F_0 - F_{N/2}$. The coefficients belonging to the negative frequencies can be found on the right end (from $F_{N/2+1} - F_{N-1}$) and are descending to the left. F_{N-1} belongs to the smallest negative frequency and $F_{N/2+1}$ to the highest. The reason is that coefficients with negative indices are wrapped on the right end due to the minus sign in the exponent of Eq. 1.18 [6, p. 98].

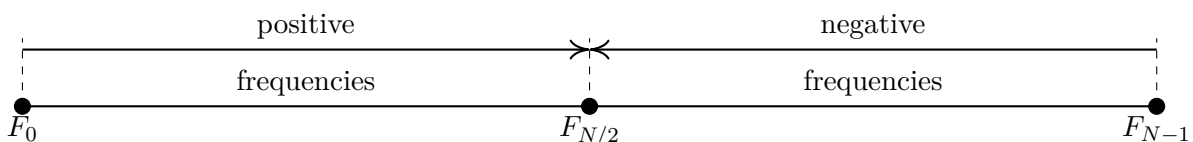


Fig. 1.10: Series of Fourier coefficients obtained by DFT.

This sequence can be easily altered to make the post-processing more convenient. Most of the time the coefficients are rearranged in a way that the frequency values range from $-\omega_{\max}, \dots, \omega_{\max}$.

Fast Fourier transformation (FFT)

The fast Fourier transformation (FFT) was invented to reduce the calculation time of the discrete FT. Cooley and Tukey⁴[9] introduced an algorithm which reduces the effort from $\mathcal{O}(N^2)$ to $\mathcal{O}(N \log(N))$, where N is the number of discrete values. The algorithm is fast (especially when $N = 2^x, x \in \mathbb{N}$) because it splits the input and reuses intermediate results. In the following, a short summary is given for completeness (taken from [6, pp. 125-126]), understanding the algorithm is not essential for following the outline of this work.

⁴Both were American Mathematicians.

The time series is split into two sub-series

$$\begin{aligned} \{f_k\} &= \{f_{1,k}\} + \{f_{2,k}\}, \\ &= \{f_{2k}\} + \{f_{2k-1}\} \quad \text{with } k = 0, \dots, M-1; M = N/2. \end{aligned} \quad (1.21)$$

A DFT is performed with both series

$$F_{1,j} = \frac{1}{M} \sum_{k=0}^{M-1} f_{1,k} W_M^{-kj} \quad \text{and} \quad F_{2,j} = \frac{1}{M} \sum_{k=0}^{M-1} f_{2,k} W_M^{-kj}, \quad (1.22a)$$

$$\begin{aligned} F_j &= \frac{1}{N} \sum_{k=0}^{N-1} f_k W_N^{-kj}, \\ &= \frac{1}{N} \sum_{k=0}^{M-1} f_{1,k} W_M^{-kj} + \frac{W_N^{-j}}{N} \sum_{k=0}^{M-1} f_{2,k} W_M^{-kj}, \\ &= \frac{1}{2} F_{1,j} + \frac{1}{2} W_N^{-j} F_{2,j} \quad \text{with } j = 0, \dots, N-1. \end{aligned} \quad (1.22b)$$

In the last step, the relation $W_N^{-(2k+1)j} = W_M^{-kj} W_N^{-j}$ was used. The coefficients are obtained by following equations

$$\begin{aligned} F_j &= \frac{1}{2} (F_{1,j} + W_N^{-j} F_{2,j}) \quad \text{and} \\ F_{j+M} &= \frac{1}{2} (F_{1,j} - W_N^{-j} F_{2,j}). \end{aligned} \quad (1.23)$$

This procedure is called *decimation in time* and can be repeated until single-part series arise [6, p. 126]. The algorithm is graphically visualized in Fig. 1.12 with $N = 4$, Fig. 1.11 shows the world famous Butterfly scheme. Both figures are modified versions of [6, pp. 129,130]. Note that the input is bit-reversed in the algorithm!

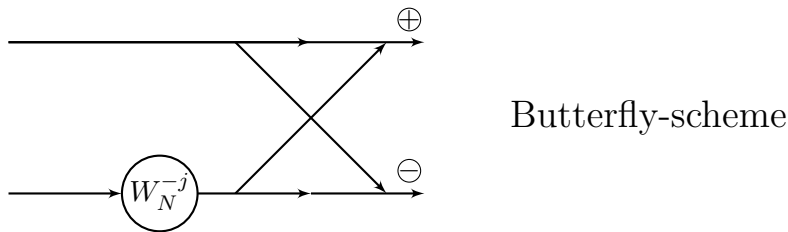
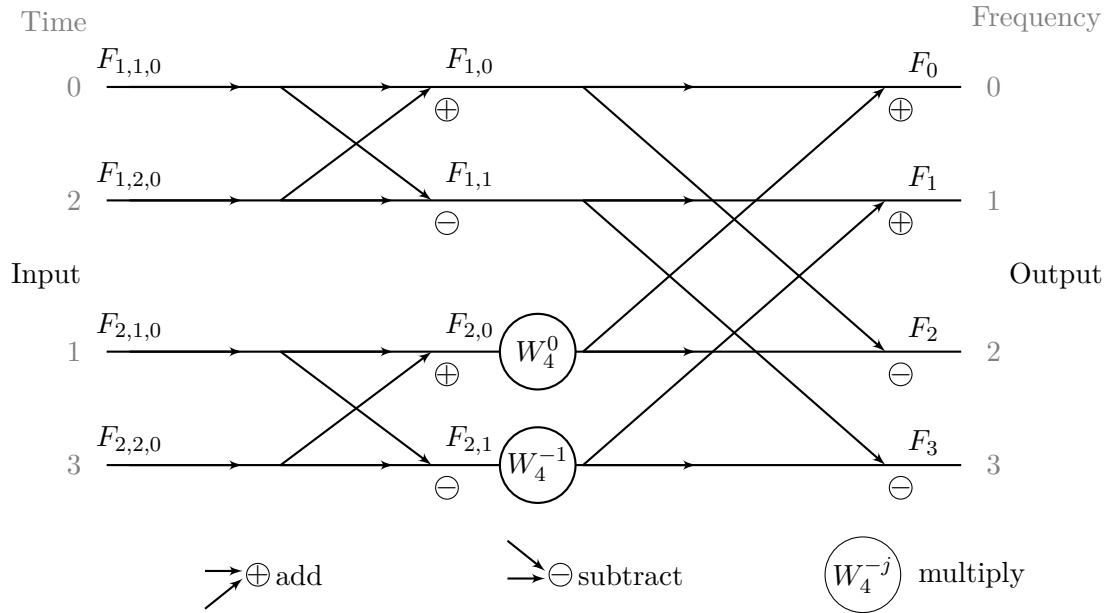


Fig. 1.11: Visualization of Butterfly-Scheme.

Fig. 1.12: Scheme of FFT-Algorithm for $N = 4$.

Nyquist-frequency

The Nyquist frequency was defined by Claude Elwood Shannon⁵ and gives a lower border for the sample rate⁶. If the sample rate is less than the Nyquist frequency, distortions known as aliasing occur. Aliasing is an effect that signals cannot be reconstructed to the original state (back transformation from frequency in time domain) as high frequencies cannot be distinguished. According to [7, p. 895] or [6, p. 102] the Nyquist frequency with the unit rad/sec is defined as

$$\omega_c = \frac{\pi}{\Delta t} > \omega_{\max}. \quad (1.24)$$

The Nyquist frequency with the unit 1/sec is defined as

$$f_c = \frac{N}{2 \cdot T} = \frac{1}{2 \cdot \Delta t} > f_{\max}. \quad (1.25)$$

Δt describes the difference in time of two neighbouring data points and is mostly chosen constant. To avoid bad affects such as aliasing it is recommended to chose Δt between the discrete data points small enough [6, p. 109].

⁵Claude Elwood Shannon, died in 2001, was an American Mathematician, electrical engineer and father of the information theory.

⁶Sample rate describes how often a value for a signal is given in a defined period of time (n/sec)

Recommendations

As mentioned previously, the DFT do have some properties which have to be kept in mind. Butz [6, p. 123] recommends three statements in order to obtain a proper frequency spectrum.

- Use lots of zeros: zero-padding is an appropriate way to circumvent the implied periodicity.
- Choose Δt small enough: a high sampling rate, i.e., a small time step prevents bad effects such as aliasing.
- Use window functions.

In this thesis, zero-padding is used to alter the input in an appropriate way, furthermore Δt is chosen small enough to detect all relevant frequencies.

1.2.4 Properties of the Fourier transformation and summary

It may be stated that the Fourier transformation transforms differential equations in a way that algebraic equations arise [5, p. 791]. Depending on the type of input, different transformations are used. Periodic functions can be transformed into the frequency domain by using the Fourier series. Non-periodic, analytically defined, functions are transformed with the help of the continuous Fourier transformation. If the input is only available at discrete time steps, the discrete Fourier transformation (or FFT) is the right choice. In the following, the most important properties for the Fourier transformation are given which are used in this thesis. The properties, taken from [6], are given with respect to the continuous Fourier transformation. The attributes can be written down analogously for the discrete Fourier transform but with sequences $\{f_n\}$ instead of closely defined functions $f(t)$. The \leftrightarrow arrow should denote the transformation between time and frequency domain. $F[f](\omega)$ is the Fourier transformed version of $f(t)$,

$$\begin{aligned} f(t) &\xrightarrow{\text{FT}} F[f](\omega) \\ f(t) &\xleftarrow{\text{IFT}} F[f](\omega). \end{aligned}$$

- The Fourier transformation is a linear operation:

$$\begin{aligned} f(t) &\leftrightarrow F[f](\omega) \\ g(t) &\leftrightarrow G[g](\omega) \\ h(t) = af(t) + bg(t) &\leftrightarrow aF[f](\omega) + bG[g](\omega) \end{aligned} \tag{1.26}$$

This property is useful to split the input and transform every single term by itself. Constant values are identical before and after the transformation.

- A shift in the time domain results in modularity in the frequency domain (first displacement law):

$$\begin{aligned} f(t) &\leftrightarrow F[f](\omega) \\ f(t - a) &\leftrightarrow F[f](\omega)e^{-i\omega a} \end{aligned} \tag{1.27}$$

A modularity means that the input function $f(t)$ is multiplied with the transformation function. This property is useful to manipulate the function in a way that the symmetry or antimetry property can be used.

- A shift in the frequency domain results in (second displacement law):

$$\begin{aligned} f(t) &\leftrightarrow F[f](\omega) \\ f(t)e^{-i\omega_0 t} &\leftrightarrow F[f](\omega + \omega_0) \end{aligned} \quad (1.28)$$

The second displacement law is the pendant to the first displacement law and is useful to alter the transformed function in order to transform back into the time domain.

- An integration in the time domain is a simple multiplication in the frequency domain:

$$\frac{d^k u}{dt^k} \leftrightarrow (i\omega)^k F[u](\omega) \quad (1.29)$$

The Fourier transformation transforms a differential equation into an algebraic equation which allows the use of fundamental mathematical operations, e.g., basic arithmetic.

- A convolution in the time domain is a multiplication in the frequency domain:

$$\begin{aligned} f(t) &\leftrightarrow F(\omega) \\ g(t) &\leftrightarrow G(\omega) \\ h(t) = f(t) * g(t) &\leftrightarrow H(\omega) = F[f](\omega) \cdot G[g](\omega) \end{aligned} \quad (1.30)$$

The convolution which is an integration in the time domain is transformed into a multiplication in the frequency domain.

- Symmetry property

$$f(t) = f(-t) \quad \forall t \quad \leftrightarrow F[f](\omega) \in \Re(\mathbb{C}) \quad (1.31)$$

If the input function is real and symmetric (even), the Fourier transform only contains the real part of a complex number [5, p. 787].

- Antimetry property

$$f(t) = -f(-t) \quad \forall t \quad \leftrightarrow F[f](\omega) \in \Im(\mathbb{C}) \quad (1.32)$$

If the input function is real and antimetric (odd), the Fourier transform only contains the imaginary part of a complex number [5, p. 787].

The following table shows the type of spectra which is produced by different types of transformations introduced in the previous sections and summarizes the information given in this thesis and literature.

Tab. 1.1: List of intervals of the spectra for different Fourier transformations.

Type of transformation	domain of x	periodicity of x	frequency spectra	Unit of output
Fourier series	continuous interval	periodic	discrete	same as input
Continuous Fourier transformation	continuous	aperiodic	continuous	input \times time
Discrete Fourier transformation	discrete, finite	aperiodic, continued periodically	discrete, finite	same as input

2 Systems with a single degree of freedom (SDOF)

Different assumptions may lead to applications, where a single degree of freedom is sufficient to obtain the desired quantity of interest. In the following, the equation of motion is derived and solution procedures are introduced.

2.1 The equation of motion

The equation of motion (later on labelled as EOM) is a mathematical equation, which describes the timely and spatial change of a physical quantity, for example the displacement [19]. There are several different ways to derive the equation of motion. The most simple one to formulate the EOM for a viscously damped system is to use the equilibrium of forces [8, p. 16]. Fig. 2.1, a modified version of [8, p. 15], shows a simplified SDOF system and its equilibrium. Throughout this thesis, it is assumed that the gravity force $m \cdot g$ is applied instantaneously on the system and therefore excites the system in the same way as an external force. The gravity force is considered in $f(t)$.

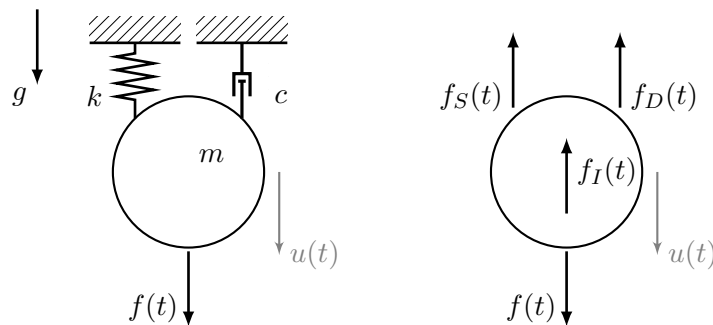


Fig. 2.1: Idealized SDOF system: (left) physical system; (right) free body diagram.

The evaluation of equilibrium of forces in vertical direction gives

$$\uparrow \sum F_V = 0 : f_S(t) + f_D(t) + f_I(t) - f(t) = 0. \quad (2.1)$$

In the following the terms are explained:

$$\text{Inertial force:} \quad f_I(t) = m \cdot \ddot{u}(t) \quad (2.2a)$$

$$\text{Linear spring force:} \quad f_S(t) = k \cdot u(t) \quad (2.2b)$$

$$\text{Viscous damping force:} \quad f_D(t) = c \cdot \dot{u}(t) \quad (2.2c)$$

$$\text{Excitation force:} \quad f(t) = m \cdot g + f_{\text{ext}}(t) \quad (2.2d)$$

The inertial force in the above product in Eq. 2.2a is acting against the displacement coordinate u according to d'Alembert's principle and Newton's second law of motion.. The spring and damping forces are also acting against the displacement coordinate u [8, p. 16].

D'Alembert's principle states that a mass develops an inertial force proportional to its acceleration [7, p. 15]

$$\mathbf{f}(t) = \frac{d}{dt} \left(m \cdot \frac{d\mathbf{u}}{dt} \right). \quad (2.3a)$$

In most cases, it is assumed that the mass does not vary over time [8, p. 9], thus giving:

$$\mathbf{f}(t) - m \cdot \ddot{\mathbf{u}}(t) = \mathbf{0}. \quad (2.3b)$$

With this, it is possible to express the equation of motion as equations of dynamic equilibrium [8, pp. 9,10].

Inserting all parts of Eq. 2.2 in Eq. 2.1 gives the EOM for a viscously damped SDOF system

$$k \cdot u(t) + c \cdot \dot{u}(t) + m \cdot \ddot{u}(t) = f(t). \quad (2.4)$$

This equation is a second order differential equation in time and therefore needs two initial conditions in order to give a unique solution. The initial conditions (ICs) are:

$$u(t = 0) = u_0, \quad (2.5a)$$

$$\dot{u}(t = 0) = v(t = 0) = v_0. \quad (2.5b)$$

The EOM may be solved in various ways such as outlined in the next sections.

2.2 Analytical solution of the EOM

In this section, the EOM from Eq. 2.4 is solved analytically and the solution is obtained in closed form. In many general cases, this is, however, not possible as the right hand side may be too complicated or not given in closed form. Nevertheless the analytical derivation of the solution yields interesting facts and is therefore included in this work.

2.2.1 Solving in the time domain

The solution of the EOM is obtained in two different ways. The first way is to calculate the homogeneous $u_h(t)$ and particular solution $u_p(t)$ separately. The superposition of both solutions yields the total response [8, p. 34]

$$u(t) = u_h(t) + u_p(t). \quad (2.6)$$

Another method is to solve the convolution integral, shown in section **Duhamels Integral**. The convolution integral yields the complete response and the splitting into homogeneous and particular solution is not possible. Both methods have benefits and drawbacks and are explained in the following.

Homogeneous solution

For obtaining the homogeneous solution, we follow the usual outline of differential calculus. The procedure of solving the homogeneous differential equation is based on [16, pp. 378-384]. The right part of Eq. 2.4 is set to zero ($f(t) = 0$), giving

$$k \cdot u(t) + c \cdot \dot{u}(t) + m \cdot \ddot{u}(t) = 0. \quad (2.7)$$

To solve a differential equation, an Ansatz needs to be made

$$u(t) = \alpha \cdot e^{\lambda \cdot t}. \quad (2.8)$$

Deriving with respect to time of Eq. 2.8 yields

$$\dot{u}(t) = \frac{du(t)}{dt} = \lambda \alpha \cdot e^{\lambda \cdot t} \quad \text{and} \quad \ddot{u}(t) = \frac{d\dot{u}(t)}{dt} = \lambda^2 \alpha \cdot e^{\lambda \cdot t}. \quad (2.9)$$

Inserting into Eq. 2.7 yields

$$m \cdot \alpha \lambda^2 e^{\lambda \cdot t} + c \cdot \alpha \lambda e^{\lambda \cdot t} + k \cdot \alpha e^{\lambda \cdot t} = 0. \quad (2.10)$$

Rearranging the coefficients and factoring out $\alpha \cdot e^{\lambda \cdot t}$ leads to

$$\alpha \cdot e^{\lambda \cdot t} \cdot (\lambda^2 + c/m \cdot \lambda + k/m) = 0, \quad (2.11)$$

with the abbreviations $k/m = \omega_0^2 := a_0$, $c/m = 2 \cdot \zeta \cdot \omega_0 := a_1$ and dividing through $(\alpha \cdot e^{\lambda \cdot t}) \neq 0$, the following equation arises

$$\lambda^2 + a_1 \cdot \lambda + a_0 = 0. \quad (2.12)$$

Eq. 2.12 is called the characteristic polynomial. The roots of this polynomial are of the following form (with the help of p-q-Formula)

$$\lambda_{1/2} = -\frac{a_1}{2} \pm \sqrt{\left(\frac{a_1}{2}\right)^2 - a_0}. \quad (2.13)$$

Depending on size of $D := a_1^2 - 4 \cdot a_0$ there are three different solutions for the roots:

$$\lambda_{1/2} = \begin{cases} (-a_1 \pm \sqrt{D})/2 & \text{if } D > 0 \\ -a_1/2 & \text{if } D = 0 \\ (-a_1 \pm i \cdot \sqrt{-D})/2 & \text{if } D < 0 \end{cases} \quad (2.14)$$

The term D directly corresponds to the type of structural system [16, p. 383]. If $D = 0 \leftrightarrow \zeta = 1$ the system is critically damped [8, p. 26], if $D < 0 \leftrightarrow \zeta \in [0, 1)$ the system is underdamped [7, p. 49] and if $D > 0 \leftrightarrow \zeta > 1$ the system is overdamped [8, p. 32].

The value $\zeta = c/c_{cr} = c/(2\omega_0 m)$ is called the damping ratio [8, p. 27] and has values ≥ 0 (compare table in [25, p. 143]). Note that in some literature the damping ratio is called D , e.g. in [13] and should not be confused with D in the derivation of the homogeneous solution in the previous lines. Systems with damping ratios ≥ 1 do not oscillate [7, p. 48], the movement is then called *creep movement* [13, p. 27]. Usual damping ratios in structural dynamics are $\zeta \in [0.002, 0.07]$ with lower values for smaller

Tab. 2.1: List of damping ratios from [23].

Stress level	Type and Condition of structure	damping ratio ζ (%)
Working stress (<50% of yield stress)	Welded steel, prestressed concrete	2-3
At or just below yield stress	Welded steel	5-7

movements and vice versa, see [25, p. 143]. Another source of damping ratios is given in [23]. A small excerpt is given in Tab. 2.1.

According to [16] theorem 8.12, the solution of Eq. 2.7 may now be written as

$$u_h(t) = \begin{cases} \alpha_1 \cdot e^{\lambda_1 t} + \alpha_2 \cdot e^{\lambda_2 t} & \text{if } D > 0 \\ (\alpha_1 + \alpha_2 t) \cdot e^{\lambda_{1/2} t} & \text{if } D = 0 \\ \alpha_1 \cdot e^{\gamma t} \cos(\beta t) + \alpha_2 \cdot e^{\gamma t} \sin(\beta t) & \text{if } D < 0 \end{cases} \quad (2.15)$$

In Eq. 2.15 the constants $\alpha_1, \alpha_2 \in \mathbb{R}$ are obtained by inserting the initial conditions from Eq. 2.5 in Eq. 2.6 and the constants β, γ are defined as

$$\beta = \frac{\sqrt{-D}}{2}, \gamma = -\frac{a_1}{2}. \quad (2.16)$$

Inserting the expression for a_0, a_1, β and γ from above in Eq. 2.15 yields the following solution for the three different cases

$$u_h(t) = \begin{cases} \alpha_1 \cdot e^{\lambda_1 t} + \alpha_2 \cdot e^{\lambda_2 t} & \text{if } \zeta > 1 \\ (\alpha_1 + \alpha_2 t) \cdot e^{-\zeta \omega_0 t} & \text{if } \zeta = 1 \\ e^{-\zeta \omega_0 t} (\alpha_1 \cdot \cos(\omega_d t) + \alpha_2 \cdot \sin(\omega_d t)) & \text{if } \zeta \in [0, 1) \end{cases} \quad (2.17)$$

with the coefficients:

$$\begin{aligned} \lambda_1 &= \omega_0(-\zeta + \sqrt{\zeta^2 - 1}), \\ \lambda_2 &= \omega_0(-\zeta - \sqrt{\zeta^2 - 1}), \\ \omega_d &= \omega_0 \cdot \sqrt{1 - \zeta^2}. \end{aligned} \quad (2.18)$$

The natural circular frequency ω_0 is directly related to the natural period of the system [13, p. 23]. The natural period describes the time needed to fulfil a whole period of movement, shown in Fig. 1.2. The relation is

$$\omega_0 = \sqrt{k/m} = 2\pi/T. \quad (2.19)$$

One may miss the solution for the undamped case but the solution is included in the underdamped case by setting the damping ratio $\zeta \equiv 0$. All the the above described oscillations are stable, except the undamped case (compare [13, Tab. 1.1]). There can be scenarios where the oscillation is unstable [13, p. 28] and the amplitude increases over time due to resonance¹ or other factors, e.g. negative stiffness [13, p. 29]. These scenarios are beyond the scope of this thesis, though.

¹The scenario where the amplitude of the oscillation increases to infinity over time is called resonance when the excitation frequency match the natural frequency of the system [8, p. 42].

The integration constants α_1 and α_2 are obtained by inserting the ICs from Eq. 2.5 into Eq. 2.6 giving two equations

$$\begin{aligned} u(t=0) &= u_0 = u_h(t=0) + u_p(t=0) \quad \text{and} \\ \dot{u}(t=0) &= v_0 = \dot{u}_h(t=0) + \dot{u}_p(t=0). \end{aligned} \quad (2.20)$$

The integration constants are, in dependency of the value ζ , of the following form

$\zeta > 1$

$$\begin{bmatrix} 1 & 1 \\ \lambda_1 & \lambda_2 \end{bmatrix} \begin{Bmatrix} \alpha_1 \\ \alpha_2 \end{Bmatrix} = \begin{Bmatrix} u_0 - u_p(t=0) \\ v_0 - \dot{u}_p(t=0) \end{Bmatrix} \quad (2.21a)$$

$\zeta = 1$

$$\begin{aligned} \alpha_1 &= u_0 - u_p(t=0) \\ \alpha_2 &= v_0 + \zeta\omega_0(u_0 - u_p(t=0)) - \dot{u}_p(t=0) \end{aligned} \quad (2.21b)$$

$\zeta \in [0, 1)$

$$\begin{aligned} \alpha_1 &= u_0 - u_p(t=0) \\ \alpha_2 &= \frac{1}{\omega_d}(v_0 + \zeta\omega_0(u_0 - u_p(t=0)) + \dot{u}_p(t=0)) \end{aligned} \quad (2.21c)$$

Note that the particular solution at time $t = 0$ is needed to compute the constants α_1, α_2 therefore the particular solution needs to be obtained first.

Particular solution

To obtain the particular solution, an Ansatz needs to be made depending on the right side $f(t)$ [8, p. 33]. An incomplete list of Ansätze is given in the following table and can be found in any mathematical collection of formulas, e.g., in [24].

Tab. 2.2: List of Ansätze for particular solution.

Right side $f(t)$	Solutionansatz $u_p(t)$
Constant function f_0	c_0
Polynomial of order n	$c_n x^n + \dots + c_1 x + c_0$
Trigonometric function	$C_1 \sin(\omega x) + C_2 \cos(\omega x)$

Inserting the Ansatz into Eq. 2.4 and doing a comparison of coefficients gives the desired particular solution $u_p(t)$. An example of this procedure can be found in Section 2.4. Obtaining the particular solution can be a very difficult and time consuming task, especially for complicated right sides of the EOM.

Therefore the convolution integral is introduced in the next section.

Solving with the convolution integral (Duhamels Integral)

This section closely follows the outline of [7, pp. 125-129]. The convolution integral can be used to obtain the total response of a linear dynamic system due to an arbitrary loading $f(t)$ [7, p. 129]. Linearity is provided because the principle is based on superposition of responses of small impulses. An arbitrary force can be divided into a sequence of infinitesimally short impulses. The response du to one of the impulses is given by multiplying the magnitude $f(\tau)d\tau$ with the unit impulse-response function $h(t - \tau)$:

$$du(t) = [f(\tau)d\tau] h(t - \tau) \quad \text{with } t > \tau. \quad (2.22)$$

The total response at t is then the sum of all impulses up to that time

$$u(t) = \int_0^t f(\tau)h(t - \tau) d\tau. \quad (2.23)$$

The focus is now on the term $h(t - \tau)$ in Eq. 2.23. This term describes the response of the system to an impulse. This impulse acts for an infinitesimally short duration, therefore the damper and the spring do not have time to respond. Only the mass gets accelerated to velocity $\dot{u}(\tau)$ [7, p. 127]. The initial conditions for the free response due to the impulse are therefore

$$v(t = 0) = \dot{u}(t = 0) = \frac{1}{m} \int_0^{T_F} F(t) dt = \frac{1}{m} \int_0^\epsilon 1 \cdot \delta(t) dt = \frac{1}{m}, \quad (2.24a)$$

where $\delta(t)$ is called the Dirac-function. For a function with duration $\epsilon \rightarrow 0$ and intensity ∞ , the product of both equals 1. The displacement at $t = 0$ is zero by definition of the convolution integral

$$u(t = 0) = 0. \quad (2.24b)$$

Inserting the initial conditions from Eq. 2.24 into the last equation of Eq. 2.17 gives the desired function

$$h(t - \tau) \equiv u(t) = \frac{1}{m\omega_d} e^{-\zeta\omega_0(t-\tau)} \sin(\omega_d(t - \tau)) \quad \text{with } t \geq \tau. \quad (2.25)$$

Inserting Eq. 2.25 into Eq. 2.23 yields Duhamels integral

$$u(t) = \frac{1}{m\omega_d} \int_0^t f(\tau) e^{-\zeta\omega_0(t-\tau)} \sin(\omega_d(t - \tau)) d\tau. \quad (2.26)$$

The consideration of the initial conditions Eq. 2.5 is possible [7, p. 129] and expands Eq. 2.26 to

$$\begin{aligned} u(t) = & \underbrace{e^{-\zeta\omega_0 t} \left(u_0 \cos(\omega_d t) + \frac{v_0 + \zeta\omega_0 u_0}{\omega_d} \sin(\omega_d t) \right)}_{\text{Response due to initial conditions} \equiv \text{free response}} \\ & + \underbrace{\frac{1}{m\omega_d} \int_0^t f(\tau) e^{-\zeta\omega_0(t-\tau)} \sin(\omega_d(t - \tau)) d\tau}_{\text{Response due to external load} \equiv \text{forced response}}. \end{aligned} \quad (2.27)$$

Solving the Duhamels integral is possible analytically in some (simpler) cases, but most of the time it is evaluated numerically [7, p. 129]. The use of Duhamels integral is demonstrated in Section 2.4.4.

2.2.2 Solving in the frequency domain

In this section, the EOM is solved in the frequency domain using Fourier theory. Similar to the situation in the time domain, the particular and the homogeneous solution need to be obtained separately. The total response is then the sum of both parts

$$F[u] = F[u_h] + F[u_p]. \quad (2.28)$$

Homogeneous solution

The homogeneous differential equation (Eq. 2.7) is transformed into the frequency domain with the help of the Fourier transform. This leads to

$$m \cdot F[\ddot{u}](\omega) + c \cdot F[\dot{u}](\omega) + k \cdot F[u](\omega) = F[0](\omega) = 0. \quad (2.29)$$

Using the properties of the Fourier transformation, that in the frequency domain a differentiation becomes a multiplication $F\left[\frac{d^k u}{dt^k}\right] = (i\omega)^k \cdot F[u](\omega)$ the following equation arises

$$F[u](\omega) \cdot (-m\omega^2 + i c \omega + k) = 0. \quad (2.30)$$

The bracketed term can be interpreted as the characteristic polynomial of the differential equation. Computing the roots and inserting in the right Ansatz leads to the homogeneous solution in the frequency domain. This can be a cumbersome procedure as one needs to deal with distributions [4]. Therefore a different approach has been made in this work. The homogeneous solution in the time domain (Eq. 2.17) is transformed into the frequency domain using the tools of Section 1.2.2. This enables the consideration of initial conditions. The derivation is in the following lines.

$\zeta > 1$

$$u_h(t) = \alpha_1 \cdot \underbrace{e^{\lambda_1 t}}_{:=g(t)} + \alpha_2 \cdot e^{\lambda_2 t} \quad \text{with } \lambda_1, \lambda_2 < 0 \quad (2.31)$$

The function $g(t)$ is transformed

$$\begin{aligned} G(\omega) &= \int_{-\infty}^{\infty} g(t) e^{-i\omega t} dt \stackrel{t \geq 0}{=} \int_0^{\infty} e^{\lambda_1 t} e^{-i\omega t} dt, \\ &= \int_0^{\infty} e^{(\lambda_1 - i\omega)t} dt = \frac{1}{\lambda_1 - i\omega} \cdot e^{(\lambda_1 - i\omega)t} \Bigg|_0^{\infty}, \\ &= \frac{1}{-\lambda_1 + i\omega}. \end{aligned} \quad (2.32)$$

This result, combined with property Eq. 1.26 yields the solution in frequency domain

$$F[u_h](\omega) = \alpha_1 \cdot \frac{1}{-\lambda_1 + i\omega} + \alpha_2 \cdot \frac{1}{-\lambda_2 + i\omega}. \quad (2.33)$$

$\zeta = 1$

$$u_h(t) = \alpha_1 \cdot \underbrace{e^{\lambda t}}_{:=\frac{1}{-\lambda + i\omega}} + \alpha_2 \cdot \underbrace{t e^{\lambda t}}_{:=h(t)} \quad \text{with } \lambda < 0 \quad (2.34)$$

$$\begin{aligned}
 H(\omega) &= \int_{-\infty}^{\infty} h(t)e^{-i\omega t} dt \stackrel{t \geq 0, \bar{\lambda} = -\lambda}{=} \int_0^{\infty} te^{-(\bar{\lambda}+i\omega)t} dt \stackrel{\text{Ad. calc.}}{\underset{\text{Part. int.}}{=}} \\
 \text{Formula of partial integration: } &\int_a^b \dot{f}g dt = [fg] \Big|_a^b - \int_a^b f\dot{g} dt \\
 &g(t) = t \leftrightarrow \dot{g}(t) = 1 \quad \text{and} \\
 &\dot{f}(t) = e^{-(\bar{\lambda}+i\omega)t} \leftrightarrow f(t) = \frac{1}{-(\bar{\lambda}+i\omega)} \cdot e^{-(\bar{\lambda}+i\omega)t} \quad (2.35) \\
 H(\omega) &= \underbrace{\frac{t}{-(\bar{\lambda}+i\omega)} \cdot e^{-(\bar{\lambda}+i\omega)t} \Big|_0^{\infty}}_{=0} - \int_0^{\infty} \frac{1}{-(\bar{\lambda}+i\omega)} \cdot e^{-(\bar{\lambda}+i\omega)t} dt, \\
 &= \frac{1}{(\bar{\lambda}+i\omega)^2} \cdot e^{-(\bar{\lambda}+i\omega)t} \Big|_{\bar{\lambda} = -\lambda}^{\infty} \frac{1}{(-\lambda+i\omega)^2}.
 \end{aligned}$$

The solution in the frequency domain is given with Eq. 1.26

$$F[u_h](\omega) = \alpha_1 \cdot \frac{1}{-\lambda + i\omega} + \alpha_2 \cdot \frac{1}{(-\lambda + i\omega)^2}. \quad (2.36)$$

$\zeta \in [0, 1)$

$$\begin{aligned}
 u_h(t) &= e^{-\zeta\omega_0 t} (\alpha_1 \cdot \cos(\omega_d t) + \alpha_2 \cdot \sin(\omega_d t)), \\
 &= \frac{1}{2} e^{-\zeta\omega_0 t} (\alpha_1 e^{-i\omega_d t} + \alpha_1 e^{i\omega_d t} + i\alpha_2 e^{-i\omega_d t} - i\alpha_2 e^{i\omega_d t}), \quad (2.37)
 \end{aligned}$$

with $(\zeta\omega_0), \omega_d \geq 0$

The homogeneous solution is reformulated with Euler's identity in order to simplify the transformation. The transformation of each term is given in the following.

$$\begin{aligned}
 F[f_1](\omega) &= \int_{-\infty}^{\infty} e^{-\zeta\omega_0 t} \cdot e^{-i\omega_d t} \cdot e^{-i\omega t} dt \stackrel{t \geq 0}{=} \int_0^{\infty} e^{-(\zeta\omega_0 + i\omega_d + i\omega)t} dt, \\
 &= \frac{-1}{\zeta\omega_0 + i\omega_d + i\omega} e^{-(\zeta\omega_0 + i\omega_d + i\omega)t} \Big|_0^{\infty} = \frac{1}{\zeta\omega_0 + i\omega_d + i\omega}. \\
 F[f_2](\omega) &= \int_{-\infty}^{\infty} e^{-\zeta\omega_0 t} \cdot e^{i\omega_d t} \cdot e^{-i\omega t} dt \stackrel{t \geq 0}{=} \int_0^{\infty} e^{-(\zeta\omega_0 - i\omega_d + i\omega)t} dt, \\
 &= \frac{-1}{\zeta\omega_0 - i\omega_d + i\omega} e^{-(\zeta\omega_0 - i\omega_d + i\omega)t} \Big|_0^{\infty} = \frac{1}{\zeta\omega_0 - i\omega_d + i\omega}. \quad (2.38)
 \end{aligned}$$

$$\begin{aligned}
 F[u_h](\omega) &= \frac{1}{2} \left[\alpha_1 \left(\frac{1}{\zeta\omega_0 + i\omega_d + i\omega} + \frac{1}{\zeta\omega_0 - i\omega_d + i\omega} \right) \right] \\
 &+ \frac{1}{2} \left[i\alpha_2 \left(\frac{1}{\zeta\omega_0 + i\omega_d + i\omega} - \frac{1}{\zeta\omega_0 - i\omega_d + i\omega} \right) \right], \\
 &= \alpha_1 \cdot \frac{\zeta\omega_0 + i\omega}{\omega_d^2 + (\zeta\omega_0 + i\omega)^2} - i\alpha_2 \cdot \frac{i\omega_d}{\omega_d^2 + (\zeta\omega_0 + i\omega)^2}.
 \end{aligned} \tag{2.39}$$

The homogeneous solutions in the frequency domain are summarized:

$$F[u_h](\omega) = \begin{cases} \alpha_1 \cdot \frac{1}{-\lambda_1 + i\omega} + \alpha_2 \cdot \frac{1}{-\lambda_2 + i\omega} & \text{if } \zeta > 1 \\ \alpha_1 \cdot \frac{1}{-\lambda + i\omega} + \alpha_2 \cdot \frac{1}{(-\lambda + i\omega)^2} & \text{if } \zeta = 1 \\ \alpha_1 \cdot \frac{\zeta\omega_0 + i\omega}{\omega_d^2 + (\zeta\omega_0 + i\omega)^2} - i\alpha_2 \cdot \frac{i\omega_d}{\omega_d^2 + (\zeta\omega_0 + i\omega)^2} & \text{if } \zeta \in [0, 1) \end{cases} \tag{2.40}$$

with the expression for $\lambda = \zeta\omega_0$ and $\lambda_1, \lambda_2, \omega_d$ from Eq. 2.18 and α_1, α_2 from Eq. 2.21. Again, in equivalence to the time domain approach, the particular solution at time $t = 0$ is needed to obtain the homogeneous solution in the frequency domain. Therefore the particular solution needs to be obtained first and transformed into the time domain.

Particular solution

This chapter is based on [13, pp. 34-63]. For obtaining the particular solution, the type of the right hand side is important. Following [13], the right hand side can be of three different types.

- Single harmonic
- General periodic
- General non-periodic

In the following all three types are discussed and an example is being made in Section 2.4. There are two number systems in which the particular solution can be obtained in the frequency domain: in terms of complex numbers \mathbb{C} or using the real numbers \mathbb{R} [13, p. 34]. In this work, complex numbers are chosen.

Single harmonic

A single harmonic excitation can be of the following form (with excitation frequency Ω)

$$f(t) = f^c \cdot \cos(\Omega t) + f^s \cdot \sin(\Omega t). \tag{2.41}$$

With Euler's formular, the force can be written as

$$f(t) = f^+ \cdot e^{i\Omega t} + f^- \cdot e^{-i\Omega t} \tag{2.42a}$$

$$\begin{aligned}
 \text{with } f^+ &= \frac{1}{2} (f^c - if^s) \\
 \text{and } f^- &= \frac{1}{2} (f^c + if^s).
 \end{aligned} \tag{2.42b}$$

With this kind of right hand side, the Ansatz for the particular solution is

$$u_p = u^+ \cdot e^{i\Omega t} + u^- \cdot e^{-i\Omega t}. \quad (2.43)$$

Inserting Eq. 2.43 and its first two derivatives with respect to time in Eq. 2.4 gives

$$\begin{aligned} m \cdot \left[-\Omega^2 u^+ e^{i\Omega t} - \Omega^2 u^- e^{-i\Omega t} \right] + c \cdot \left[i\Omega u^+ e^{i\Omega t} - i\Omega u^- e^{-i\Omega t} \right] \\ + k \cdot \left[u^+ \cdot e^{i\Omega t} + u^- \cdot e^{-i\Omega t} \right] = f^+ \cdot e^{i\Omega t} + f^- \cdot e^{-i\Omega t}. \end{aligned} \quad (2.44)$$

Comparing coefficients gives two equations for u^+ and u^-

$$u^+ \cdot \left[-\Omega^2 m + ic\Omega + k \right] = f^+, \quad (2.45a)$$

$$u^- \cdot \left[-\Omega^2 m - ic\Omega + k \right] = f^-$$

$$\Rightarrow u^+ = f^+ H^+ \quad \text{and} \quad u^- = f^- H^-, \quad (2.45b)$$

with the complex valued frequency response function H

$$\begin{aligned} H^+ &= \frac{1}{[-\Omega^2 m + ic\Omega + k]} = \frac{1}{k(1 - \eta^2 + 2i\zeta\eta)}, \\ H^- &= \frac{1}{[-\Omega^2 m - ic\Omega + k]} = \frac{1}{k(1 - \eta^2 - 2i\zeta\eta)}, \end{aligned} \quad (2.45c)$$

and $\eta = \Omega/\omega_0$.

Note that the two values obtained in Eq. 2.45b are conjugate complex². u^+ and u^- build the particular solution in the frequency domain. $\{a; b\}$ denotes a point in the $\omega - u$ plain. The solution for a harmonic load is therefore given by only two values in the frequency spectrum

$$F[u_p] = \{+\Omega / -\Omega; u^+ / u^-\}. \quad (2.46)$$

The solution in the time domain is obtained by inserting Eq. 2.45b into Eq. 2.43. Using the fact that the coefficients are conjugate complex, the transformation back into the time domain can be written as

$$u_p(t) = 2 \cdot \Re(u^+) \cdot e^{+i\Omega t}. \quad (2.47)$$

This formulation is possible because transforming two conjugate complex values back eliminates the imaginary part and doubles the real part [13, p. 55].

²Conjugated complex numbers do have an equal real part and an imaginary part with equal value but different sign.

General periodic

Every periodic function can be expressed as a Fourier series described in Section 1.2.1. With a slight change in the notation of Eq. 1.9 and Eq. 1.10 the load $f(t)$ can be written as

$$f(t) = \sum_{n=-\infty}^{+\infty} f_n e^{in\omega t}, \quad (2.48)$$

with the coefficients

$$f_n = \frac{1}{T} \int_{-T/2}^{T/2} f(t) e^{-in\omega t} dt, \quad (2.49)$$

where T describes the length of one period and $\omega = 2\pi/T$. To solve Eq. 2.4 with this kind of right side it is useful to use the superposition principle of differential calculus. The solution for each term of $f(t)$ is obtained and the superposition is the particular solution.

The coefficients of Eq. 2.49 are conjugate complex to each other for n equal in absolute value [13, p. 60], therefore the situation is the same as for a single harmonic excitation. Solving for one harmonic has been described above in detail. The main steps are repeated here.

Choose Ansatz

$$u_{pn} = u_n^+ \cdot e^{in\omega t} + u_n^- \cdot e^{-in\omega t}, \quad (2.50)$$

insert Eq. 2.50 and it's derivatives in the EOM and comparing coefficients gives

$$u_n^+ \cdot [-(n\omega)^2 m + ic(n\omega) + k] = f_n^+, \quad (2.51a)$$

$$u_n^- \cdot [-(n\omega)^2 m - ic(n\omega) + k] = f_n^-$$

$$\Rightarrow u_n^+ = f_n^+ H_n^+ \quad \text{and} \quad u_n^- = f_n^- H_n^-, \quad (2.51b)$$

with the complex-valued frequency response function H

$$H_n^+ = \frac{1}{[-(n\omega)^2 m + ic(n\omega) + k]} \quad \text{and} \quad (2.51c)$$

$$H_n^- = \frac{1}{[-(n\omega)^2 m - ic(n\omega) + k]} \quad \text{and} \quad H_0 = \frac{1}{k}.$$

The final particular solution in the time domain is given by

$$u_p(t) = H_0 f_0 + \sum_{n=1}^{\infty} H_n^+ f_n^+ e^{in\omega t} + \sum_{n=1}^{\infty} H_n^- f_n^- e^{-in\omega t}, \quad (2.52a)$$

or in short form

$$u_p(t) = \sum_{n=-\infty}^{\infty} \underbrace{H_n f_n}_{u_n} e^{in\omega t}, \quad (2.52b)$$

with the frequency response function H_n

$$H_n = \frac{1}{-(n\omega)^2 m + ic(n\omega) + k}. \quad (2.52c)$$

u_n is independent of t and therefore the solution in the frequency domain

$$F[u_p] = \{n\omega; u_n\}. \quad (2.53)$$

The solution in the frequency domain is a series of discrete values in the $\omega - u$ plain.

General non-periodic

For obtaining the particular solution for a general non-periodic right hand side, the knowledge from the previous situations can be used. The derivation is not done in detail here but may be found, e.g., in [13, p. 62]. The fact that in case of a general non-periodic right side the derivation is similar to general periodic right sides but, with introduction of an imaginary period T^* , the Fourier series evolves into the continuous Fourier transformation

$$f(t) = \frac{1}{2\pi} \int_{-\infty}^{\infty} F[f](\omega) e^{i\omega t} d\omega. \quad (2.54)$$

The spectral lines will be plotted over a frequency continua ω instead of discrete frequency values $\{n\omega\}$.

The particular solution is then given by multiplying the Fourier transformed load with the complex valued frequency response function $H(i\omega) = \frac{1}{-\omega^2 m + i c \omega + k}$. The solution is a closely defined function

$$F[u_p] = U(i\omega) = H(i\omega) \cdot F[f](\omega). \quad (2.55)$$

The solution in the time domain is then easily obtained by inserting Eq. 2.55 in Eq. 1.14

$$u_p(t) = \frac{1}{2\pi} \cdot \int_{-\infty}^{\infty} U(i\omega) e^{+i\omega t} dt. \quad (2.56)$$

Remark: The evaluation of the particular solution for difficult right hand sides can only be handled by numerically solving Eq. 2.56.

With this the general response from Eq. 2.28 is found. Fig. 2.2 summarizes the step needed to obtain the solution in the frequency domain.

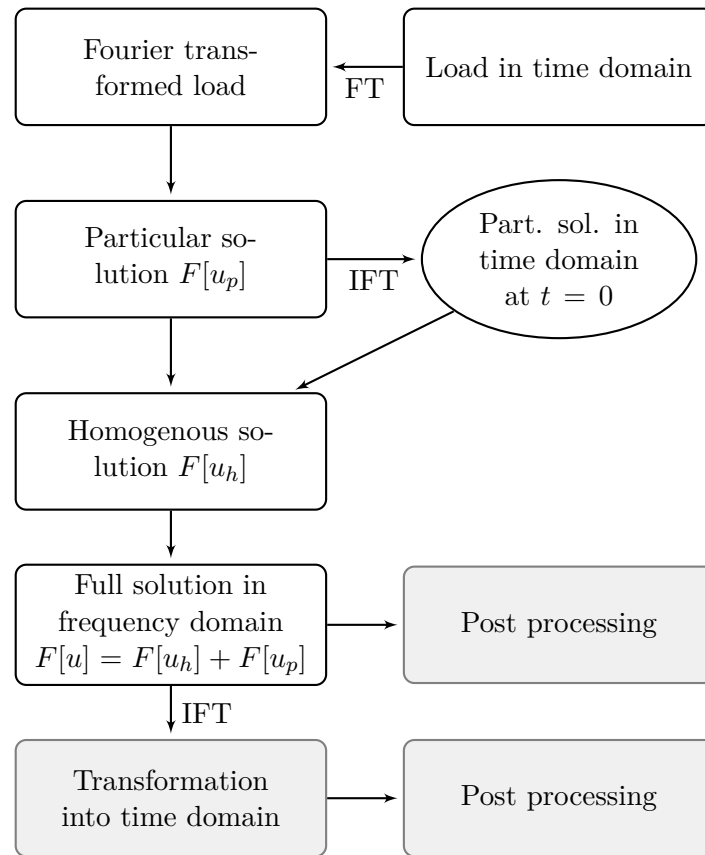


Fig. 2.2: Flow chart of obtaining the analytical solution in the frequency domain.

2.2.3 Comparison of calculation methods

The following flow chart summarizes the calculation in both, time and frequency domain and also shows the connections between the calculations. Furthermore it is shown whether initial conditions can be considered or not ([7, p. 40]). The abbreviations FT and IFT denote the Fourier transform and the inverse Fourier transform respectively.

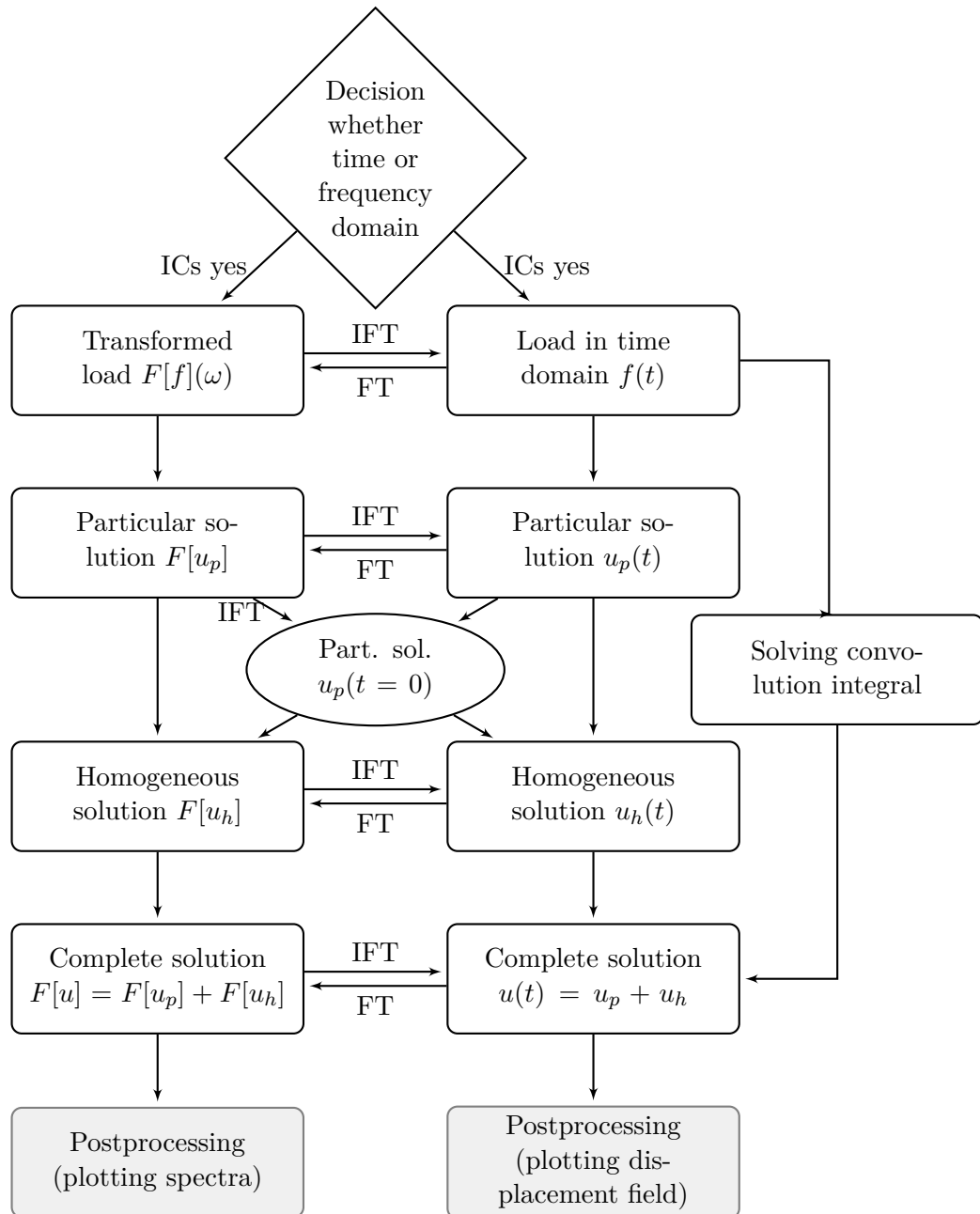


Fig. 2.3: Flow chart of analytically solving the equation of motion.

2.3 Numerical solution of the EOM

In many practical applications, the right hand side is not available in closed form but rather as a series of discrete values at discrete time steps or the right hand side $f(t)$ is in such form that an analytical solution cannot be obtained (with reasonable effort). In the following section, numerical procedures are discussed in both, time and frequency domain.

2.3.1 Numerical solution in the time domain

For solving the differential equation (which is an initial value problem of second order) numerically, a discretisation (in time) needs to be made [5, p. 969]. There are various different methods to do this and one may distinguish the methods based on the data of previous time steps employed:

- Multi-step methods, where informations of multiple former time steps are used (e.g. central difference method [7, pp. 171-174]).
- Single-step methods, where information of only *one* former step is needed (e.g. Newmark's method).

In this work, the Newmark's method [22] is used and introduced in the following, following the outline of [7, pp. 174-178]. The consideration of the initial conditions from Eq. 2.5 is possible [7, p. 165].

The EOM of Eq. 2.4 is discretised at time step t_{n+1}

$$k \cdot u_{n+1} + c \cdot \dot{u}_{n+1} + m \cdot \ddot{u}_{n+1} = f_{n+1}. \quad (2.57)$$

For u_{n+1} and \dot{u}_{n+1} special finite differences are used

$$u_{n+1} \approx u_n + \Delta t \cdot \dot{u}_n + [(1/2 - \beta)\ddot{u}_n + \beta \cdot \ddot{u}_{n+1}] \cdot \Delta t^2 \quad (2.58a)$$

$$\dot{u}_{n+1} \approx \dot{u}_n + [(1 - \gamma)\ddot{u}_n + \gamma \cdot \ddot{u}_{n+1}] \cdot \Delta t \quad (2.58b)$$

where Δt is the size of one time step which is most of the time chosen constant [7, p. 166].

Inserting Eq. 2.58 into Eq. 2.57 and reformulating gives

$$\begin{aligned} & (m + \gamma\Delta t \cdot c + \beta\Delta t^2 \cdot k) \cdot \ddot{u}_{n+1} = \\ & f_{n+1} - c \cdot (\dot{u}_n + (1 - \gamma)\Delta t \cdot \ddot{u}_n) - k \cdot (u_n + \Delta t \cdot \dot{u}_n + (1/2 - \beta)\Delta t^2 \cdot \ddot{u}_n). \end{aligned} \quad (2.59)$$

In Eq. 2.59 all quantities except \ddot{u}_{n+1} are known from the previous time step and the equation can be evaluated immediately. The quantities \dot{u}_{n+1} and u_{n+1} are then given by evaluating Eq. 2.58.

At time step $t = 0$, the acceleration \ddot{u}_0 is unknown but can be obtained by analysing the EOM at time $t = 0$. Reformulating said equation gives

$$\ddot{u}_0 = \frac{1}{m} (f_0 - c \cdot \dot{u}_0 - k \cdot u_0). \quad (2.60)$$

Newmark proposes in [22] to chose the values $\gamma = 1/2$ and $\beta \geq 1/8$ and recommends $\beta = 1/6$ for the best convergence properties. Choosing $\beta = 1/4$ makes Newmark's method unconditionally stable [8, p. 122].

Linear systems enable the evaluation of a modified Newmark's method without iteration [7, p. 175]. The displacement at time step t_{n+1} is calculated first and then the velocity and acceleration. According to [7, pp. 175-176], the direct evaluation is achieved by reformulating Eq. 2.58a and Eq. 2.58b to

$$\ddot{u}_{n+1} = a_0 \cdot (u_{n+1} - u_n) - a_2 \cdot \dot{u}_n - a_3 \cdot \ddot{u}_n \quad (2.61a)$$

$$\dot{u}_{n+1} = a_1 \cdot (u_{n+1} - u_n) + a_4 \cdot \dot{u}_n + a_5 \cdot \ddot{u}_n \quad (2.61b)$$

with the coefficients

$$a_0 = \frac{1}{\beta \Delta t^2}, \quad a_1 = \frac{\gamma}{\beta \Delta t}, \quad a_2 = \frac{1}{\beta \Delta t}, \quad a_3 = \frac{1}{2\beta} - 1, \quad (2.62)$$

$$a_4 = 1 - \frac{\gamma}{\beta}, \quad a_5 = \Delta t \left(1 - \frac{\gamma}{2\beta} \right).$$

Inserting Eq. 2.61 into Eq. 2.57 enables the calculation of u_{n+1} directly

$$(a_0 m + a_1 c + k) \cdot u_{n+1} = f_{n+1} + m \cdot (a_0 u_n + a_2 \dot{u}_n + a_3 \ddot{u}_n) + c \cdot (a_1 u_n - a_4 \dot{u}_n - a_5 \ddot{u}_n). \quad (2.63)$$

The whole procedure can be summarized in three major steps and is graphically shown in Fig. 2.4.

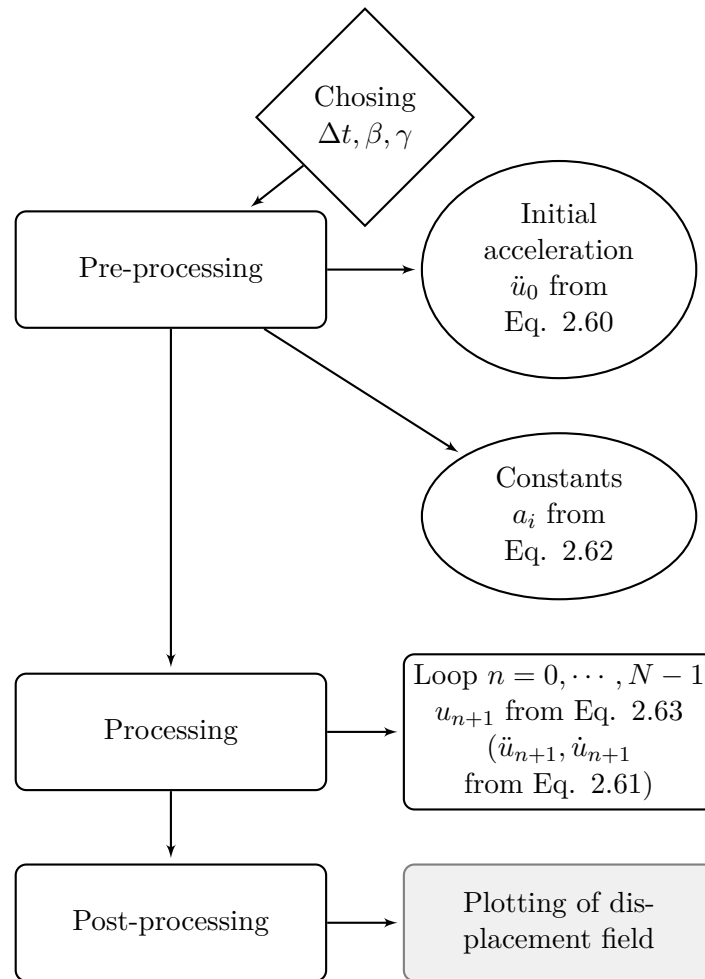


Fig. 2.4: Flow chart of numerically solving the EOM with Newmark's method.

The time step size Δt has to be chosen appropriately. Newmark proposes to chose the time step size to be one fifth to one sixth of the smallest natural period of the system in order to achieve reasonable convergence rates and small errors [22, p. 79].

The Newmark's method gives the total response of the system to arbitrary loads. Distinguishing damping scenarios according to D as in Eq. 2.15 or the splitting into homogeneous and particular solutions does not apply. One can obtain the response due to initial conditions and due to external load separately by setting the ICs or the load zero though.

2.3.2 Numerical solution in the frequency domain

The derivation of the numerical solution is done very quickly and follows the outline of [21, p. 6]. The response obtained is the total one [7, p. 891], which means it is not possible to extract the homogeneous or particular solution. Furthermore the initial conditions from Eq. 2.5 are assumed to be zero with this kind of formulation ([8, p. 108], [7, p. 900], [20, p. 57]). By considering the pseudo-force techniques, the consideration of ICs would be possible [20, p. 57]. This technique is not followed in this thesis.

The general steps for solving the differential equation is very similar as for obtaining the homogeneous solution. Eq. 2.4 is Fourier transformed and gives

$$m \cdot F[\ddot{u}](\omega) + c \cdot F[\dot{u}](\omega) + k \cdot F[u](\omega) = F[f](\omega). \quad (2.64)$$

With the property Eq. 1.29 the equation is of following form

$$F[u](\omega) \cdot (-m\omega^2 + ic\omega + k) = F[f](\omega). \quad (2.65)$$

Reformulating the equation gives the solution of the EOM in the frequency domain

$$F[u](\omega) = \frac{1}{(-m\omega^2 + ic\omega + k)} \cdot F[f](\omega) = H(\omega) \cdot F[f](\omega). \quad (2.66)$$

The numerical part comes into play when considering the Fourier transformed load, wherefore the FFT from Section 1.2.3 is used. Discrete frequency values are inserted in the frequency response function meaning that for every frequency value the response function needs to be evaluated. In Fig. 2.5, a flow chart of the calculation is shown where the last step is obviously optional.

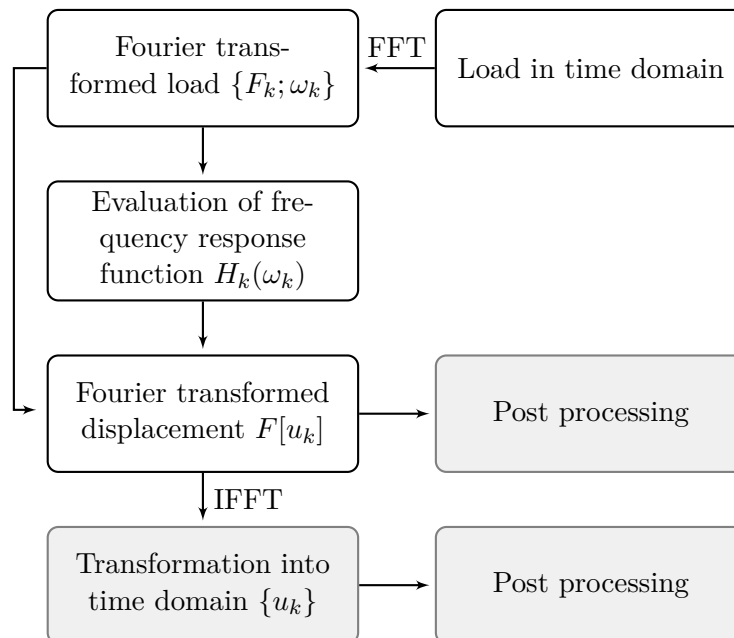


Fig. 2.5: Flow chart of numerically solving the EOM in the frequency domain.

Chopra [7] stated in appendix A, that depending on the damping ratio ζ and the observed calculation time, the results may vary dramatically. Therefore it is once again shown that choosing the right amount of zero-padding and/or modification of the calculation time is crucial for a good approximation of the result. To keep the errors in the frequency analysis below some selected tolerance limit $\epsilon \ll 1$, it is necessary to choose the calculation time t_f longer for systems with less damping [7, p. 901].

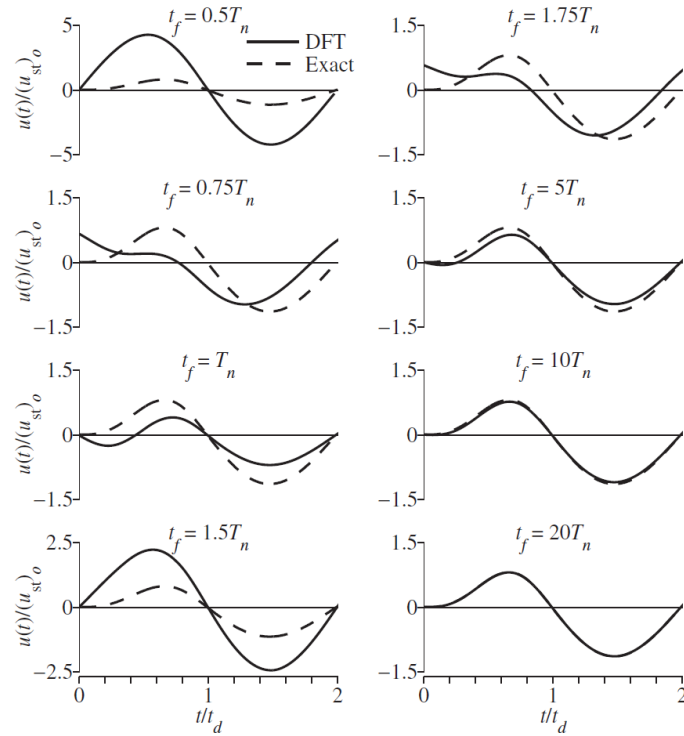


Fig. 2.6: Influence of the time t_f on the results obtained by using the FFT in frequency analysis, taken from [7, p. 900]

2.3.3 Comparison of calculation methods

The following flow chart should summarize the calculation in both, time and frequency domain and also shows the connections between the calculations. Furthermore it is shown whether initial conditions can be considered or not ([7, p. 165], [7, p. 129] and [20, p. 57]). The abbreviations FFT and IFFT denote the Fast Fourier transform and the inverse Fast Fourier transform respectively.

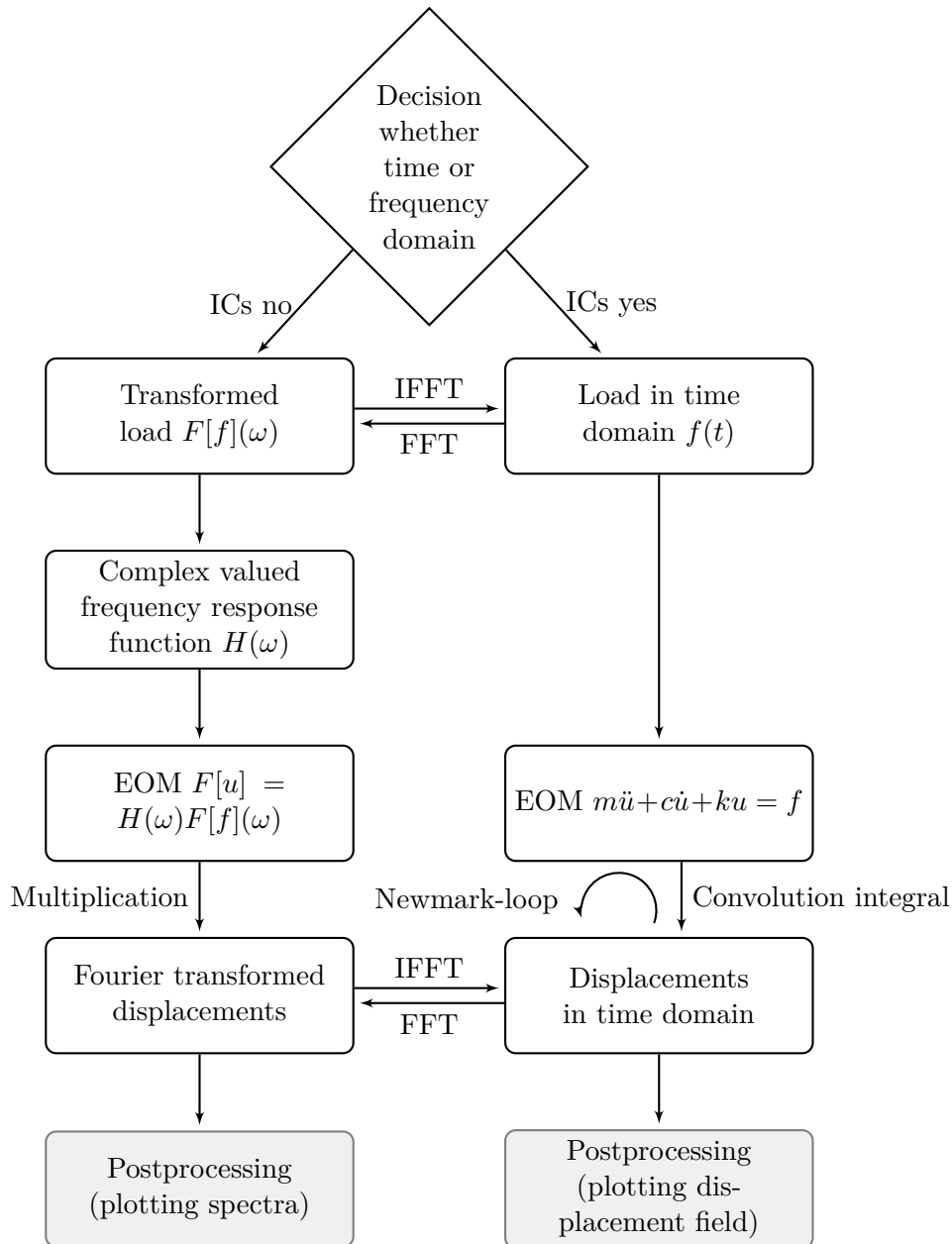


Fig. 2.7: Flow chart of numerically solving EOM in both domains

2.4 Examples

In this sections some solutions for a single degree of freedom system are presented. The system as well as the system parameters are shown in the following figure. As the goal of this thesis is to compare the computations in the time and frequency domain, both approaches are used for each example. The example's geometry is taken from the lecture notes "Structural Dynamics"³ of Dr. Dünser [10].

2.4.1 Introduction to example

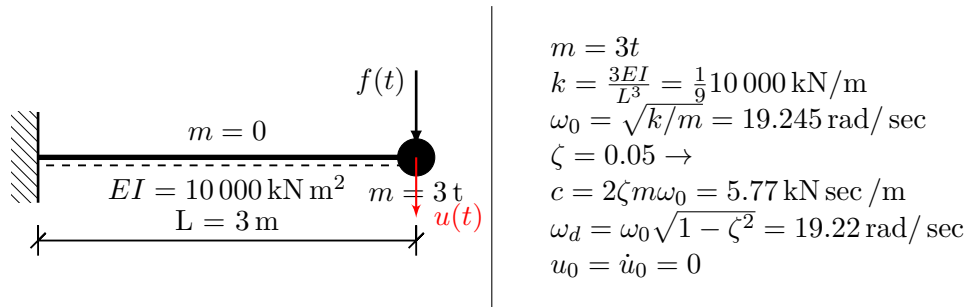


Fig. 2.8: Geometrical configuration of a cantilever beam with load on end.

Four different loadings are applied on the mass on the right end of the cantilever beam. The observed time is always 10 seconds.

- Single harmonic: $f(t) = f^c \cos(\Omega t) + f^s \sin(\Omega t) = 50 \cdot \cos(10t) + 25 \cdot \sin(10t)$ shown in Fig. 2.9(a)
- General periodic: load from Fig. 1.3 with $\hat{y} = 50 \text{ kN}$ and $T = 10 \text{ sec}$ shown in Fig. 2.9(b)
- General non-periodic: load from Fig. 1.6 with $f_0 = 50 \text{ kN}$ and $\hat{T} = 5 \text{ sec}$ shown in Fig. 2.10(a)
- Arbitrary: with discrete values at time steps (marked with x) as shown in Fig. 2.10(b)

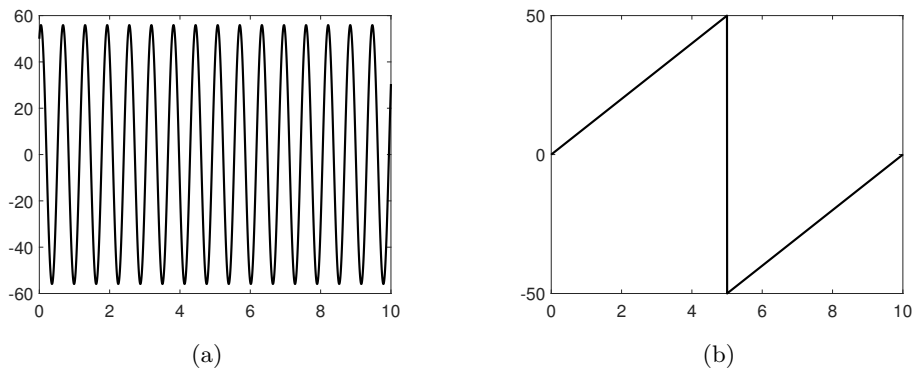


Fig. 2.9: Example of a (a) harmonic load and (b) periodic load.

³The lecture Structural Dynamics is taught by Dr.techn. C. Dünser at TU Graz in 2020. The lecture slides and notes are only published for students enrolled in this course but not to the general public [10].

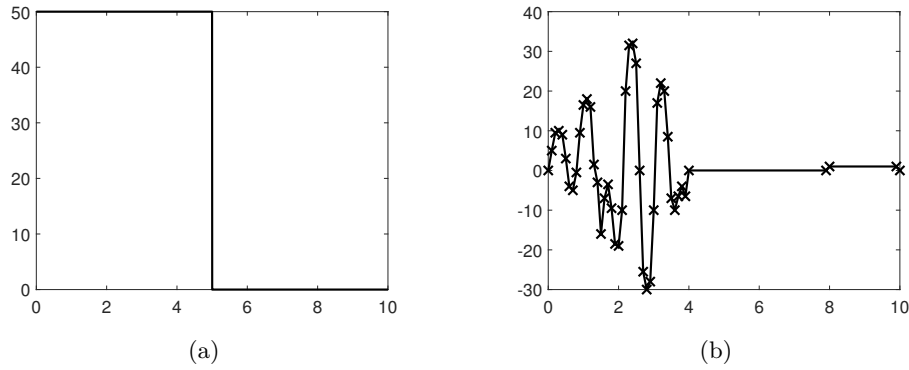


Fig. 2.10: Example of a (a) non-periodic load and (b) arbitrary load.

2.4.2 Harmonic excitation

The EOM is solved in the time and frequency domain. Firstly, the solution is derived in the time domain.

Solution in time domain

The Ansatz for the particular solution is chosen as proposed in Tab. 2.2

$$u_p(t) = u^c \cos(\Omega t) + u^s \sin(\Omega t). \quad (2.67)$$

Obtaining the first and second derivative with respect to time gives

$$\dot{u}_p(t) = \frac{du_p}{dt} = -\Omega u^c \sin(\Omega t) + \Omega u^s \cos(\Omega t) \quad \text{and} \quad (2.68a)$$

$$\ddot{u}_p(t) = \frac{d\dot{u}_p}{dt} = -\Omega^2 u^c \cos(\Omega t) - \Omega^2 u^s \sin(\Omega t). \quad (2.68b)$$

Inserting in the EOM Eq. 2.4 gives

$$\begin{aligned} f^c \cos(\Omega t) + f^s \sin(\Omega t) &= m \cdot \left(-\Omega^2 u^c \cos(\Omega t) - \Omega^2 u^s \sin(\Omega t) \right) \\ &\quad + c \cdot \left(-\Omega u^c \sin(\Omega t) + \Omega u^s \cos(\Omega t) \right) \\ &\quad + k \cdot \left(u^c \cos(\Omega t) + u^s \sin(\Omega t) \right). \end{aligned} \quad (2.69)$$

Rearranging and factoring out gives the following system of equations (with $\Delta = (k - \Omega^2 m)^2 + (\Omega c)^2$)

$$\begin{bmatrix} k - \Omega^2 m & \Omega c \\ -\Omega c & k - \Omega^2 m \end{bmatrix} \begin{Bmatrix} u^c \\ u^s \end{Bmatrix} = \begin{Bmatrix} f^c \\ f^s \end{Bmatrix}, \quad (2.70a)$$

with the coefficients

$$\begin{aligned} u^c &= \frac{k - \Omega^2 m}{\Delta} f^c - \frac{\Omega c}{\Delta} f^s = 0.0594 \text{ m} \quad \text{and} \\ u^s &= \frac{k - \Omega^2 m}{\Delta} f^s + \frac{\Omega c}{\Delta} f^c = 0.0352 \text{ m}. \end{aligned} \quad (2.70b)$$

Therefore the particular solution is

$$u_p(t) = 0.0594 \cos(10t) + 0.0352 \sin(10t), \quad (2.71)$$

with values of the displacement and velocity at time $t = 0$

$$\begin{aligned} u_p(t=0) &= 0.0594 \text{ m} \quad \text{and} \\ \dot{u}_p(t=0) &= 0.352 \text{ m/sec.} \end{aligned} \quad (2.72)$$

The homogeneous solution is then straightforwardly obtained by inserting the integration constants from Eq. 2.21 in Eq. 2.17

$$\begin{aligned} \alpha_1 &= u_0 - u_p(t=0) = -0.0594, \\ \alpha_2 &= \frac{1}{\omega_d} (v_0 + \zeta\omega_0(u_0 - u_p(t=0)) + \dot{u}_p(t=0)) = 0.0153, \end{aligned} \quad (2.73)$$

$$u_h(t) = e^{-0.05 \cdot 19.245 \cdot t} (-0.0594 \cdot \cos(19.22t) + 0.0153 \cdot \sin(19.22t)). \quad (2.74)$$

The full solution is the sum of particular and homogeneous solution and is plotted in Fig. 2.11.

Solution in frequency domain

The solution in the frequency domain is calculated next by inserting in Eq. 2.45b with Eq. 2.42b and Eq. 2.45c. Therefore the harmonic loading needs to be rewritten with complex notation

$$\begin{aligned} f(t) &= f^+ \cdot e^{i\Omega t} + f^- \cdot e^{-i\Omega t}, \\ \text{with } f^+ &= 25 - 12.5i \quad \text{and} \quad f^- = 25 + 12.5i. \end{aligned} \quad (2.75)$$

Inserting the complex load in Eq. 2.45b together with the frequency response function gives

$$\begin{aligned} u^+ &= f^+ H^+ = \frac{25 - 12.5i}{-100 \cdot 3 + 5.77 \cdot 10i + 1111.11} \quad \text{and} \\ u^- &= f^- H^- = \frac{25 + 12.5i}{-100 \cdot 3 - 5.77 \cdot 10i + 1111.11}. \end{aligned} \quad (2.76)$$

The particular solution in the frequency domain is therefore

$$u^+ = 0.0296 - 0.0175i \quad \text{and} \quad u^- = 0.0296 + 0.0175i. \quad (2.77)$$

The homogeneous solution then follows by inserting the coefficients α_i from Eq. 2.73 into Eq. 2.40

$$\begin{aligned} F[u_h](\omega) &= -0.0594 \cdot \frac{0.05 \cdot 19.245 + i\omega}{19.22^2 + (0.05 \cdot 19.245 + i\omega)^2} \\ &\quad + 0.0153i \cdot \frac{19.22i}{19.22^2 + (0.05 \cdot 19.245 + i\omega)^2}. \end{aligned} \quad (2.78)$$

The amplitude spectrum of $F[u]$ is graphically shown in Fig. 2.13. The peaks in the spectrum show the dominant frequencies at $\omega = 10 \text{ rad/sec}$ and $\omega = \omega_0$. The dominant frequency of the particular

solution is the excitation frequency $\Omega = 10 \text{ rad/sec}$ as expected. The transient part oscillates with the natural period of the system ω_0 .

After transforming this solution into the time domain, results are shown in Fig. 2.12 and Fig. 2.11, split into homogeneous, particular and total response. It can be seen that the homogeneous (transient) solution decays over time leading to $u(t) \rightarrow u_p(t)$ for large t . This is typical for damped systems.

A comparison of the two solutions in the time domain is given in Fig. 2.14. The blue line shows the solution in the time domain. The black line marks the displacement obtained in the frequency domain. Both calculated displacement fields behave equally, confirming the equivalence of the two approaches. The amplitudes of the oscillations are similar. The phases match well, meaning the time difference of the two displacements is close to zero.

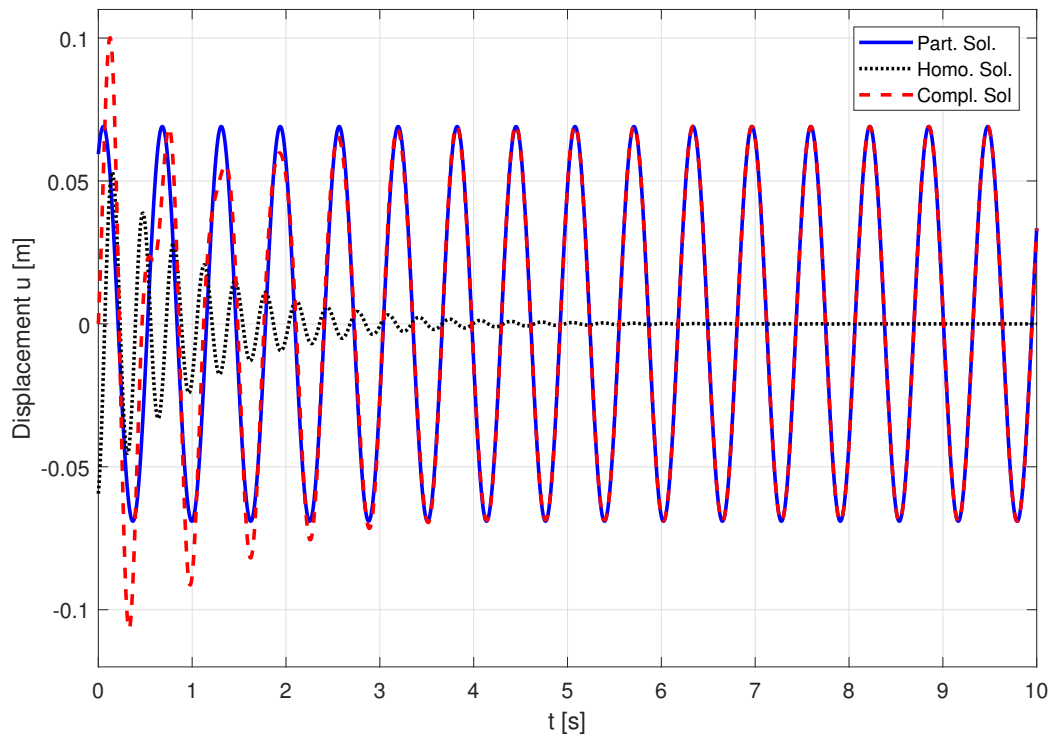


Fig. 2.11: Displacement in the time domain with harmonic load obtained in time domain.

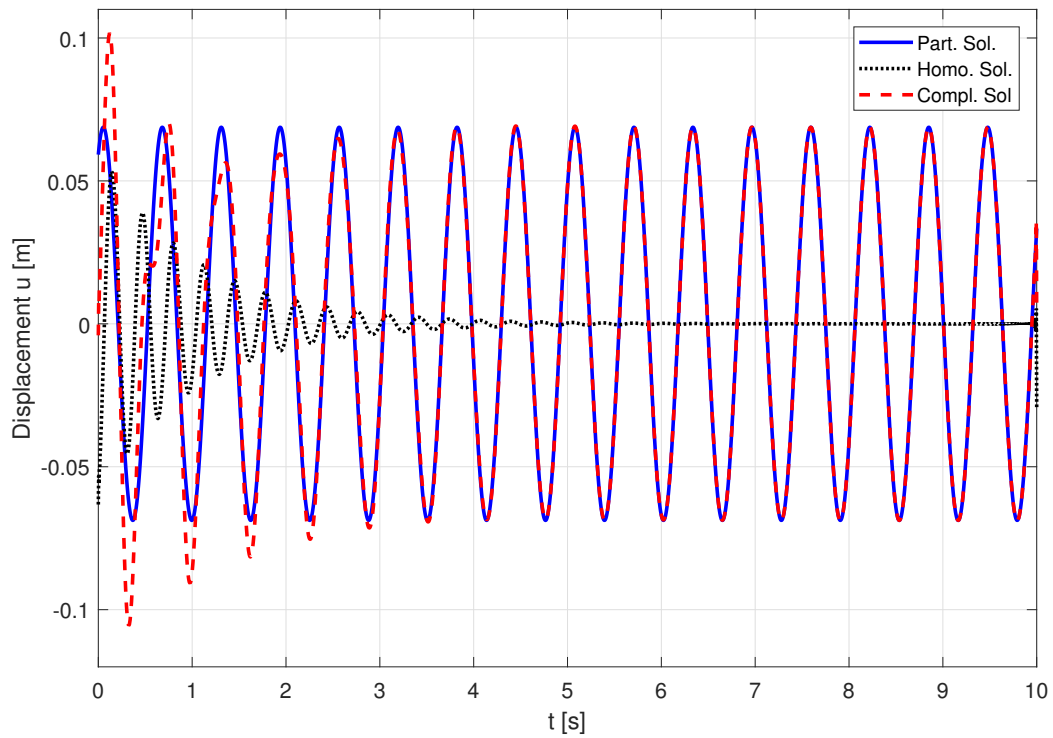


Fig. 2.12: Displacement in the time domain with harmonic load obtained in frequency domain.

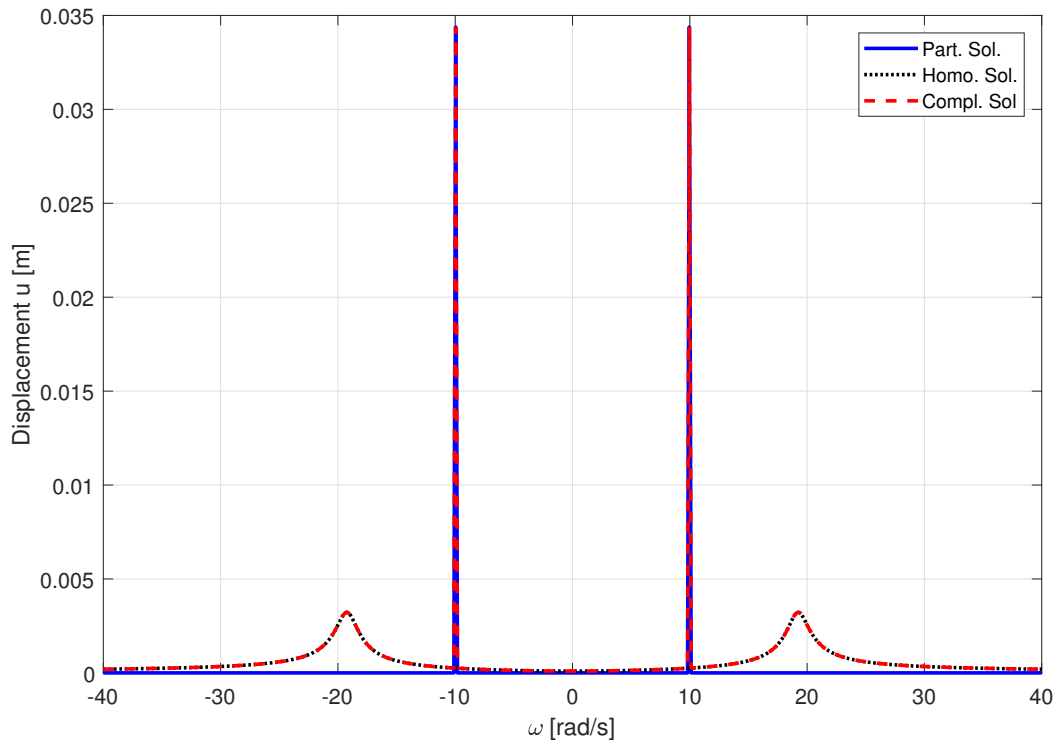


Fig. 2.13: Amplitude spectrum of response with harmonic load obtained in frequency domain.

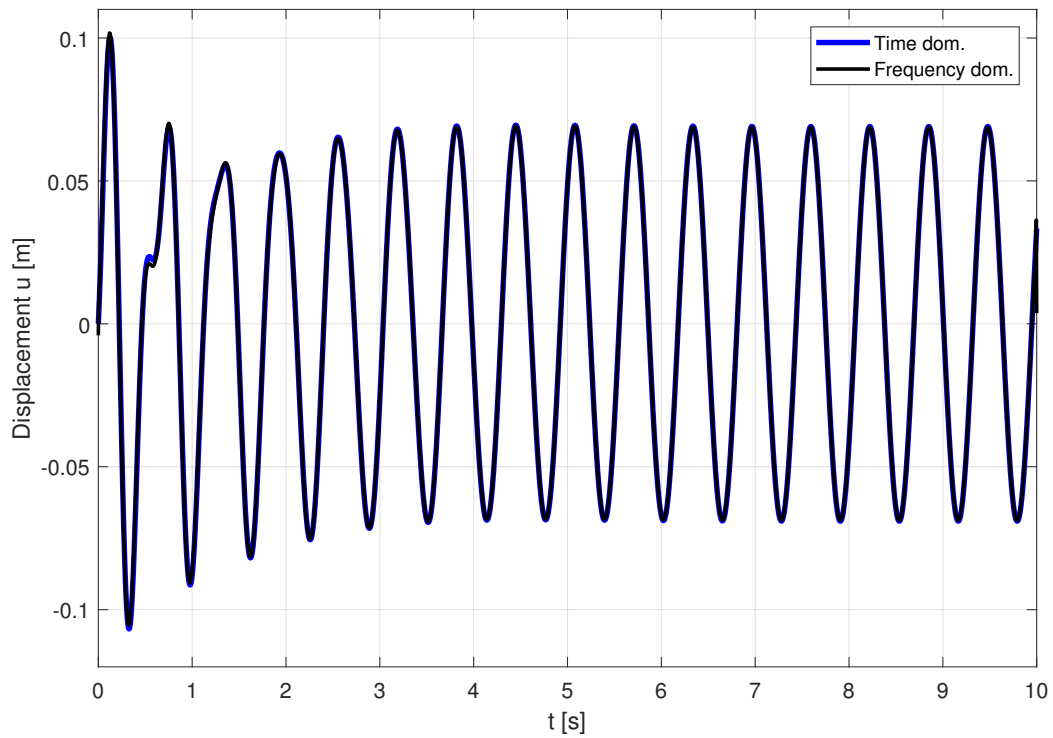


Fig. 2.14: Comparison of displacements due to harmonic load in the time and frequency domain.

2.4.3 Periodic excitation

Solution in time domain

For obtaining the solution in the time domain, it is necessary to disassemble the sawtooth function into the corresponding harmonics. This is shown in Section 1.2.1. The load can be expressed as (with the help of Eq. 1.11 and Eq. 1.12)

$$f(t) = \sum_{n=1}^{+\infty} \frac{100}{\pi n} \cdot (-1)^{n+1} \sin(n\omega t) = \sum_{n=1}^{+\infty} f_n^s \sin(n\omega t). \quad (2.79)$$

The particular solution can be obtained by the sum of the particular solutions of the harmonics of $f(t)$. The n th particular solution is derived next and is very similar to the harmonic case.

The Ansatz is similar to Eq. 2.67

$$u_{p,n}(t) = u_n^c \cos(n\omega t) + u_n^s \sin(n\omega t). \quad (2.80)$$

Inserting the antiderivative and the first two derivatives with respect to time in the EOM Eq. 2.4 gives a system of equations (with $\Delta = (k - (n\omega)^2 m)^2 + (n\omega c)^2$)

$$\begin{bmatrix} k - (n\omega)^2 m & n\omega c \\ -n\omega c & k - (n\omega)^2 m \end{bmatrix} \begin{Bmatrix} u_n^c \\ u_n^s \end{Bmatrix} = \begin{Bmatrix} f_n^c = 0 \\ f_n^s \end{Bmatrix}, \quad (2.81a)$$

giving the coefficients

$$\begin{aligned} u_n^c &= -\frac{n\omega c}{\Delta} f_n^s \quad \text{and} \\ u_n^s &= \frac{k - (n\omega)^2 m}{\Delta} f_n^s. \end{aligned} \quad (2.81b)$$

Therefore the particular solution is

$$u_p(t) = \sum_{n=1}^{\infty} -\frac{n\omega c}{\Delta} f_n^s \cos(n\omega t) + \frac{k - (n\omega)^2 m}{\Delta} f_n^s \sin(n\omega t), \quad (2.82)$$

with the displacement and velocity at time $t = 0$

$$\begin{aligned} u_p(t=0) &= -2.177 \cdot 10^{-5} \text{ m} \quad \text{and} \\ \dot{u}_p(t=0) &= -0.0034 \text{ m/sec.} \end{aligned} \quad (2.83)$$

The homogeneous solution is then immediately obtained by evaluating the integration constants α_1 and α_2 from Eq. 2.21

$$\begin{aligned} \alpha_1 &= u_0 - u_p(t=0) = 2.177 \cdot 10^{-5} \quad \text{and} \\ \alpha_2 &= \frac{1}{\omega_d} (v_0 + \zeta \omega_0 (u_0 - u_p(t=0)) + \dot{u}_p(t=0)) = -1.684 \cdot 10^{-4}, \end{aligned} \quad (2.84)$$

and inserting the coefficients in Eq. 2.17, giving

$$u_h(t) = e^{-0.05 \cdot 19.245 \cdot t} \left(2.1773 \cdot 10^{-5} \cdot \cos(19.22t) - 1.684 \cdot 10^{-4} \cdot \sin(19.22t) \right). \quad (2.85)$$

The full solution is the sum of particular and homogeneous solution and is shown in Fig. 2.15 For computing purposes, the infinite sum was stopped after the 100th term.

Solution in frequency domain

To obtain the solution in the frequency domain, it is necessary to calculate the complex Fourier coefficients of the sawtooth function ($\Omega = 2\pi/T$)

$$\begin{aligned} f_n &= \frac{1}{T} \int_{-T/2}^{T/2} f(t) e^{-in\Omega t} dt, \\ &= \frac{1}{T} \int_{-T/2}^{T/2} f(t) (\cos(n\Omega t) - i \sin(n\Omega t)) dt. \end{aligned} \quad (2.86)$$

As the sawtooth function is an antimetric function, the cosine part of Eq. 2.86 is zero. The Fourier coefficients are

$$\begin{aligned} f_n &= \frac{-i}{T} \int_{-T/2}^{T/2} \frac{2\hat{y}}{T} t \sin(n\Omega t) dt = \frac{-2\hat{y}i}{T^2} \int_{-T/2}^{T/2} t \sin(n\Omega t) dt, \\ &= \frac{(\sin(\pi n) - \pi n \cos(\pi n)) T^2}{2\pi^2 n^2} \cdot \frac{-2\hat{y}i}{T^2}. \end{aligned} \quad (2.87)$$

The particular solution is obtained by inserting the coefficients in Eq. 2.51b

$$\begin{aligned} F[u_p] &= \{u_n; n\Omega\} \quad \text{with} \quad \Omega = 0.628 \text{ rad/sec} \quad \text{and} \\ u_n &= -\frac{1}{-3(n\Omega)^2 + 5.77i(n\Omega) + 1111.11} \cdot \frac{50i}{\pi^2 n^2} (\sin(\pi n) - \pi n \cos(\pi n)). \end{aligned} \quad (2.88)$$

The solution in the time domain is then obtained by inserting in Eq. 2.52b. The homogeneous solution is similarly obtained as in the points above (see Eq. 2.78) and is

$$\begin{aligned} F[u_h](\omega) &= 2.177 \cdot 10^{-5} \cdot \frac{0.05 \cdot 19.245 + i\omega}{19.22^2 + (0.05 \cdot 19.245 + i\omega)^2} \\ &\quad - 1.684 \cdot 10^{-4} i \cdot \frac{19.22i}{19.22^2 + (0.05 \cdot 19.245 + i\omega)^2}. \end{aligned} \quad (2.89)$$

The amplitude spectrum of $F[u]$ is graphically shown in Fig. 2.17. The amplitude spectrum shows the response of the system for every frequency. In this example, it is clearly seen that the system oscillates with its natural circular frequency ω_0 .

The solution in the time domain is shown in Fig. 2.16, split into homogeneous, particular and total response. The homogeneous solution is nearly zero in this example because the initial conditions are zero and the particular solution is close to zero at time $t = 0$.

A comparison of the two solutions is given in Fig. 2.18. In equivalence to the harmonic test case the solution obtained in the time domain is plotted blue and the solution in the frequency domain black. It can be seen that both responses are similar. The phases and amplitudes of the oscillations are equal, showing the equivalence of both approaches.

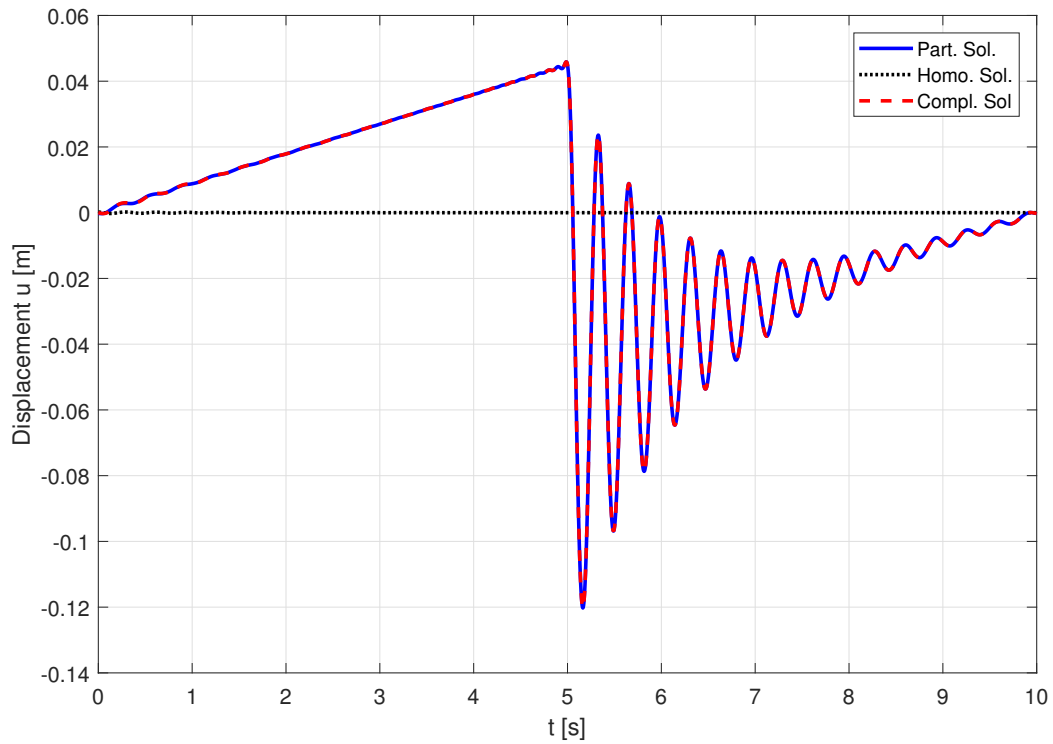


Fig. 2.15: Displacement in the time domain with periodic load obtained in time domain.

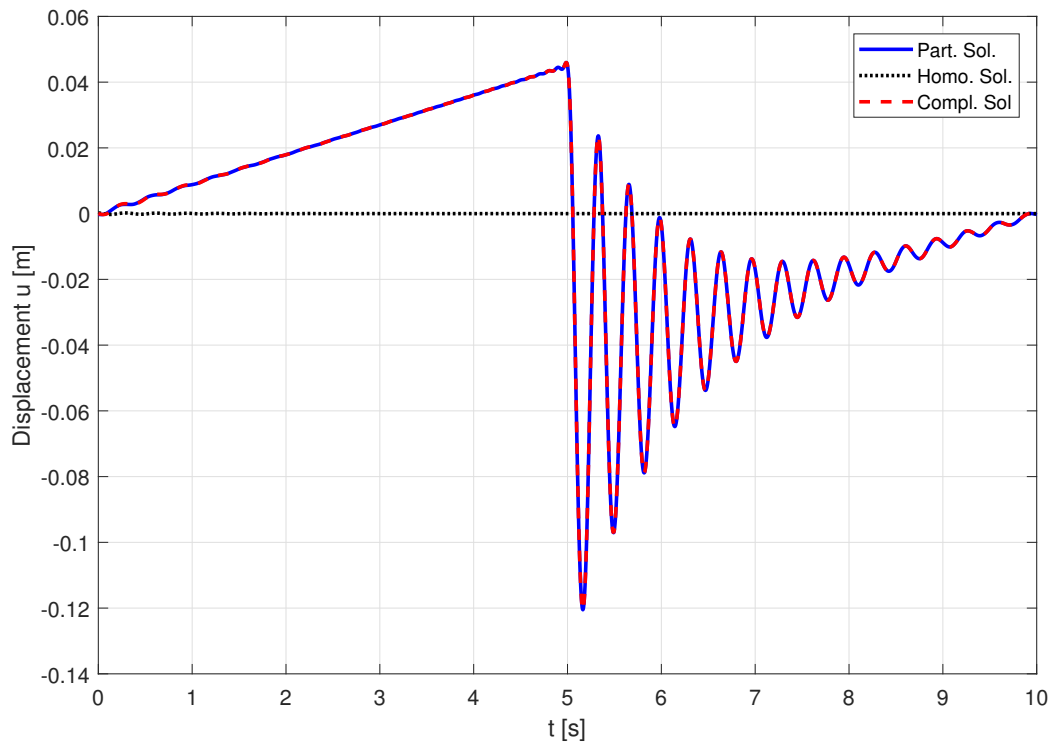


Fig. 2.16: Displacement in the time domain with periodic load obtained in frequency domain.

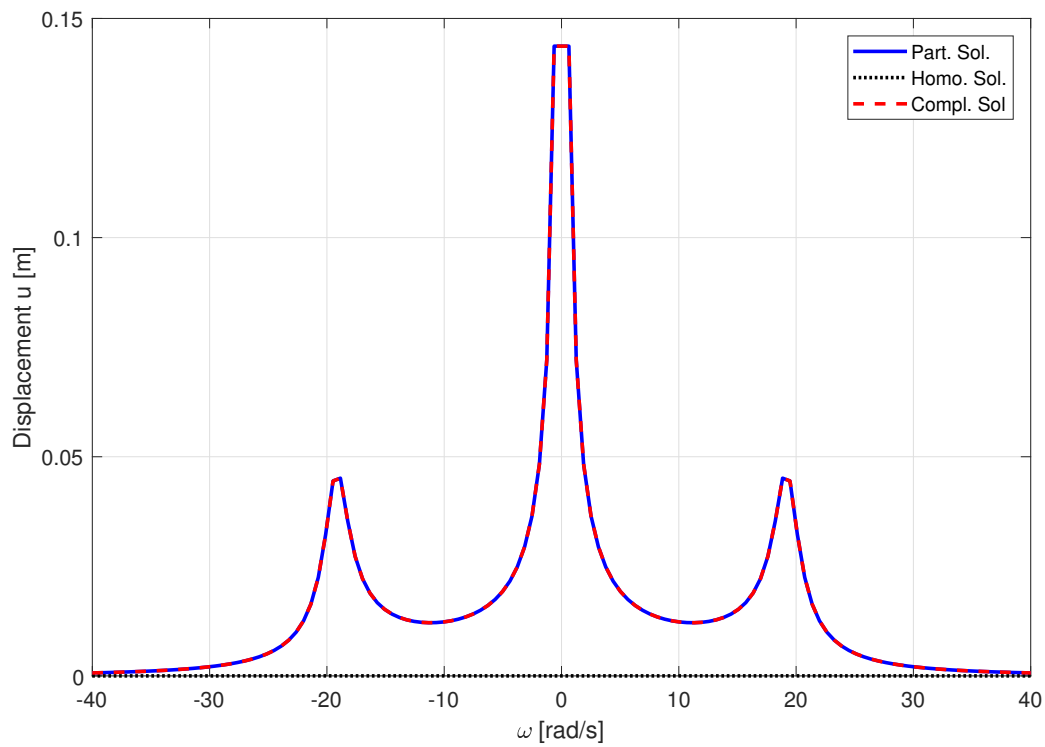


Fig. 2.17: Amplitude spectrum of response with periodic load obtained in frequency domain.

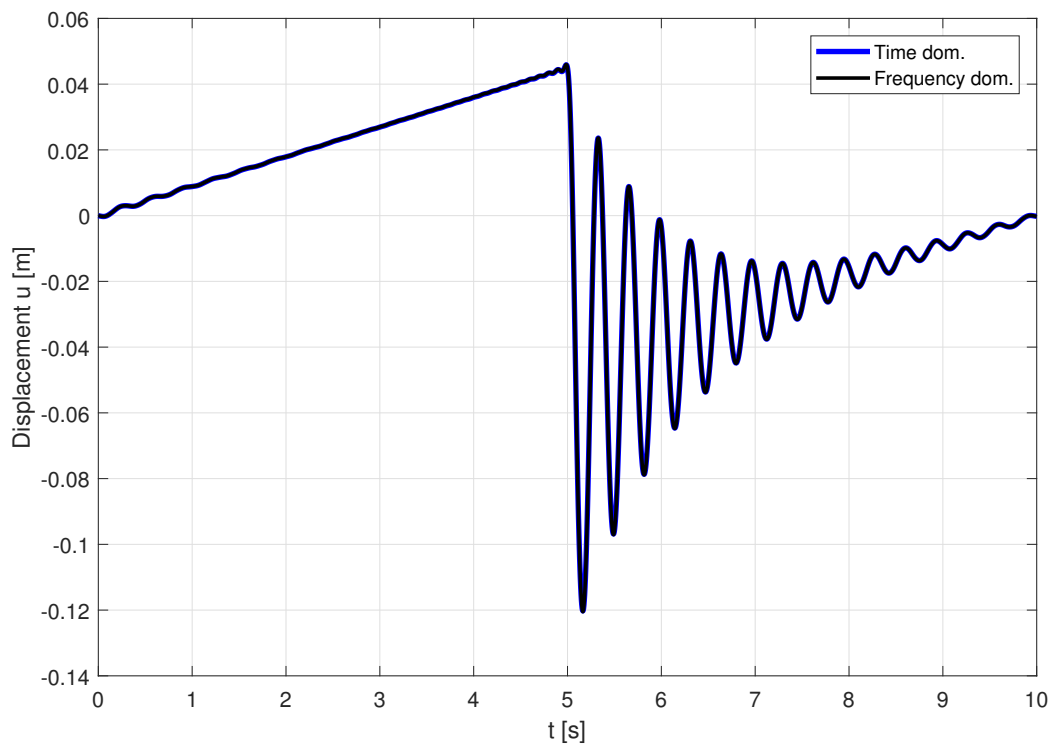


Fig. 2.18: Comparison of displacements due to periodic load in the time and frequency domain.

In order to verify the results once again, the response due to the periodic loading is obtained with Newmark's method. Fig. 2.19 shows the total response in the time domain.

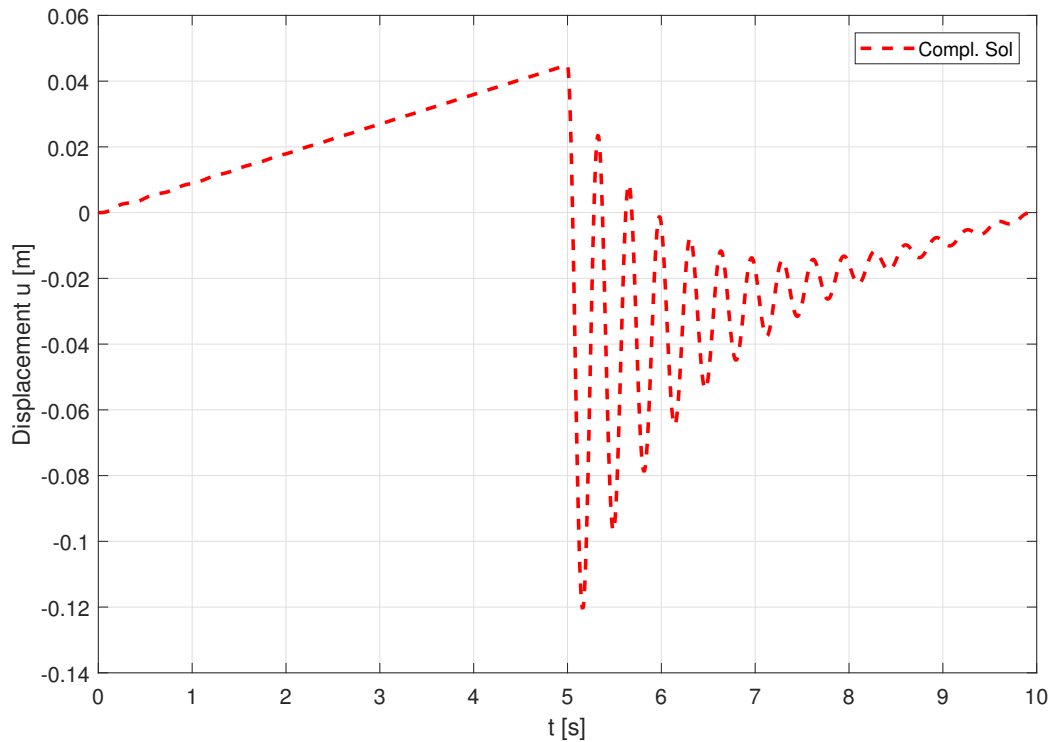


Fig. 2.19: Displacement in the time domain with periodic load obtained with Newmark's method.

Comparing Fig. 2.18 and Fig. 2.19, it can be seen that equivalent results are obtained. It is thus confirmed that all three methods (analytical time, analytical frequency and numerical time) are suitable to perform the calculation with the given excitation and yield equivalent results.

2.4.4 Non-periodic excitation

Solution in time domain

The response of this loading is calculated with help of the convolution integral. As the load jumps from f_0 to 0, the integral needs to be split and separately solved with Eq. 2.27. The forced vibration phase⁴ $t \leq \hat{T}$ is given by

$$u(t) = \underbrace{e^{-\zeta\omega_0 t} \left(u_0 \cos(\omega_d t) + \frac{v_0 + \zeta\omega_0 u_0}{\omega_d} \sin(\omega_d t) \right)}_{u_0=v_0=0 \rightarrow 0} + \frac{1}{m\omega_d} \int_0^t f_0 \cdot e^{-\zeta\omega_0(t-\tau)} \cdot \sin(\omega_d(t-\tau)) \, d\tau. \quad (2.90)$$

Applying the partial integration rule twice gives

$$u(t) = \frac{f_0}{m\omega_d} \cdot \left(\frac{\cos(\omega_d(t-\tau)) \cdot e^{-\zeta\omega_0(t-\tau)}}{\omega_d} \Big|_0^t \right) - \frac{f_0}{m\omega_d} \cdot \left(\frac{\zeta\omega_0 \sin(\omega_d(t-\tau)) \cdot e^{-\zeta\omega_0(t-\tau)}}{\omega_d^2} \Big|_0^t - \int_0^t -\frac{\zeta\omega_0 \sin(\omega_d(t-\tau)) \cdot e^{-\zeta\omega_0(t-\tau)}}{\omega_d^2} \, d\tau \right). \quad (2.91)$$

For the partial integration the trigonometric function was integrated twice and the exponential function was derived twice.

Inserting the boundaries gives

$$u(t) = \frac{f_0}{m\omega_d} \cdot \frac{\omega_d - e^{-\zeta\omega_0 t} (\zeta\omega_0 \sin(\omega_d t) + \omega_d \cos(\omega_d t))}{\omega_d^2 + (\zeta\omega_0)^2}. \quad (2.92)$$

After rearranging the coefficients, the solution for the forced vibration phase follows as

$$u(t) = \underbrace{\frac{f_0}{k}}_{u_{\text{stat},0}} \cdot \left(1 - e^{-\zeta\omega_0 t} \left(\cos(\omega_d t) + \frac{\zeta}{\sqrt{1-\zeta^2}} \sin(\omega_d t) \right) \right), \quad (2.93)$$

$$= \frac{50}{1111.11} \cdot \left(1 - e^{-0.05 \cdot 19.245 \cdot t} \left(\cos(19.22t) + \frac{0.05}{\sqrt{1-0.05^2}} \sin(19.22t) \right) \right).$$

Once the force is removed, the system oscillates until the damping stops the motion until rest. The free vibration phase⁵ $t \geq \hat{T}$ can be described by inserting in Eq. 2.27

$$u(t) = e^{-\zeta\omega_0 t} \left(u_0 \cos(\omega_d t) + \frac{v_0 + \zeta\omega_0 u_0}{\omega_d} \sin(\omega_d t) \right) + \underbrace{\frac{1}{m\omega_d} \int_0^t f_0 e^{-\zeta\omega_0(t-\tau)} \sin(\omega_d(t-\tau)) \, d\tau}_{f(t)=0 \rightarrow 0}. \quad (2.94)$$

⁴The vibration due to external load is called forced vibration.

⁵The free vibration phase describes the vibration due to initial condition and zero external load.

The free vibration phase is given by

$$\begin{aligned} u(t) &= e^{-\zeta\omega_0(t-\hat{T})} \left(u(t=\hat{T}) \cdot \cos(\omega_d(t-\hat{T})) + \frac{1}{\omega_d} (\dot{u}(t=\hat{T}) + \zeta\omega_0 u(t=\hat{T})) \cdot \sin(\omega_d(t-\hat{T})) \right), \\ &= e^{-0.05 \cdot 19.245(t-5)} (0.0451 \cdot \cos(19.22(t-5)) + 0.0101 \cdot \sin(19.22(t-5))), \end{aligned} \quad (2.95)$$

with the constants $u(t=\hat{T}) = 0.0451$ m and $\frac{1}{\omega_d} (\dot{u}(t=\hat{T}) + \zeta\omega_0 u(t=\hat{T})) = 0.0101$. Fig. 2.20 shows the displacement for the non-periodic load.

Solution in frequency domain

To solve the problem in the frequency domain, the load has to be transformed into the frequency domain and was already done for the rectangular force in Eq. 1.17. The particular solution in the frequency domain follows with Eq. 2.55

$$\begin{aligned} F[u_p](\omega) &= \frac{1}{-\omega^2 m + i\omega k + k} \cdot \hat{T} \cdot f_0 \cdot \frac{\sin(\omega\hat{T}/2)}{\omega\hat{T}/2} \cdot e^{-i\omega\hat{T}/2}, \\ &= \frac{1}{-3\omega^2 + i5.77\omega + 1111.11} \cdot 250 \cdot \frac{\sin(2.5\omega)}{2.5\omega} \cdot e^{-2.5i\omega}. \end{aligned} \quad (2.96)$$

At time $t = 0$ the particular solution has the values $u_p(t = 0) = 1.4366 \cdot 10^{-4}$ m and $\dot{u}_p(t = 0) = 0.1206$ m/sec. The values are obtained by transforming the solution back into the time domain.

The homogeneous solution is given analogously to Eq. 2.78 by inserting the integration constants

$$\begin{aligned} \alpha_1 &= u_0 - u_p(t = 0) = -1.4366 \cdot 10^{-4} \quad \text{and} \\ \alpha_2 &= \frac{1}{\omega_d} (v_0 + \zeta\omega_0(u_0 - u_p(t = 0)) + \dot{u}_p(t = 0)) = 6.267 \cdot 10^{-3} \end{aligned} \quad (2.97)$$

into Eq. 2.40

$$\begin{aligned} F[u_h](\omega) &= -1.4366 \cdot 10^{-4} \cdot \frac{0.05 \cdot 19.245 + i\omega}{19.22^2 + (0.05 \cdot 19.245 + i\omega)^2} \\ &\quad + 6.267 \cdot 10^{-3} \cdot i \cdot \frac{19.22 \cdot i}{19.22^2 + (0.05 \cdot 19.245 + i\omega)^2}. \end{aligned} \quad (2.98)$$

Fig. 2.20 shows the complete response obtained with the convolution integral. Fig. 2.21 shows the solution in the time domain obtained with a frequency analysis. The figure shows the particular, the homogeneous and the total response. Fig. 2.22 shows the solution (amplitude spectrum) in the frequency domain. It can be nicely seen, that the system oscillates with its natural circular frequency ω_0 . As done for the other loading scenarios, Fig. 2.23 shows the solution in the time domain obtained by the two different approaches. Both methods result in similar outcomes with expected displacements. In the forced vibration phase, the system oscillates around the static solution with the maximum displacement of approximately $2 \cdot u_{\text{stat}}$. The system starts to oscillate around the state of rest once the load is being removed due to the ideal elastic material law. The amplitudes of the time domain solution are slightly smaller than the ones in the frequency domain. The phases do match well, although they are slightly shifted.

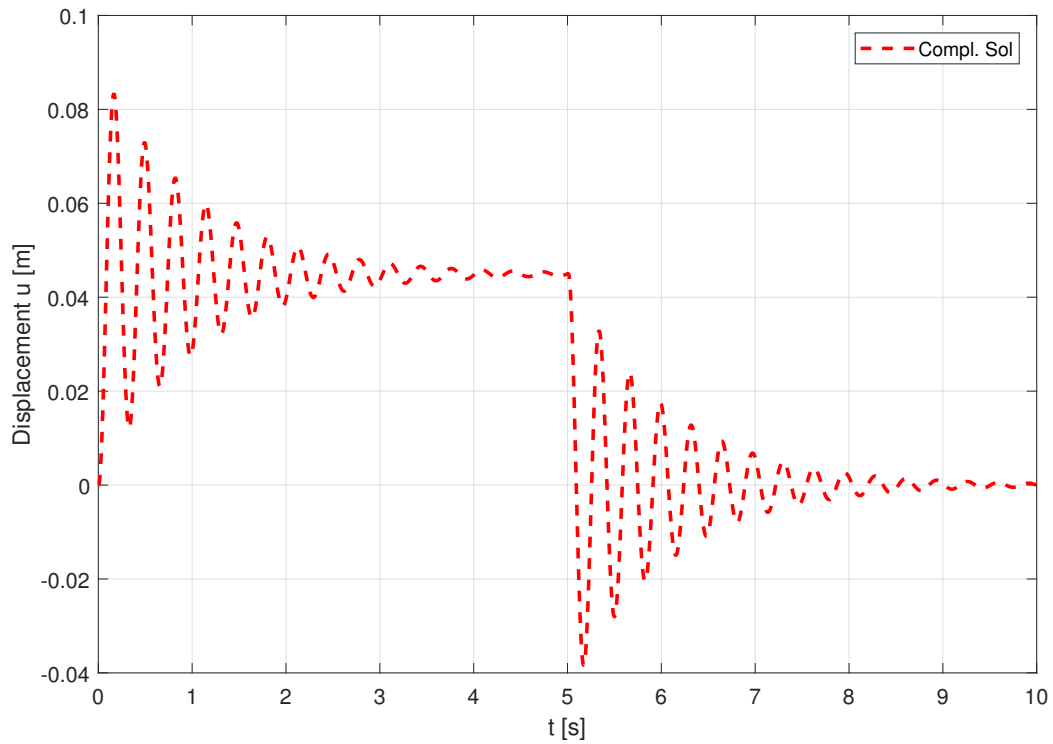


Fig. 2.20: Displacement in the time domain with nonperiodic load obtained in time domain.

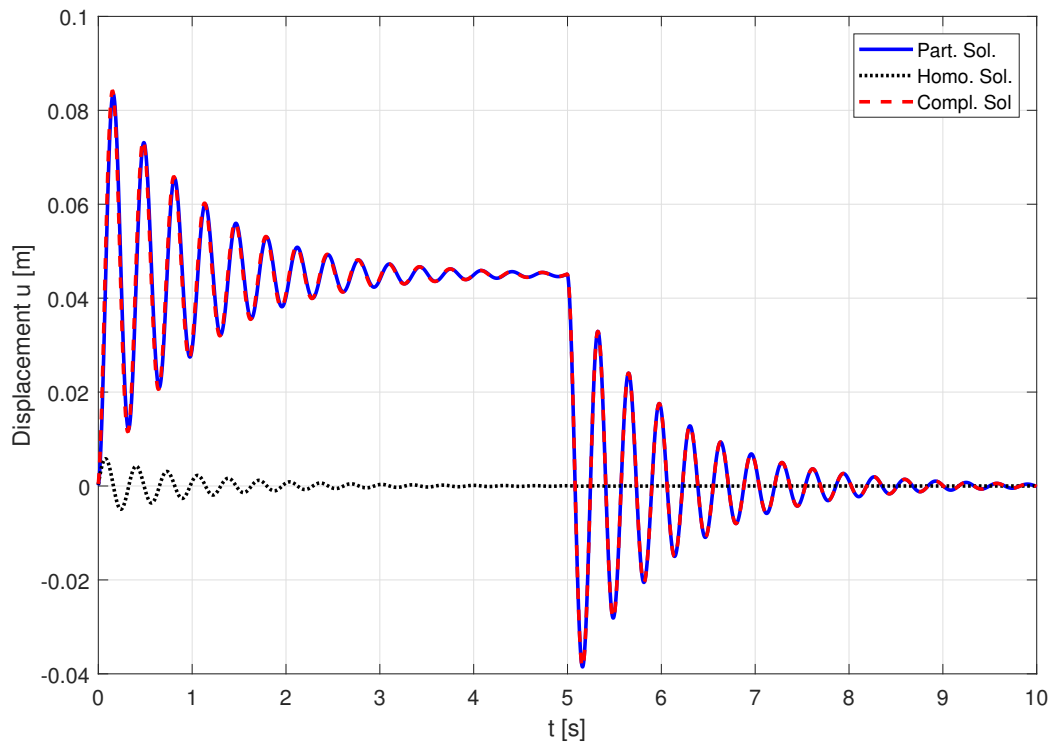


Fig. 2.21: Displacement in the time domain with nonperiodic load obtained in frequency domain.

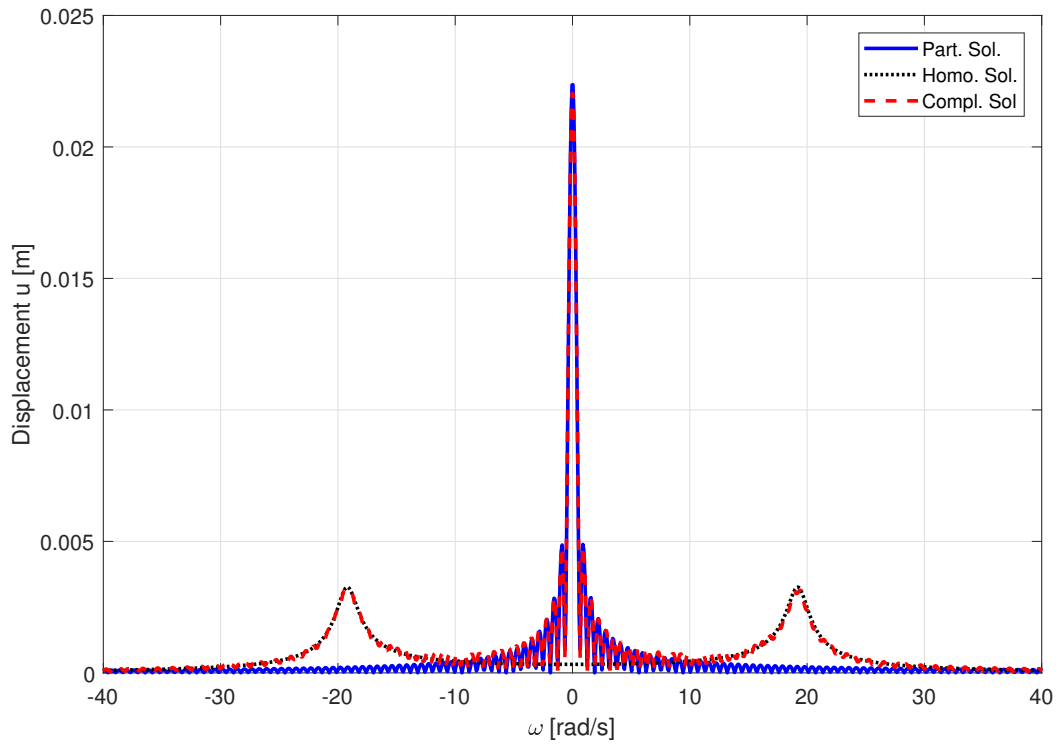


Fig. 2.22: Amplitude spectrum of response with nonperiodic load obtained in frequency domain.

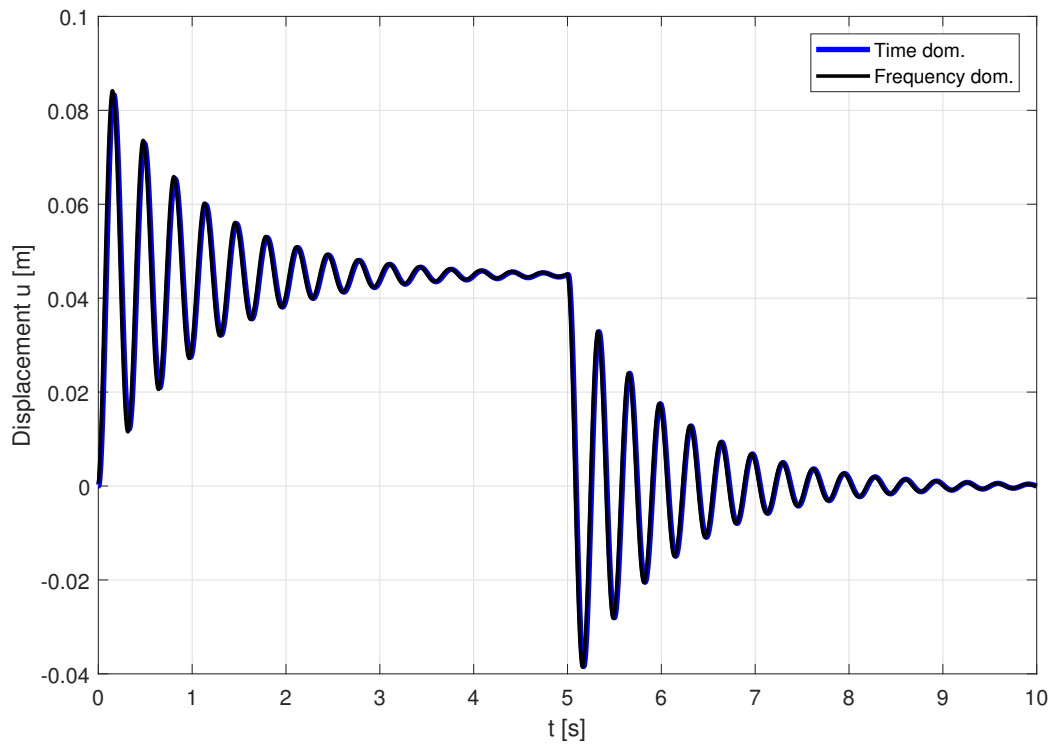


Fig. 2.23: Comparison of displacements due to nonperiodic load in the time and frequency domain.

2.4.5 Arbitrary excitation

The solution for the given load in Fig. 2.10(b) is shown in the figure below. As the load is only available at discrete time steps, a numerical treatment is required. The solution in the time domain was obtained by following the steps in Section 2.3.1 and the solution in the frequency domain with the methods shown in Section 2.3.2 and transformed into the time domain by an inverse fast Fourier transformation (IFFT). Note that the load was interpolated linearly between the given values in order to obtain function values at each time step n .

Fig. 2.24 shows the displacement obtained in both domains. The blue line shows the solution in the time domain, calculated with Newmark's method. The black line marks the displacement obtained in the frequency domain. The result is as expected, meaning that the displacement amplitudes are highest when the load reaches its maximum. The displacements converge to zero while the load is removed. There is little to no offset between the two lines. The amplitudes of displacement match very well. The amplitudes of displacement are very important for the design of a building. The phases also match nicely, which means the time change of displacements are nearly identical in both domains. Consequently, it can be stated that both methods yield similar outcomes.

Fig. 2.25 shows the relative difference $\epsilon = |(u_{\text{Newm}} - u_{\text{Freq}})|/|u_{\text{Newm}}|$ between the two calculations. The outliers can be explained by the fact that the displacement in this points have different signs which lead to a very high relative difference. This fact is considered less important as the displacements are very small at those values. The amplitude spectra is not shown for this test case.

2.4.6 Conclusions

As shown in the examples, both methods in the time and frequency domain yield very similar results. The computation effort is nearly identical when calculating the solutions analytically. Depending on the application, the relative differences vary. Considering the results of the previous examples, one may state that the frequency domain yields advantages over the time domain approach for harmonic and periodic loadings and non-periodic loads in closed form because algebraic equations need to be solved instead of integrating an equation [13, p. 34]. When it comes to arbitrary loadings (and numerical treatment in general), the time domain may be the better choice as the input needs to be altered in the frequency domain in order to obtain good results (zero-padding, windowing,...). In conclusion, it may be stated that both methods do have advantages and drawbacks over the other and the individual user needs to be careful what type of loading is present in the application. One disadvantage of the frequency domain is that one needs to chose the calculation time very carefully and pay close attention to alter the input to obtain an accurate result when carrying out calculations numerically. One major advantage of calculating in the frequency domain is that frequency depended properties can easily be considered. In case of frequency dependent properties Eq. 2.66 can be written as

$$F[u](\omega) = \frac{1}{-m\omega^2 + ic(\omega) + k(\omega)} \cdot F[f](\omega) = H(\omega) \cdot F[f](\omega), \quad (2.99)$$

where $k(\omega)$ and $c(\omega)$ can be depending on the frequency [8, p. 97]. Another advantage of the approach in the frequency domain is that the interpretation of results may be easier.

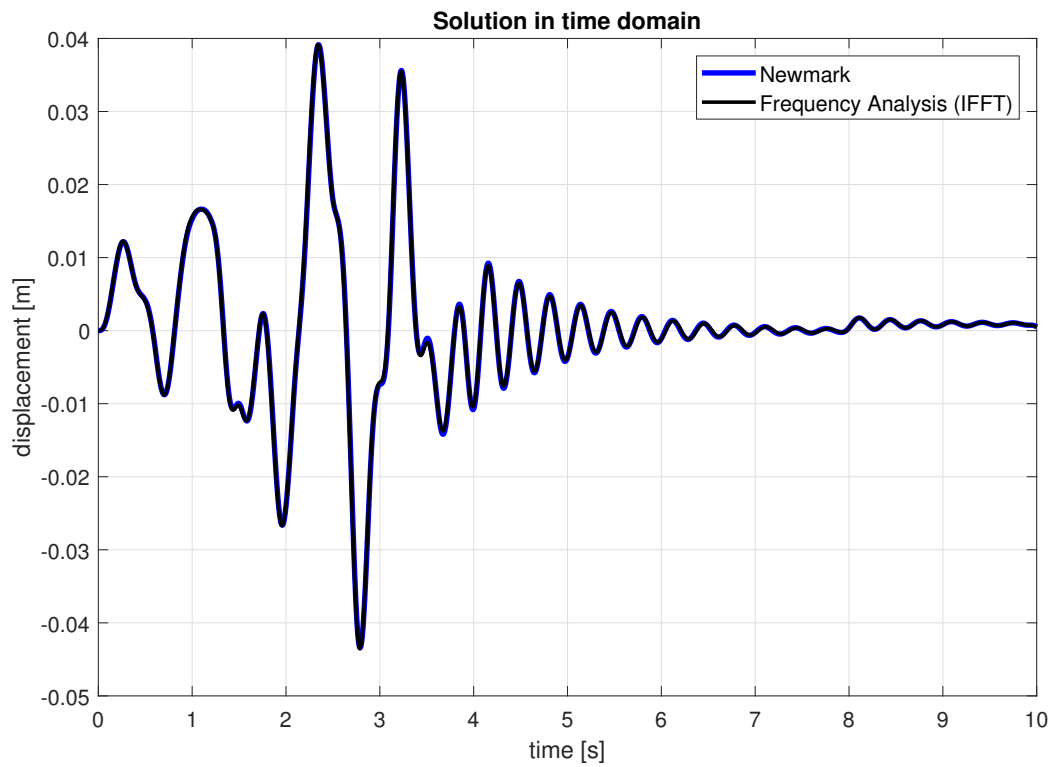


Fig. 2.24: Comparison of displacements due to arbitrary load in the time and frequency domain.

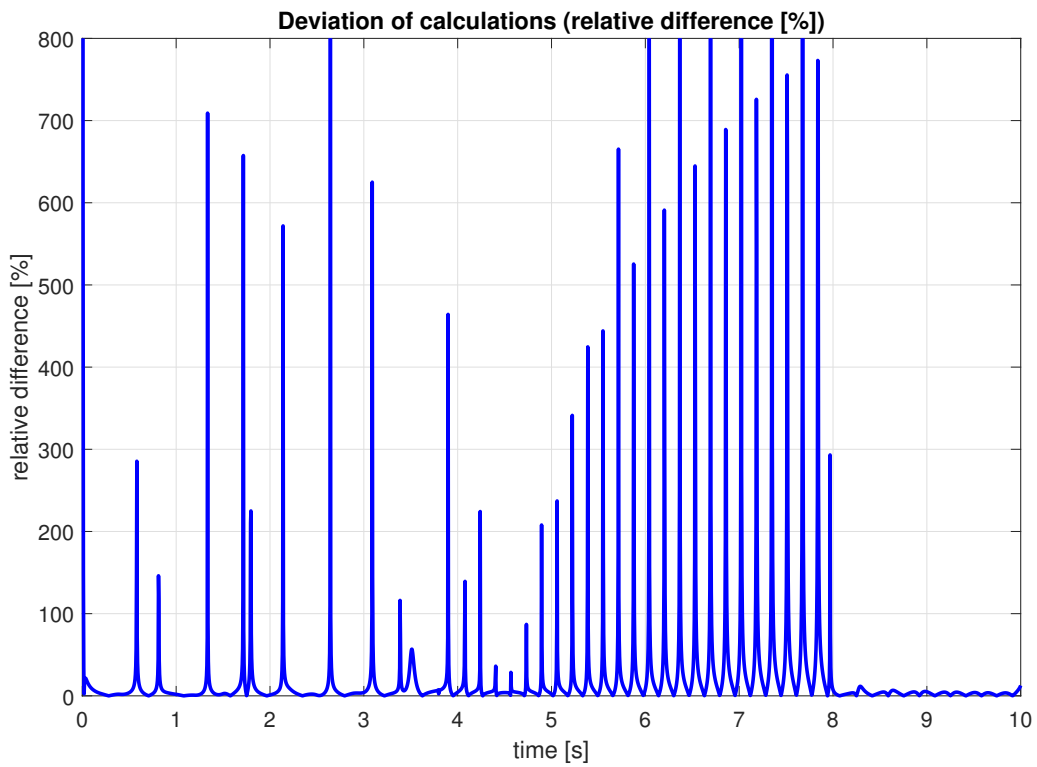


Fig. 2.25: Relative difference of displacements in the time and frequency domain.

3 Systems with multiple degrees of freedom (MDOF)

As already mentioned in the introduction, it is often not sufficient to describe an application with one single degree of freedom. Systems with many DOFs need similar techniques to be handled as SDOF systems, with appropriate adaptations. This chapter derives the EOM for MDOF systems and introduces methods to solve the EOM being a system of coupled equations.

3.1 The equation of motion

MDOF systems arise in many different applications. In some applications, the properties (mass, stiffness, damping) are concentrated at specific places within the domain, e.g., several masses interact through springs and/or dampers. Other applications have continuously distributed properties which, as a result of some discretization also result in MDOFs. We will see that both systems lead to formally equivalent EOMs.

3.1.1 Systems with discrete masses

This section is based on Clough [8, pp. 171-173]. The EOM of MDOF systems with discrete properties can be formulated by expressing the equilibrium of all effective forces associated with each of the degrees of freedom of the system [8, p. 171]. In other words, the sum of all effective reaction forces needs to be zero for each DOF. This is the same principle as for the SDOF case (compare Section 2.1). The arising sums of forces can be written as a set of equations in the following way

$$\begin{aligned} f_{S1}(t) + f_{D1}(t) + f_{I1}(t) - f_1(t) &= 0 \\ f_{S2}(t) + f_{D2}(t) + f_{I2}(t) - f_2(t) &= 0 \\ f_{S3}(t) + f_{D3}(t) + f_{I3}(t) - f_3(t) &= 0 \\ &\dots\dots\dots \end{aligned} \tag{3.1a}$$

or when the forces are written in vector form

$$\mathbf{f}_S(t) + \mathbf{f}_D(t) + \mathbf{f}_I(t) - \mathbf{f}(t) = 0, \tag{3.1b}$$

with the elastic force vector $\mathbf{f}_S(t)$, the damping force vector $\mathbf{f}_D(t)$, the inertia force vector $\mathbf{f}_I(t)$ and the vector of external loads $\mathbf{f}(t)$.

Eq. 3.1b is the MDOF-equivalent to the EOM of SDOF systems

$$f_S(t) + f_D(t) + f_I(t) - f(t) = 0. \tag{3.2}$$

Clough stats that expressing each of the forces in Eq. 3.1 by means of an appropriate set of influence coefficients is the most convenient way [8, p. 171]. The information behind these coefficients is how much each of the DOFs influence the force at one specific DOF. The calculation of the coefficients can be done by applying unit-properties (unit-displacements $u_j = 1$, unit-velocities $\dot{u}_j = 1$ and unit-accelerations $\ddot{u}_j = 1$) on each degree of freedom j and computing the response (reaction) forces at each degree of freedom i . The coefficients can be written as

$$k(c/m)_{ij} = \text{force corresponding to DOF } i \text{ due to an} \quad (3.3)$$

$$\text{unit displacement (velocity/acceleration) of DOF } j.$$

This leads to following matrix-vector-products.

Set of elastic force relationships obtained by applying unit displacements

$$\begin{Bmatrix} f_{S1} \\ f_{S2} \\ \cdot \\ f_{Si} \\ \cdot \end{Bmatrix} = \begin{bmatrix} k_{11} & k_{12} & \cdots & k_{1i} & \cdots & k_{1N} \\ k_{21} & k_{22} & \cdots & k_{2i} & \cdots & k_{2N} \\ \cdots & \cdots & \cdots & \cdots & \cdots & \cdots \\ k_{i1} & k_{i2} & \cdots & k_{ii} & \cdots & k_{iN} \\ \cdots & \cdots & \cdots & \cdots & \cdots & \cdots \end{bmatrix} \cdot \begin{Bmatrix} u_1 \\ u_2 \\ \cdot \\ u_i \\ \cdot \end{Bmatrix}. \quad (3.4a)$$

Set of damping forces obtained by applying unit velocities

$$\begin{Bmatrix} f_{D1} \\ f_{D2} \\ \cdot \\ f_{Di} \\ \cdot \end{Bmatrix} = \begin{bmatrix} c_{11} & c_{12} & \cdots & c_{1i} & \cdots & c_{1N} \\ c_{21} & c_{22} & \cdots & c_{2i} & \cdots & c_{2N} \\ \cdots & \cdots & \cdots & \cdots & \cdots & \cdots \\ c_{i1} & c_{i2} & \cdots & c_{ii} & \cdots & c_{iN} \\ \cdots & \cdots & \cdots & \cdots & \cdots & \cdots \end{bmatrix} \cdot \begin{Bmatrix} \dot{u}_1 \\ \dot{u}_2 \\ \cdot \\ \dot{u}_i \\ \cdot \end{Bmatrix}. \quad (3.4b)$$

Set of inertial forces obtained by applying unit accelerations

$$\begin{Bmatrix} f_{I1} \\ f_{I2} \\ \cdot \\ f_{Ii} \\ \cdot \end{Bmatrix} = \begin{bmatrix} m_{11} & m_{12} & \cdots & m_{1i} & \cdots & m_{1N} \\ m_{21} & m_{22} & \cdots & m_{2i} & \cdots & m_{2N} \\ \cdots & \cdots & \cdots & \cdots & \cdots & \cdots \\ m_{i1} & m_{i2} & \cdots & m_{ii} & \cdots & m_{iN} \\ \cdots & \cdots & \cdots & \cdots & \cdots & \cdots \end{bmatrix} \cdot \begin{Bmatrix} \ddot{u}_1 \\ \ddot{u}_2 \\ \cdot \\ \ddot{u}_i \\ \cdot \end{Bmatrix}. \quad (3.4c)$$

Inserting Eq. 3.4 in Eq. 3.1b gives the complete dynamic equilibrium of the structure

$$\mathbf{M} \cdot \ddot{\mathbf{u}}(t) + \mathbf{C} \cdot \dot{\mathbf{u}}(t) + \mathbf{K} \cdot \mathbf{u}(t) = \mathbf{f}(t) \quad (3.5)$$

Eq. 3.5 is a system of coupled differential equations of second order in time. Analogously to the SDOF case, initial conditions (ICs) are needed to obtain a unique solution. The ICs can be of the following form

$$\mathbf{u}(t = 0) = \mathbf{u}_0 \quad (3.6a)$$

$$\dot{\mathbf{u}}(t = 0) = \mathbf{v}(t = 0) = \mathbf{v}_0 \quad (3.6b)$$

Example

An example shall demonstrate this procedure (taken from the slides of Dr. Dünser [10]). The EOM for the two-story frame is sought. The geometry is shown in Fig. 3.1(left). It is assumed that the mass of the columns are zero and the columns as well as the ceilings can not change their length ($EA \rightarrow \infty$). The mass of the ceilings is concentrated in the middle and the flexural stiffness is infinitely high ($EI \rightarrow \infty$). The corners of the frame cannot rotate. Because of the above described properties the system is a two DOF system. The following figures (Fig. 3.1, Fig. 3.2, Fig. 3.3 and Fig. 3.4) show the application of the unit-properties and the calculation of the influence coefficients. The red arrows and values symbolizes the unit properties.

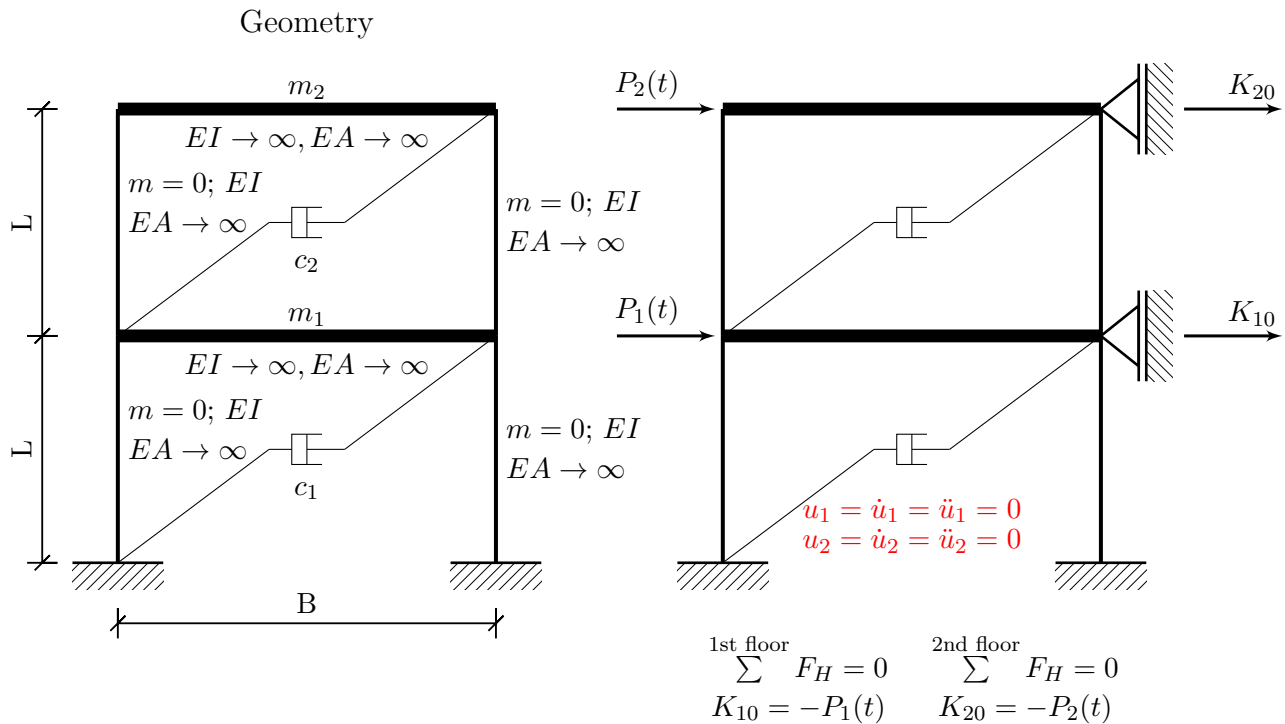


Fig. 3.1: (left) Geometry and (right) force coefficients of example frame.

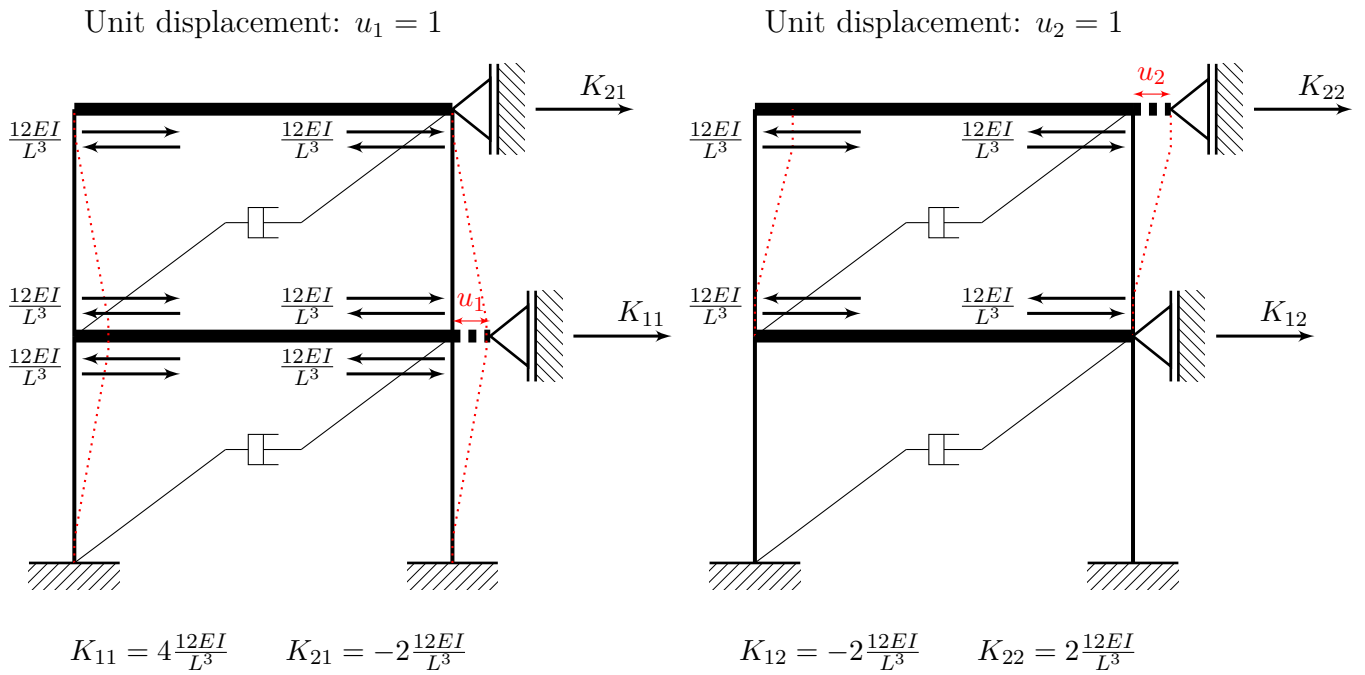


Fig. 3.2: Stiffness coefficients of example frame.

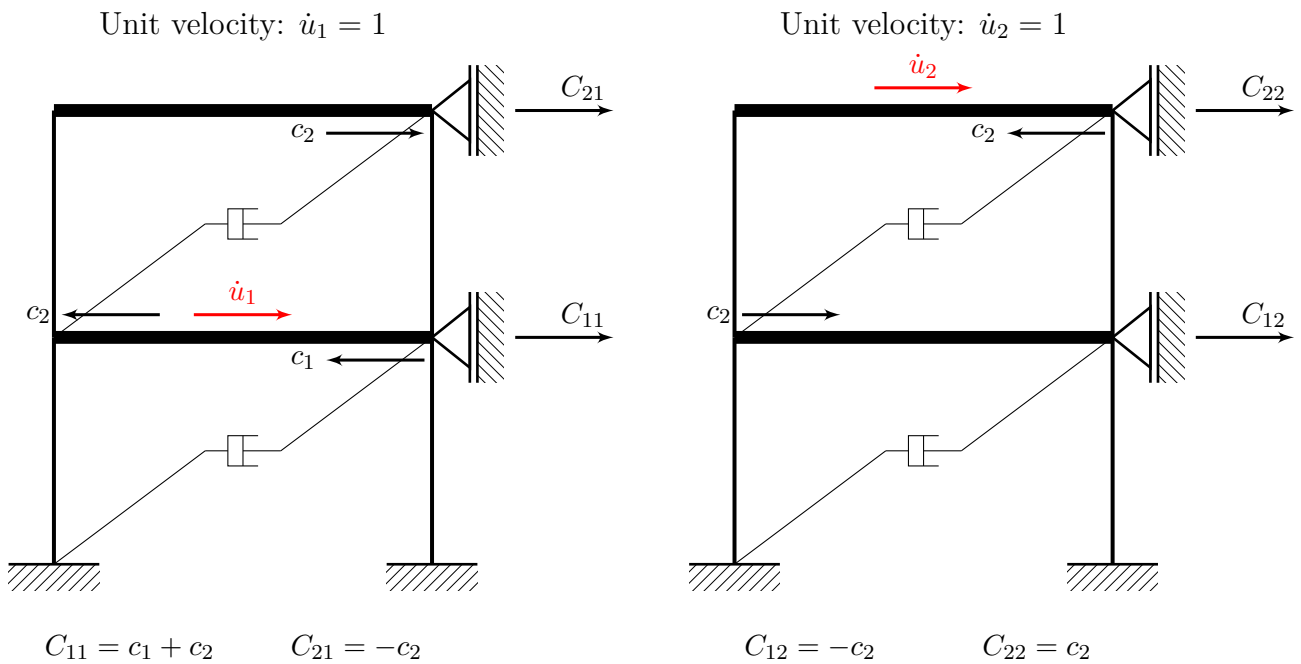


Fig. 3.3: Damping coefficients of example frame.

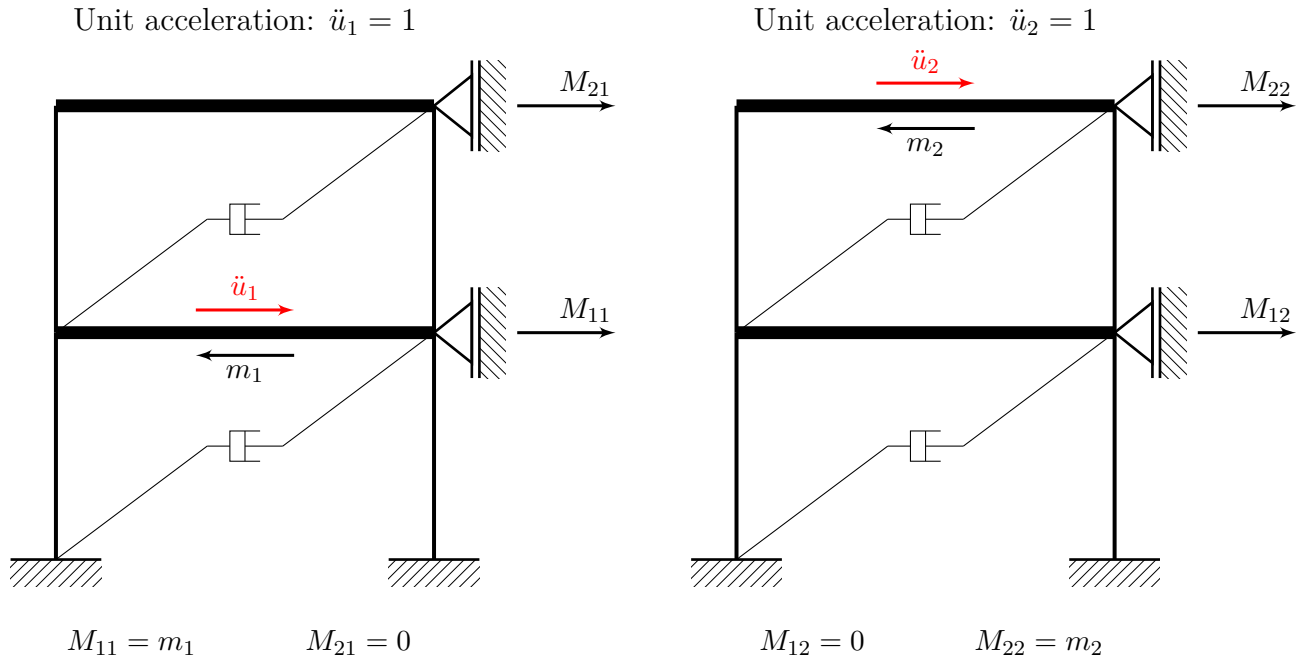


Fig. 3.4: Inertia coefficients of example frame.

For equilibrium, all support forces of all response states need to vanish, in other words the sum of forces of each DOF needs to be zero. The equilibrium for each degree of freedom needs to be fulfilled and can be written as

$$\sum_{\text{first floor}} F_x = 0 : M_{11}\ddot{u}_1 + M_{12}\ddot{u}_2 + C_{11}\dot{u}_1 + C_{12}\dot{u}_2 + K_{11}u_1 + K_{12}u_2 + K_{10} \quad (3.7a)$$

$$\sum_{\text{second floor}} F_x = 0 : M_{21}\ddot{u}_1 + M_{22}\ddot{u}_2 + C_{21}\dot{u}_1 + C_{22}\dot{u}_2 + K_{21}u_1 + K_{22}u_2 + K_{20} \quad (3.7b)$$

Rewriting the equations in matrix-vector notation yields

$$\begin{bmatrix} M_{11} & M_{12} \\ M_{21} & M_{22} \end{bmatrix} \cdot \begin{Bmatrix} \ddot{u}_1 \\ \ddot{u}_2 \end{Bmatrix} + \begin{bmatrix} C_{11} & C_{12} \\ C_{21} & C_{22} \end{bmatrix} \cdot \begin{Bmatrix} \dot{u}_1 \\ \dot{u}_2 \end{Bmatrix} + \begin{bmatrix} K_{11} & K_{12} \\ K_{21} & K_{22} \end{bmatrix} \cdot \begin{Bmatrix} u_1 \\ u_2 \end{Bmatrix} + \begin{Bmatrix} K_{10} \\ K_{20} \end{Bmatrix} = 0. \quad (3.7c)$$

The procedure of obtaining the EOM for a simplified two story frame is therefore shown.

3.1.2 Systems with distributed properties (FEM-systems)

In many applications, the properties of a system are not available at discrete spatial points but rather distributed continuously over the domain. In this section the EOM is derived and later discretised with the Finite Element Method. The derivation is done with respect to systems where only small displacements and small strains occur. In linear elasticity, no distinction between Lagrangian¹ and Eulerian² framework needs to be done [2, p. 307]. In the following all quantities of the domain are given with respect to the spatial position vector \mathbf{x} [2, p. 307].

Strong form

Later on, the discrete weak form of the initial boundary value problem (IBVP) is needed wherefore the strong form is given as a starting point here. According to [2, pp. 307-308] the strong form of the elastodynamics is given as

$$\nabla \cdot \boldsymbol{\sigma} + \underbrace{\rho \mathbf{k}}_{:=\mathbf{f}} = \rho \ddot{\mathbf{u}} \quad \text{with} \quad \boldsymbol{\sigma} = \boldsymbol{\sigma}^T \quad \text{on} \quad \Omega_S \times (0, T) \quad (3.8)$$

There, ρ is the density of the solid, \mathbf{f} the volume force vector, Ω_S the structural domain and T the calculation time.

The linearised constitution law (Hooke's law) is given as

$$\boldsymbol{\sigma} = \lambda(\boldsymbol{\varepsilon} : \mathbf{I})\mathbf{I} + 2\mu\boldsymbol{\varepsilon} = 2G \left(\frac{\nu}{1-2\nu}(\boldsymbol{\varepsilon} : \mathbf{I})\mathbf{I} + \boldsymbol{\varepsilon} \right), \quad (3.9)$$

and the linear strain-displacement relation as

$$\boldsymbol{\varepsilon} = \frac{1}{2} [\nabla \mathbf{u} + (\nabla \mathbf{u})^T]. \quad (3.10)$$

\mathbf{I} describes the unity tensor. The material parameters are defined as

$$\nu = \frac{\lambda}{2(\lambda + \mu)}, \quad E = \frac{\mu(3\lambda + 2\mu)}{\lambda + \mu}, \quad G = \mu. \quad (3.11)$$

The Lamé constants λ and μ are defined as (reformulation of Eq. 3.11)

$$\lambda = \frac{E\nu}{(1+\nu)(1-2\nu)}, \quad \mu = \frac{E}{2(1+\nu)}, \quad (3.12)$$

with Young's modulus E and Poisson's ratio ν .

¹In the Lagrangian framework, the observer sits on a particle which moves in space and time [2, p. 76].

²In the Eulerian framework, the observer stays fixed at one point in space and observes the movement of particles [2, p. 76].

Weak form

The weak form, or to be more precise the discrete weak form is necessary when using the Finite Element Method (FEM). For readers not familiar with the FEM it is recommended to look at the example in [18, 78ff]. Further reading on the FEM is given, e.g., in Hughes [17]. The derivation is made with respect to the lecture slides of Prof. Fries³ [12].

The strong form of the initial boundary problem is:

Given the information in the equations below, find \mathbf{u} , such that

$$\rho \ddot{\mathbf{u}}(\mathbf{x}, t) = \nabla \cdot \boldsymbol{\sigma} + \mathbf{f} \quad \text{on } \Omega_S \times (0, T) \quad (3.13a)$$

$$\mathbf{u}(\mathbf{x}, t) = \mathbf{u}_{\Gamma_D}(t) \quad \text{on } \Gamma_D \times (0, T) \quad (3.13b)$$

$$\boldsymbol{\sigma} \cdot \mathbf{n} = \mathbf{f}_{\Gamma_N}(t) \quad \text{on } \Gamma_N \times (0, T) \quad (3.13c)$$

$$\mathbf{u}(\mathbf{x}, t = 0) = \mathbf{u}_0(\mathbf{x}) \quad \mathbf{x} \in \Omega_S \quad (3.13d)$$

$$\dot{\mathbf{u}}(\mathbf{x}, t = 0) = \dot{\mathbf{u}}_0(\mathbf{x}) \quad \mathbf{x} \in \Omega_S \quad (3.13e)$$

holds. Γ_D denotes the part of the boundary of the domain where Dirichlet (or kinematic) BCs are prescribed, Γ_N denotes the part of the boundary where Neumann (or traction) BCs are prescribed. \mathbf{n} is the normal vector to the boundary of Ω_S . Eq. 3.13a is a second order initial value problem in time (and space) therefore the initial conditions \mathbf{u}_0 and $\dot{\mathbf{u}}_0$ are needed as well.

To obtain the continuous weak form it is necessary to multiply Eq. 3.8 with a test function vector \mathbf{w} , integrate over the whole domain Ω_S and apply the divergence theorem. The continuous weak form can be then written as: Given \mathbf{f} , $\mathbf{u}_{\Gamma_D}(t)$, $\mathbf{f}_{\Gamma_N}(t)$, \mathbf{u}_0 and $\dot{\mathbf{u}}_0$, find $\mathbf{u}(t) \in \mathcal{S}_t$, $t \in (0, T)$, such that for all $\mathbf{w} \in \mathcal{V}$

$$\int_{\Omega_S} \rho \mathbf{w} \cdot \ddot{\mathbf{u}} \, d\Omega + \int_{\Omega_S} \nabla \mathbf{w} : \boldsymbol{\sigma} \, d\Omega = \int_{\Omega_S} \mathbf{w} \cdot \mathbf{f} \, d\Omega + \int_{\Gamma} \mathbf{w} \cdot \hat{\mathbf{t}} \, d\Gamma \quad (3.14)$$

holds. $\hat{\mathbf{t}}$ is the traction along the Neumann boundary Γ_N .

It is essential to *discretize* the nodal displacements \mathbf{u} and the test function \mathbf{w} using the Ansätze

$$\mathbf{u} \approx \mathbf{u}^h = \sum_i N_i u_i = \mathbf{N}^T \cdot \mathbf{u} \quad (3.15a)$$

$$\mathbf{w} \approx \mathbf{w}^h = \sum_i N_i w_i = \mathbf{N}^T \cdot \mathbf{w} \quad (3.15b)$$

With these approximations, it is possible to find one solution for \mathbf{u}^h with \mathbf{w}^h . Inserting Eq. 3.15 into Eq. 3.14 gives the discrete weak form needed to find a solution with the FEM: Given \mathbf{f} , $\mathbf{u}_{\Gamma_D}(t)$, $\mathbf{f}_{\Gamma_N}(t)$, \mathbf{u}_0 and $\dot{\mathbf{u}}_0$, find $\mathbf{u}^h(t) \in \mathcal{S}_t^h$, such that for all $\mathbf{w}^h \in \mathcal{V}^h$

$$\int_{\Omega_S} \rho \mathbf{w}^h \cdot \ddot{\mathbf{u}}^h \, d\Omega + \int_{\Omega_S} \nabla \mathbf{w}^h : \boldsymbol{\sigma} \, d\Omega = \int_{\Omega_S} \mathbf{w}^h \cdot \mathbf{f} \, d\Omega + \int_{\Gamma} \mathbf{w}^h \cdot \hat{\mathbf{t}}^h \, d\Gamma \quad (3.16)$$

holds. The spatial discretisation of Eq. 3.8 with the help of FEM gives a semi-discrete system of equations of the form equivalent to Eq. 3.5.

$$\mathbf{M} \cdot \ddot{\mathbf{u}}(t) + \mathbf{C} \cdot \dot{\mathbf{u}}(t) + \mathbf{K} \cdot \mathbf{u}(t) = \mathbf{f}(t) \quad (3.17)$$

³The lectures Finite Element Method I and II are taught by Prof. T.-P. Fries at TU Graz in 2020. The lecture slides and notes are only published for students enrolled in this course but not for the general public [12]

where \mathbf{M} is the mass matrix, \mathbf{K} the stiffness matrix and \mathbf{C} the damping matrix. It is thus confirmed that formally this EOM coincides with MDOF systems as described in the previous section. \mathbf{M} and \mathbf{K} are calculated as below. A short comment to the damping matrix \mathbf{C} is given in the subsection **Damping**.

The terms in Eq. 3.17 are calculated as shown below in case of a 2D setting

$$\mathbf{K} = \sum_{i=1}^{n_{\text{Elem}}} \begin{bmatrix} \int_{\Omega_i} (\lambda + 2\mu) \mathbf{N}_{,x} \mathbf{N}_{,x}^T + \mu \mathbf{N}_{,y} \mathbf{N}_{,y}^T \, d\Omega_i & \int_{\Omega_i} \lambda \mathbf{N}_{,x} \mathbf{N}_{,y}^T + \mu \mathbf{N}_{,y} \mathbf{N}_{,x}^T \, d\Omega_i \\ \int_{\Omega_i} \lambda \mathbf{N}_{,y} \mathbf{N}_{,x}^T + \mu \mathbf{N}_{,x} \mathbf{N}_{,y}^T \, d\Omega_i & \int_{\Omega_i} (\lambda + 2\mu) \mathbf{N}_{,y} \mathbf{N}_{,y}^T + \mu \mathbf{N}_{,x} \mathbf{N}_{,x}^T \, d\Omega_i \end{bmatrix} \quad (3.18a)$$

$$\mathbf{M} = \sum_{i=1}^{n_{\text{Elem}}} \int_{\Omega_i} \rho \mathbf{N} \mathbf{N}^T \, d\Omega_i \quad (3.18b)$$

$$\mathbf{f} = \sum_{i=1}^{n_{\text{Elem}}} \begin{bmatrix} \int_{\Omega_i} \mathbf{N} f_x \, d\Omega_i + \int_{\Gamma_i} \mathbf{N} \hat{t}_x \, d\Gamma_i \\ \int_{\Omega_i} \mathbf{N} f_y \, d\Omega_i + \int_{\Gamma_i} \mathbf{N} \hat{t}_y \, d\Gamma_i \end{bmatrix} \quad (3.18c)$$

where $N_{,j}$ denotes the partial derivative of N in j -direction $N_{,j} = \frac{\partial N}{\partial j}$ with $j = x, y$. The matrices \mathbf{K} and \mathbf{M} are sparsely filled⁴ due to the use of shape functions N provided by the finite elements and featuring local supports. The Ansatz functions fulfil the Kronecker-Delta property, which means the shape functions are zero at all nodes except for the one function belonging to that node (which is 1 there) [18, p. 255].

In the next chapters the EOM is solved in the time and frequency domain.

Damping

Damping in a structure reduces the amplitudes of a motion over time. This happens because energy dissipates through internal and external mechanisms [25, p. 101]. Damping properties are difficult to specify and have to be extracted from tests or chosen with respect to similar structures [7, p. 453]. Various different models were introduced over the years, the most commonly and convenient one is the Rayleigh damping⁵.

The Rayleigh damping (also called "proportional viscous damping" [8, p. 234] or "classical damping" [7, p. 456]) is proportional to a combination of the mass and the stiffness of the system [8, p. 235] where the mass-proportional part can be interpreted as damping due to air resistance and the stiffness-proportional part as damping due to internal friction by deformation of the structure [7, p. 455].

The Rayleigh damping is defined as

$$\mathbf{C} = a_0 \mathbf{M} + a_1 \mathbf{K}. \quad (3.19)$$

The Rayleigh damping allows the definition of two damping ratios at two frequency values. Switching to index notation and with the relations $c_n = 2\omega_n m_n \zeta_n = a_0 m_n = a_1 k_n$ and $k_n = \omega_n^2 m_n$, the damping ratio ζ_n can be expressed as

$$\zeta_n = \frac{a_0}{2\omega_n} + \frac{a_1 \omega_n}{2}. \quad (3.20)$$

It can be seen that the mass-proportional damping is linearly dependent on the frequency while the stiffness-proportional damping is inversely proportional to the frequency.

The two Rayleigh damping factors a_0 and a_1 can be evaluated by inserting two specific frequencies

⁴Sparsely filled means that only the main diagonal and few off diagonals have entries $\neq 0$.

⁵Named after John Strutt, third baron Rayleigh who was an English physician.

(modes) and two damping ratios in Eq. 3.20. Written in matrix notation the system of equation becomes

$$\begin{Bmatrix} \zeta_m \\ \zeta_n \end{Bmatrix} = \frac{1}{2} \begin{bmatrix} 1/\omega_m & \omega_m \\ 1/\omega_n & \omega_n \end{bmatrix} \begin{Bmatrix} a_0 \\ a_1 \end{Bmatrix}. \quad (3.21a)$$

The solutions are given as

$$\begin{Bmatrix} a_0 \\ a_1 \end{Bmatrix} = 2 \frac{\omega_m \omega_n}{\omega_n^2 - \omega_m^2} \begin{bmatrix} \omega_n & -\omega_m \\ -1/\omega_n & 1/\omega_m \end{bmatrix} \begin{Bmatrix} \zeta_m \\ \zeta_n \end{Bmatrix}. \quad (3.21b)$$

Usually, the two damping ratios are chosen the same, i.e., $\zeta_m = \zeta_n = \zeta$ [8, p. 236] and Eq. 3.21b simplifies to

$$\begin{Bmatrix} a_0 \\ a_1 \end{Bmatrix} = \frac{2\zeta}{\omega_n + \omega_m} \begin{Bmatrix} \omega_m \omega_n \\ 1 \end{Bmatrix}. \quad (3.22)$$

It is recommended to chose ω_m as the fundamental frequency (frequency belonging to the first mode \equiv smallest eigenfrequency [7, p. 408]) of the system and ω_n to be set among higher frequencies [8, p. 236]. The reason behind this statement is that good damping properties should be achieved in the range of frequency which is of interest for the calculation. Fig. 3.5 shows the relationship between the damping ratio and frequency for Rayleigh damping. The figure is slightly modified and taken from [8, p. 235].

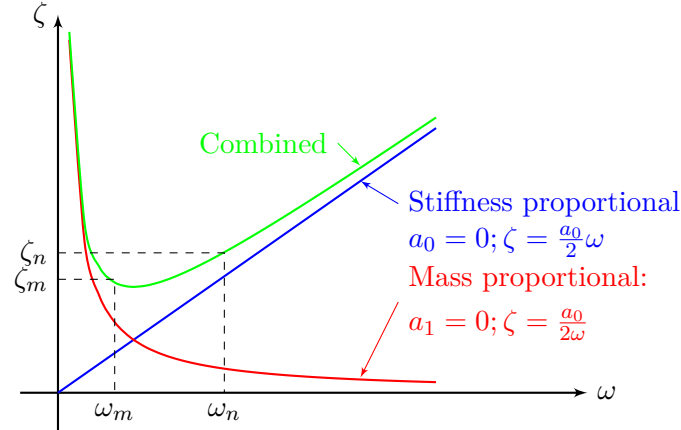


Fig. 3.5: Relationship between damping ratio and frequency.

A very positive aspect of the Rayleigh damping is, next to the fact that very good damping properties are achieved, that the viscous damping allows a full decoupling of the system of equation (see Chapter 4 for further explanation). In the following, two other damping models are described in order to give the reader a better overview.

The **Extended Rayleigh Damping** allows to specify damping ratios at more than 2 frequencies [8, p. 237] and therefore improves the damping properties at those frequency values. The damping matrix can be written as

$$\mathbf{C}_n = \sum_b a_b \omega_n^{2b} \mathbf{M}_n. \quad (3.23)$$

The coefficients a_b can be obtained by choosing ζ_n and ω_n and solving the following system of equations

$$\zeta_n = \frac{1}{2\omega_n} \sum_b a_b \omega_n^{2b}. \quad (3.24)$$

Another possible way to consider damping is the **complex-stiffness damping**. It has advantages over the linear viscous damping as the energy loss per cycle at a fixed displacement amplitude is independent of the response frequency [8, p. 230]. The damping is defined as

$$\hat{\mathbf{K}}_n = \mathbf{K}_n [1 + 2i\zeta_n]. \quad (3.25)$$

ζ_n is chosen with respect to the material of the structure in any of the presented cases. A small excerpt can be found in Tab. 2.1. In this thesis, only the **Rayleigh damping** is used.

3.2 Numerical solution of the EOM

Large systems of equation are very time consuming or may quickly become impossible to solve analytically. Therefore numerical procedures are typically preferred. In the following, procedures are introduced in both, the time and frequency domain.

3.2.1 Solving in the time domain

In this work, Newmark's method is used to solve the EOM numerically in the time domain. The procedure introduced in Section 2.3.1 is straightforwardly extended to systems of equations [7, p. 676]. In equivalence to the SDOF case, the consideration of initial conditions is possible [7, p. 674]. The most important equations are given in the following.

The EOM of Eq. 3.5 is discretised at time step t_{n+1}

$$\mathbf{K} \cdot \mathbf{u}_{n+1} + \mathbf{C} \cdot \dot{\mathbf{u}}_{n+1} + \mathbf{M} \cdot \ddot{\mathbf{u}}_{n+1} = \mathbf{f}_{n+1}. \quad (3.26)$$

The special differences outlined in Eq. 2.58 are extended to vectors

$$\mathbf{u}_{n+1} \approx \mathbf{u}_n + \Delta t \cdot \dot{\mathbf{u}}_n + [(1/2 - \beta)\ddot{\mathbf{u}}_n + \beta \cdot \ddot{\mathbf{u}}_{n+1}] \cdot \Delta t^2 \quad (3.27a)$$

$$\dot{\mathbf{u}}_{n+1} \approx \dot{\mathbf{u}}_n + [(1 - \gamma)\ddot{\mathbf{u}}_n + \gamma \cdot \ddot{\mathbf{u}}_{n+1}] \cdot \Delta t \quad (3.27b)$$

and are inserted in Eq. 3.26. The equilibrium at time t_{n+1} is

$$\begin{aligned} & (\mathbf{M} + \gamma\Delta t \cdot \mathbf{C} + \beta\Delta t^2 \cdot \mathbf{K}) \cdot \ddot{\mathbf{u}}_{n+1} = \\ & \mathbf{f}_{n+1} - \mathbf{C} \cdot (\dot{\mathbf{u}}_n + (1 - \gamma)\Delta t \cdot \ddot{\mathbf{u}}_n) - \mathbf{K} \cdot (\mathbf{u}_n + \Delta t \cdot \dot{\mathbf{u}}_n + (1/2 - \beta)\Delta t^2 \cdot \ddot{\mathbf{u}}_n). \end{aligned} \quad (3.28)$$

All quantities are known except the acceleration $\ddot{\mathbf{u}}_{n+1}$ at time t_{n+1} and the initial acceleration $\ddot{\mathbf{u}}_0$ for the first time step. The initial acceleration is a vector in case of a MDOF system and achieved by evaluating the EOM at time $t = 0$

$$\ddot{\mathbf{u}}_0 = \frac{1}{\mathbf{M}} (\mathbf{f}_0 - \mathbf{C} \cdot \dot{\mathbf{u}}_0 - \mathbf{K} \cdot \mathbf{u}_0). \quad (3.29)$$

In some applications displacements are of major importance. In order to get these, the reformulated differences (see Eq. 2.58 for SDOF systems) are inserted in Eq. 3.26 and the displacement at time t_{n+1} can be calculated directly

$$\mathbf{f}_{n+1} + \mathbf{M} \cdot (a_0 \mathbf{u}_n + a_2 \dot{\mathbf{u}}_n + a_3 \ddot{\mathbf{u}}_n) + \mathbf{C} \cdot (a_1 \mathbf{u}_n - a_4 \dot{\mathbf{u}}_n - a_5 \ddot{\mathbf{u}}_n), \quad (a_0 \mathbf{M} + a_1 \mathbf{C} + \mathbf{K}) \cdot \mathbf{u}_{n+1} = \quad (3.30)$$

with the constants a_i from Eq. 2.62.

It can be seen that for every time step, a matrix needs to be inverted. This can become very expensive and can be circumvented for linear time invariant systems (LTI-systems). For these systems the properties (mass, stiffness and damping) do not change over time and the matrix only needs to be inverted once. Improvement of calculation time can be achieved by LU-decomposition⁶ of the matrix.

3.2.2 Solving in the frequency domain

The goal of this section is to solve the EOM for MDOF systems in the frequency domain. The approach is taken from [21, pp. 8-10]. With this approach one needs to keep in mind that the initial conditions from Eq. 3.6 are assumed zero [20, p. 57]. In equivalence to the SDOF case, the consideration of pseudo-forces would make the consideration of ICs possible. The EOM was derived in Section 3.1 and is of following form

$$\mathbf{M} \cdot \ddot{\mathbf{u}}(t) + \mathbf{C} \cdot \dot{\mathbf{u}}(t) + \mathbf{K} \cdot \mathbf{u}(t) = \mathbf{f}(t), \quad (3.31)$$

where \mathbf{M} , \mathbf{K} and \mathbf{C} are matrices and \mathbf{u} , \mathbf{f} are vectors. The Fourier transform is applied on both sides of the EOM and gives

$$\mathbf{M} \cdot F[\ddot{\mathbf{u}}](\omega) + \mathbf{C} \cdot F[\dot{\mathbf{u}}](\omega) + \mathbf{K} \cdot F[\mathbf{u}](\omega) = F[\mathbf{f}](\omega). \quad (3.32)$$

With property Eq. 1.29 the equation becomes

$$\mathbf{M} \cdot (i\omega)^2 \cdot F[\mathbf{u}](\omega) + \mathbf{C} \cdot (i\omega) \cdot F[\mathbf{u}](\omega) + \mathbf{K} \cdot F[\mathbf{u}](\omega) = F[\mathbf{f}](\omega). \quad (3.33)$$

Factoring out $F[\mathbf{u}](\omega)$ gives

$$F[\mathbf{u}](\omega) \cdot (-\mathbf{M} \cdot \omega^2 + i\mathbf{C}\omega + \mathbf{K}) = F[\mathbf{f}](\omega). \quad (3.34)$$

The solution in the frequency domain is written as a multiplication

$$F[\mathbf{u}](\omega) = \mathbf{H}(\omega) \cdot F[\mathbf{f}](\omega), \quad (3.35)$$

with

$$\mathbf{H}(\omega) = (-\mathbf{M} \cdot \omega^2 + i\mathbf{C}\omega + \mathbf{K})^{-1}, \quad (3.36)$$

with $F[\mathbf{u}](\omega)$ being the Fourier transformed unknown displacements and $F[\mathbf{f}](\omega)$ being the Fourier transformed load and $\mathbf{H}(\omega)$ the frequency response function. This equation is handled numerically by means of the fast Fourier transformation. The calculation time of large systems with many DOFs can be very high because the frequency response function needs to be evaluated and inverted for every single discrete frequency value [13, p. 174]. The scheme is identical to Fig. 2.5. Note that every entry of the load vector $\mathbf{f}(t)$ needs to be transformed with an FFT.

⁶LU-decomposition was invented by the Polish mathematician Tadeusz Banachiewicz and decomposes the matrix \mathbf{A} in two triangular matrices in order to solve systems of linear equations, invert \mathbf{A} or compute $\det \mathbf{A}$.

3.3 Example

Two very typical structures are considered to demonstrate the similarities of both calculation procedures. The structures are chosen as nearly every civil engineer has to deal with in his/her life. The first example is a cantilever beam typically found in balcony structures. The second structure is a multi-story frame which schematically represents a high rise building.

3.3.1 Example 1 - Cantilever beam

In this section a 20 meter long cantilever beam is observed. The beam is excited with a load on the right end. It is assumed that the dead load is applied suddenly leading to a further excitation of the structure. The load on the right end is released after half of the calculation time. Fig. 3.6 shows the geometrical configuration of the beam. The special node at \mathbf{x}_{SN} is a reference point in the upper right corner used to show results of the calculations. The system is at rest at time $t = 0$.

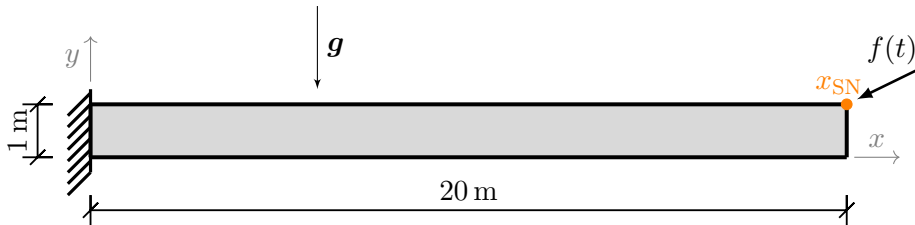


Fig. 3.6: Geometrical configuration of the cantilever beam.

The parameters of the example are listed below:

- Density of material $\rho = 7850 \text{ kg/m}^3$
- Gravity constant $\mathbf{g} = 9.81 \text{ m/s}^2$
- Young's modulus $E = 210\,000\,000 \text{ kN/m}^2$
- Poisson's ratio $\nu = 0.3 [-]$
- Lamé's parameter λ is used for thick plates, given as

$$\lambda = \frac{E \cdot \nu}{(1 + \nu)(1 - 2\nu)} \quad (3.37)$$

- Rayleigh damping with $\zeta = 0.05 [-]$
- Loading
 - Dead load $\rho \cdot \mathbf{g}$
 - Single force on right end acting the first half of calculation $f_x = -2000 \text{ kN}$, $f_y = -500 \text{ kN}$
- Initial conditions
 - Displacement $\mathbf{u}_0 = \mathbf{0}$

- Velocity $\dot{\mathbf{u}}_0 = \mathbf{0}$
- Time discretization done using Newmark's method
 - Length of calculation $t = 5$ sec
 - Time step size $\Delta t = 0.005$ sec
 - Number of time steps $N = 1000$
 - Nyquist frequency $f_c = 100 / \text{sec} \rightarrow \omega_c = f_c \cdot 2\pi = 628$ rad/sec
- Spatial discretization done using the FEM with $5 \times 50 = 250$ quadratic Lagrangian elements
- The input (load) is zero-padded for the FFT calculation; $2N$ zeros are added.

The cantilever beam is discretized with 250 quadratic Lagrangian elements. Fig. 3.7 shows the mesh (yellow), highlighting the nodes on the Dirichlet (blue) and Neumann (red) boundary.

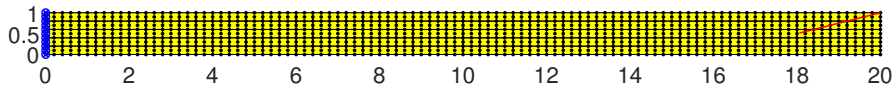


Fig. 3.7: Mesh and boundary conditions of the cantilever beam.

The following figures show the horizontal and vertical displacements of the special node at \mathbf{x}_{SN} . Fig. 3.8 shows the horizontal displacements in the time domain and Fig. 3.10 the vertical displacements. The *relative* differences are plotted in Fig. 3.9 as well as in Fig. 3.11.

Tab. 3.1 summarizes the most important comparisons.

Tab. 3.1: Comparison of the calculation in time and frequency domain - Cantilever beam.

	Time domain	Frequency domain
Calculation time [s]	3	116
max. hor. displacement [m]	0.0086	0.0086
time of max. hor. displ. [s]	0.2252	0.2202
min. ver. displacement [m]	-0.2580	-0.2580
time of min. ver. displ. [s]	0.2252	0.2202

Taking the figures and the table into consideration, it can be seen that the results match very well. The maximas and minimas of the amplitudes are nearly equal. The phases are only slightly shifted. The peaks in the relative difference plot (Fig. 3.9) can be explained that the displacements have different signs and are close to zero from time to time and thus may give a huge *relative* differences. The displacement fields behave as expected. The system oscillates around the static solution and is coming to rest at the static solution. Once the load is released, the system oscillates around the static deformation due to dead load and comes to rest right there after a while. The computation times are very different. The calculation with the frequency analysis takes nearly 40 times longer than the calculation in the time domain⁷. The reason is the high effort for obtaining the frequency response function \mathbf{H} at every discrete frequency value.

⁷The calculations were done on a commercially available laptop, but the absolute times are not of interest, rather the *relative* computation times.

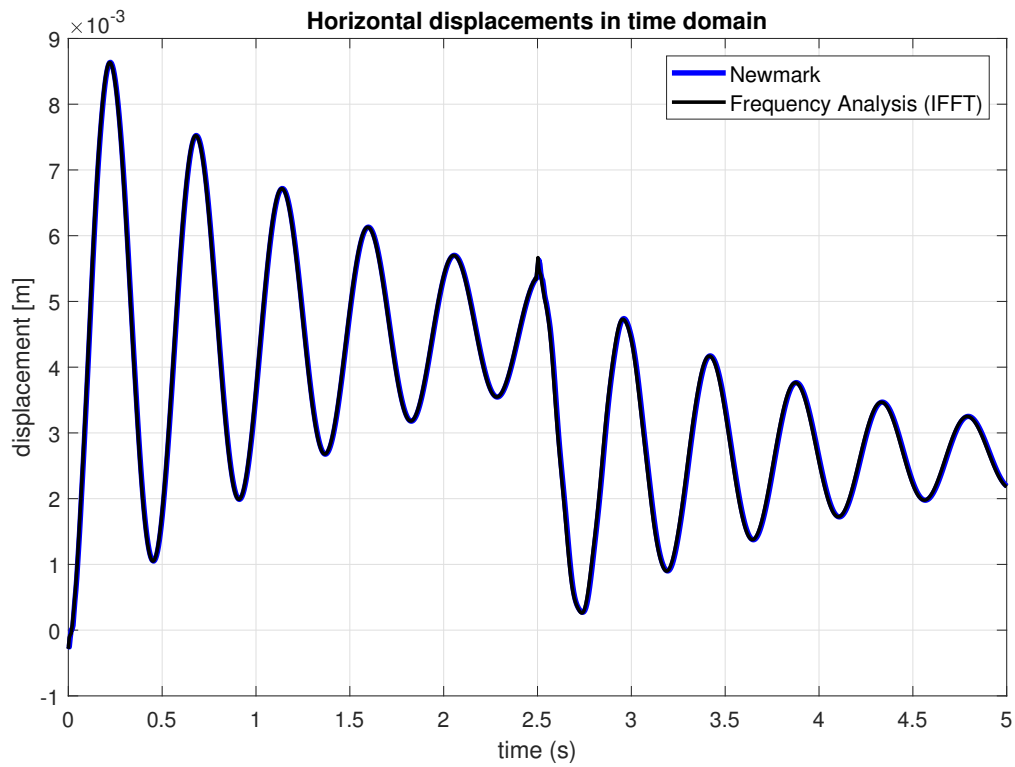


Fig. 3.8: Comparison of the horizontal displacement in the time domain.

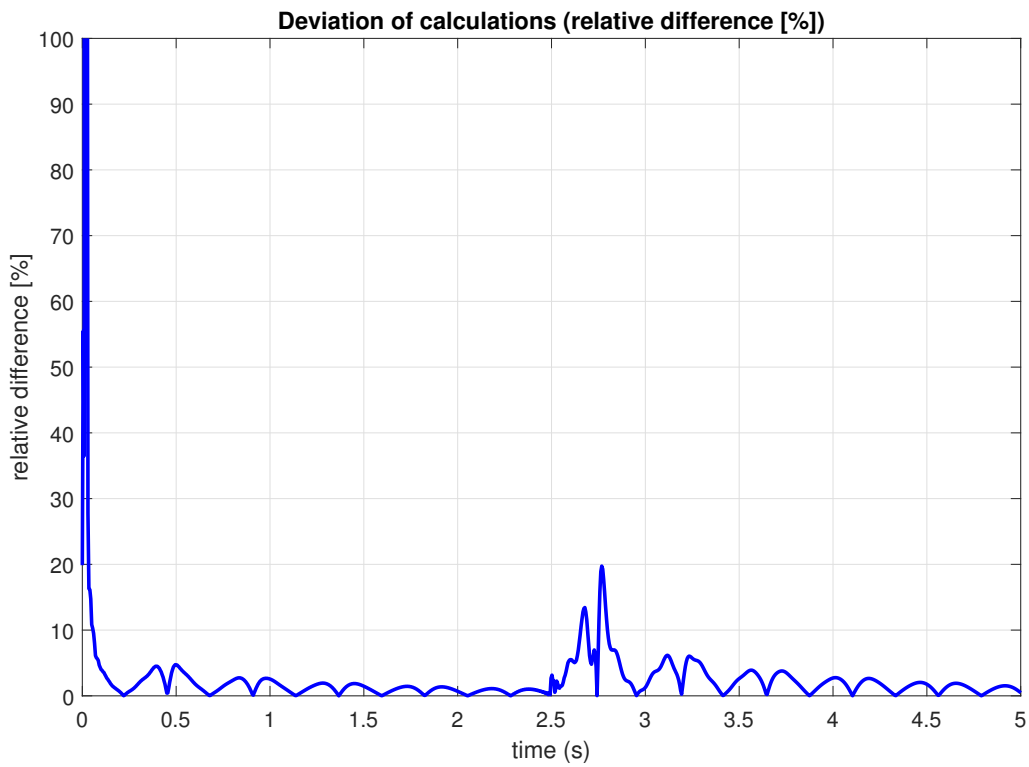


Fig. 3.9: Relative difference of the two calculation methods.

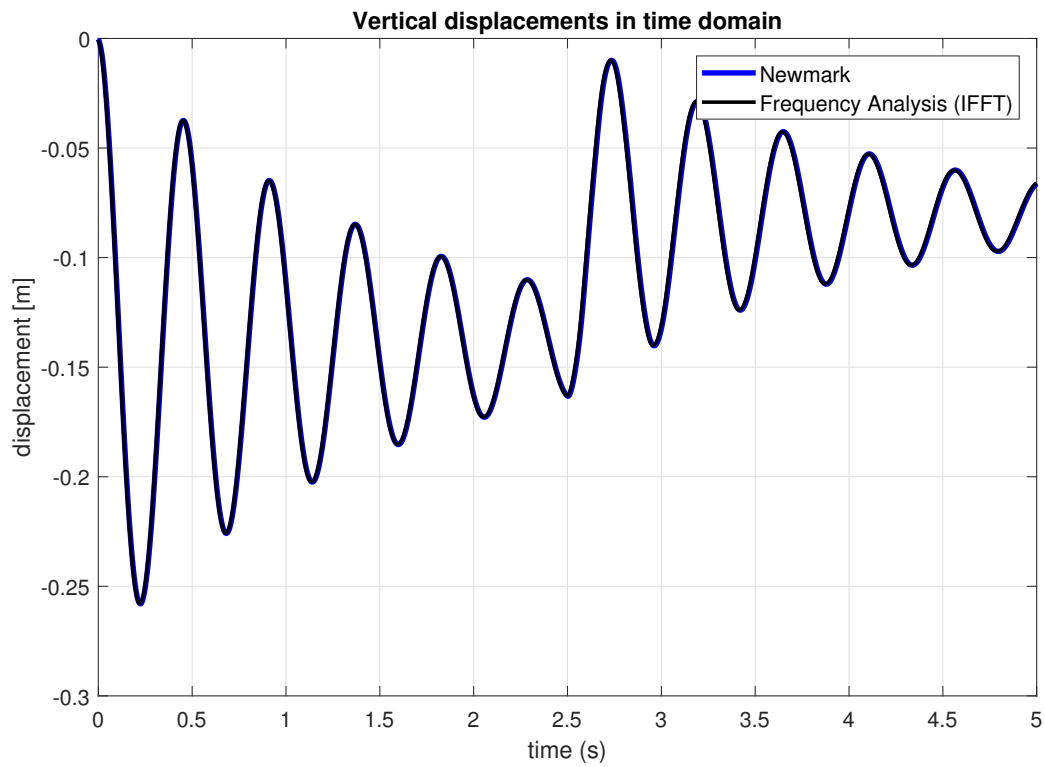


Fig. 3.10: Comparison of the vertical displacement in the time domain.

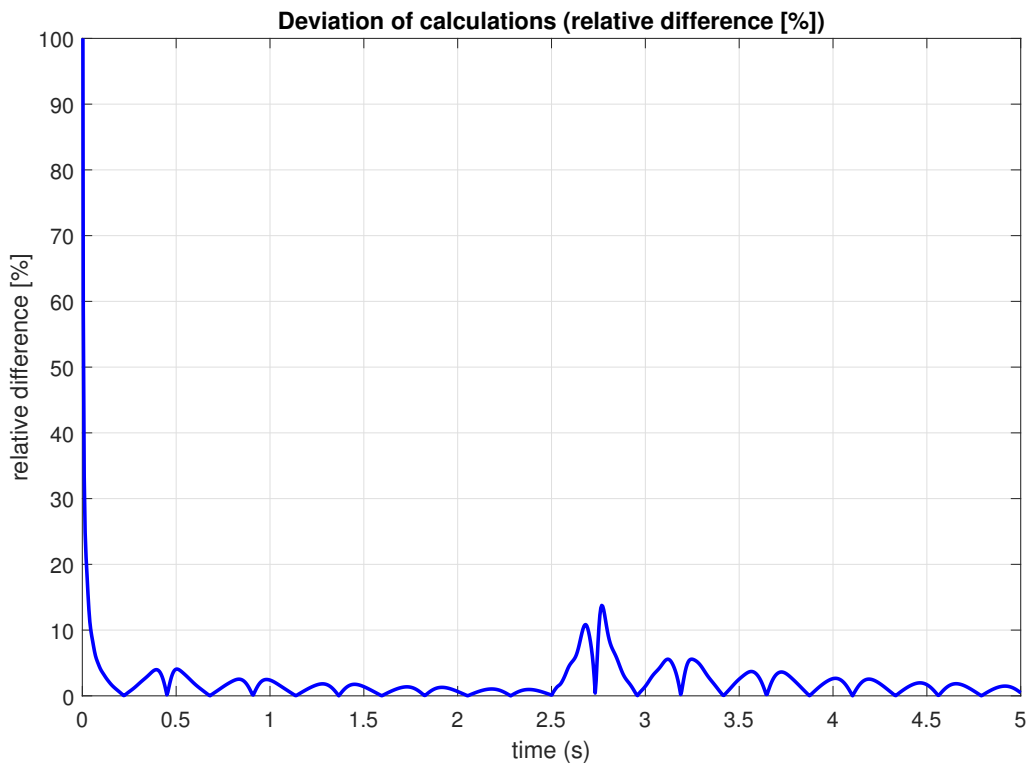


Fig. 3.11: Relative difference of the two calculation methods.

3.3.2 Example 2 - Multi-story frame

The next example is a highrise building, being a typical structure in civil engineering. Many simplifications in the geometry may lead to the system shown in Fig. 3.12. A machine in the last floor with rotating parts (e.g., a huge washing mashine) excites the whole building harmonically. The dead load of the structure is applied suddenly as in Section 3.3.1 and loads the building as well. The system is at rest at the beginning $t = 0$. The special node at x_{SN} is the reference point below the machine to visualize results.

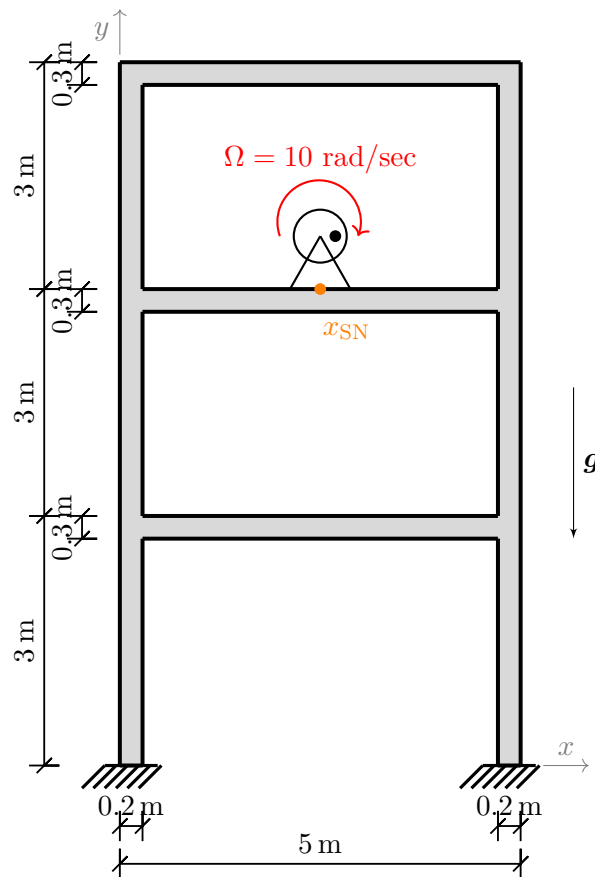


Fig. 3.12: Geometrical configuration of the multi-story frame.

The parameters of the example are listed below:

- Density of material $\rho = 7850 \text{ kg/m}^3$
- Gravity constant $g = 9.81 \text{ m/s}^2$
- Young's modulus $E = 210\,000\,000 \text{ kN/m}^2$
- Poisson's ratio $\nu = 0.3$ [-]
- Lamé's parameter λ is used for thick plates, given as

$$\lambda = \frac{E \cdot \nu}{(1 + \nu)(1 - 2\nu)} \quad (3.38)$$

- Rayleigh damping with $\zeta = 0.05$ [-]
- Loading
 - Dead load $\rho \cdot \mathbf{g}$
 - Washing machine running with a circular frequency of $\Omega = 10$ rad/sec
 - $\mathbf{F}(t) = \mathbf{A} \cdot \sin(\Omega t)$ with $\mathbf{A} = \begin{Bmatrix} F_x \\ F_y \end{Bmatrix} = \begin{Bmatrix} -200 \text{ kN} \\ -2000 \text{ kN} \end{Bmatrix}$
- Initial conditions
 - Displacement $\mathbf{u}_0 = \mathbf{0}$
 - Velocity $\dot{\mathbf{u}}_0 = \mathbf{0}$
- Time discretization done using Newmark's method
 - Length of calculation $t = 5$ sec
 - Time step size $\Delta t = 0.005$ sec
 - Number of time steps $N = 1000$
 - Nyquist frequency $f_c = 100$ / sec $\rightarrow \omega_c = f_c \cdot 2\pi = 628$ rad/sec
- Spatial discretization done using the FEM
- The input (load) is zero-padded for the FFT calculation; $2N$ zeros are added.

Fig. 3.13 shows the mesh (yellow) and shows the highlighted nodes with Dirichlet (blue) and Neumann (red) boundary.

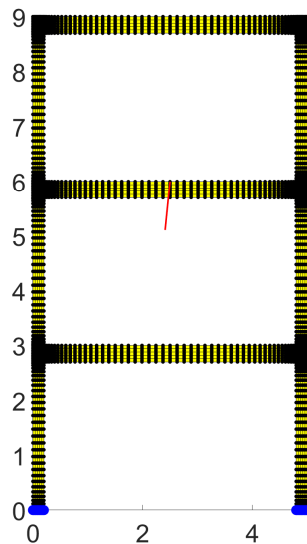


Fig. 3.13: Mesh and boundary conditions of the multi-story frame.

The following figures show the horizontal and vertical displacements at \mathbf{x}_{SN} . Fig. 3.14 shows the horizontal displacements in the time domain and the vertical displacements are given in Fig. 3.16. The *absolute* differences are plotted in Fig. 3.15 as well as in Fig. 3.17.

Tab. 3.2 summarizes the most important comparisons.

Tab. 3.2: Comparison of the calculation in time and frequency domain - Multi-story frame.

	Time domain	Frequency domain
Calculation time [s]	22	1155
min. hor. displacement [m]	-0.0050	-0.0053
time of min. hor. displ. [s]	0.1552	0.1451
min. ver. displacement [m]	-0.0049	-0.0049
time of min. ver. displ. [s]	0.1552	0.1552

The results given in the table and figures once again show that both, the approach in the time and in the frequency domain, yields similar results. The minima and maxima of the amplitudes are nearly equal. The phases are again slightly shifted. The displacements behave in an expected way. The system oscillates with the excitation frequency once the transient oscillation is damped out.

It is noteworthy that there is nearly no transient response in the vertical displacement field. The steady state response dominates heavily as soon as calculation begins. It can be said that the vertical damping properties of the frame are good.

The oscillation of the vertical response obtained by Newmark may be explained that the time step size is not chosen small enough to converge to a solution immediately.

The calculation time difference is even higher than for the cantilever beam test case. Obtaining the response with a frequency analysis takes 60 times longer than in the time domain. The reason can once again be found in evaluating the frequency response function \mathbf{H} .

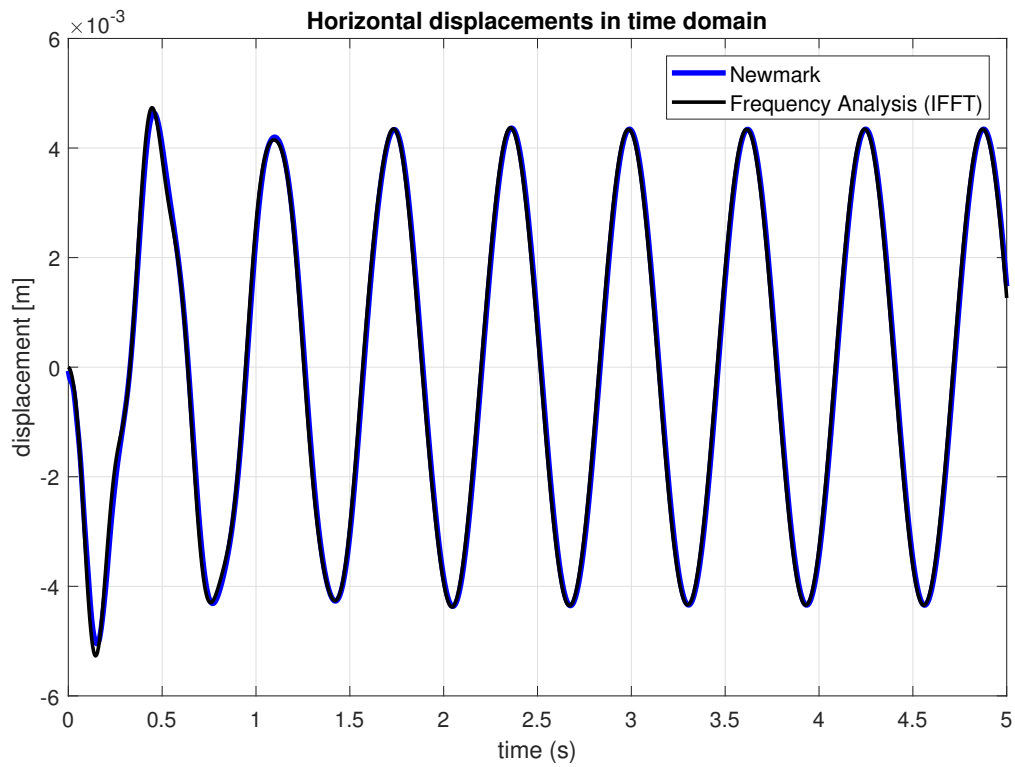


Fig. 3.14: Comparison of the horizontal displacement in the time domain.

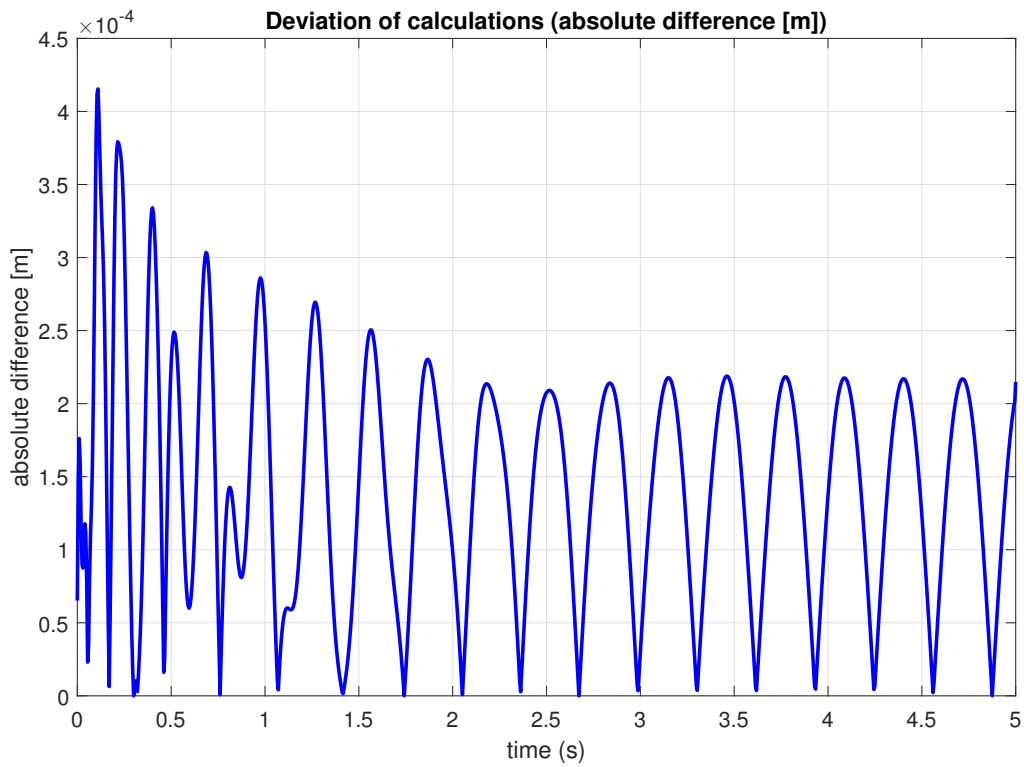


Fig. 3.15: Absolute difference of the two calculation methods.

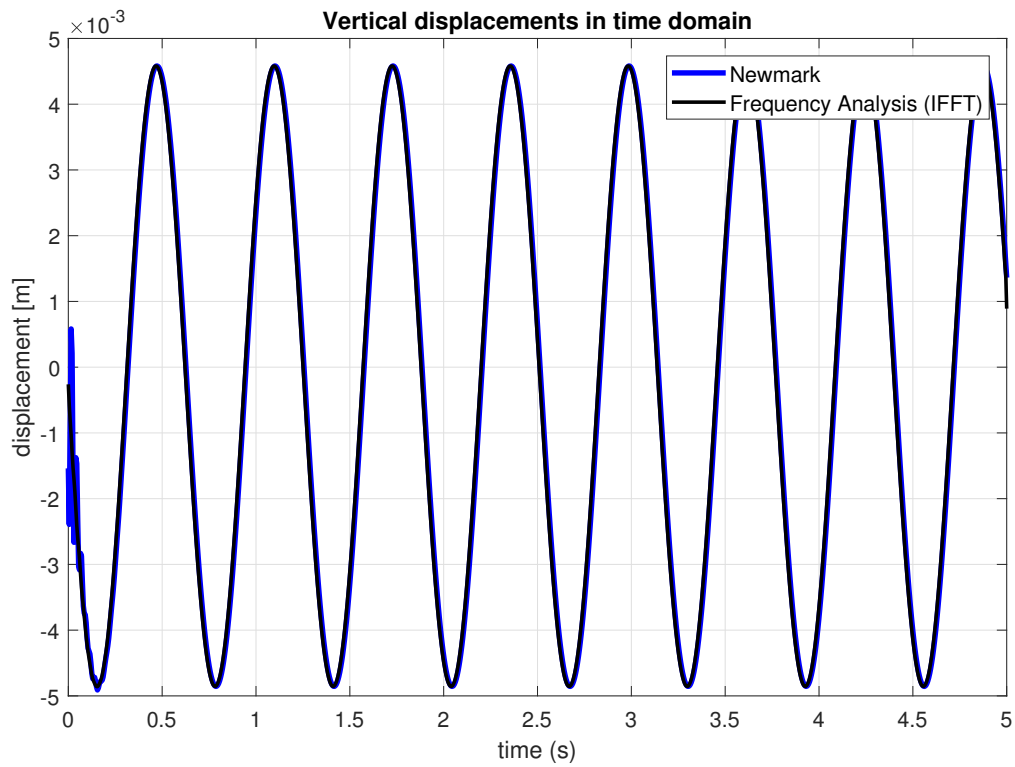


Fig. 3.16: Comparison of the vertical displacement in the time domain.

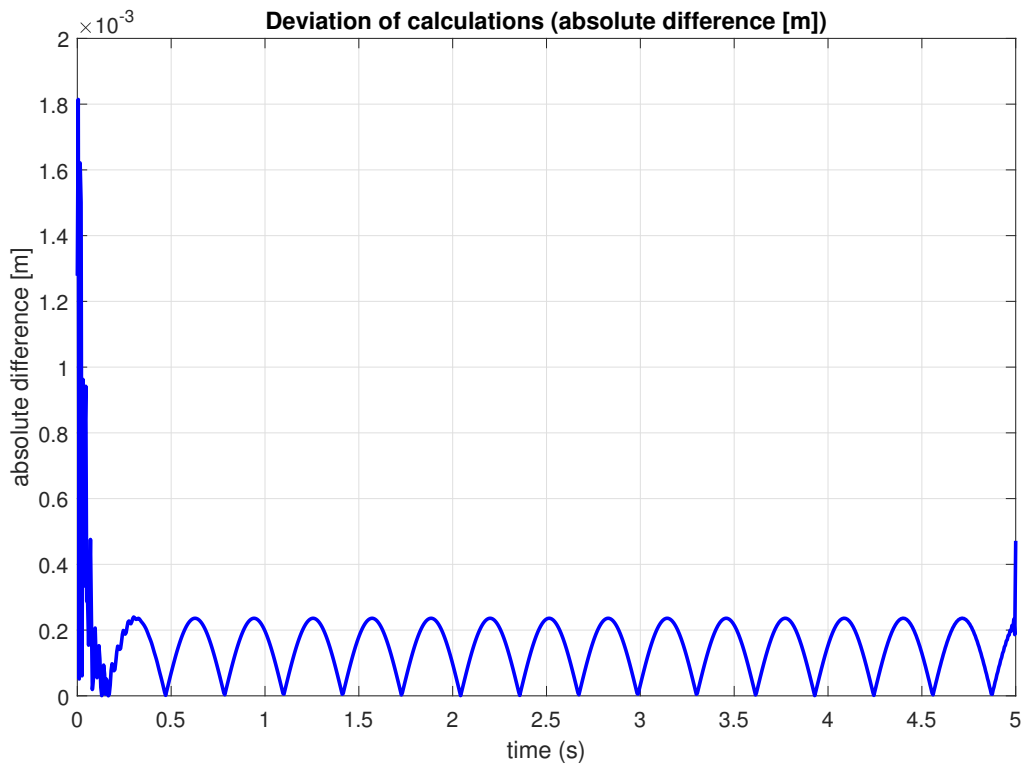


Fig. 3.17: Absolute difference of the two calculation methods.

4 Modal analysis for systems with multiple degrees of freedom (MDOF)

As already mentioned in the introduction, the decoupling of the system of equations enables the use of all methods described in Chapter 2, applied to every single (decoupled) scalar equation of the MDOF. Furthermore, the decoupling enables a reduction of the model, i.e., the DOFs, leading to reduced calculation times. This chapter introduces the procedure of decoupling by *modal analysis* and explains the steps to obtain a solution in the time and frequency domain.

4.1 Decoupling by modal analysis

The section follows closely the outline of Chopra [7], chapter 10 and 12. In the first step, the undamped EOM is considered. Later on, the context will be extended for viscously damped systems relevant in this thesis. To recall the EOMs of an undamped and damped system are given below:

$$\text{Undamped:} \quad \mathbf{M} \cdot \ddot{\mathbf{u}}(t) + \mathbf{K} \cdot \mathbf{u}(t) = \mathbf{f}(t) \quad (4.1a)$$

$$\text{and damped:} \quad \mathbf{M} \cdot \ddot{\mathbf{u}}(t) + \mathbf{C} \cdot \dot{\mathbf{u}}(t) + \mathbf{K} \cdot \mathbf{u}(t) = \mathbf{f}(t). \quad (4.1b)$$

To solve the EOM with the help of a modal analysis, it is necessary to transform the physical coordinates $\mathbf{u}(t)$ into modal coordinates $\mathbf{q}(t)$. This leads to a decoupled system of equations where, for each modal equation, the modal contribution to the response is calculated. These modal contributions are then superposed to obtain the total response. The transformation formula is given as

$$\mathbf{u}(t) = \sum_{n=1}^N \phi_n q_n(t) = \mathbf{\Phi} \mathbf{q}(t), \quad (4.2)$$

where $\mathbf{\Phi}$ is called *modal matrix* and contains the N natural modes ϕ_n . The modal matrix is time invariant which means the matrix remains constant over time. The natural eigenmodes and frequencies are obtained in the following.

Calculation of natural modes and frequencies

This section applies to **undamped** and **viscously damped** systems. For systems with different damping properties, it is advised to follow further literature, eg [7], [8] or [25]. The natural modes and frequencies are the results of the eigenvalue problem which shall be seen later. The derivation is done for the free vibration and is valid for forced vibrations as well.

The displacements $\mathbf{u}(t)$ are described mathematically by Ansatz in Eq. 4.2, where ϕ_n does not change with time. The displacements due to free vibration ($\mathbf{f}(t) = 0$) can be described by a simple harmonic function

$$q_n(t) = A_n \cos(\omega_0 t) + B_n \sin(\omega_0 t), \quad (4.3)$$

where the constants A_n and B_n are obtained by inserting the initial conditions. Inserting Eq. 4.3 in Eq. 4.2 and then inserting in Eq. 4.1a (with $\mathbf{f}(t) = 0$) gives following equation

$$\left[-\omega_0^2 \mathbf{M} \phi_n + \mathbf{K} \phi_n \right] q_n(t) = \mathbf{0}. \quad (4.4)$$

There are two possibilities to satisfy Eq. 4.4. The first one is trivial because $q_n(t) = 0 \rightarrow \mathbf{u}(t) = \mathbf{0}$ which corresponds to a system without displacements. As it is the goal to find the modes of motion, the other possibility to satisfy the other term in Eq. 4.4 is used. The natural frequencies and modes must satisfy the algebraic equation

$$\omega_0^2 \mathbf{M} \phi_n = \mathbf{K} \phi_n. \quad (4.5)$$

Eq. 4.5 is called the matrix eigenvalue problem and is formally rewritten as

$$\left[\mathbf{K} - \omega_0^2 \mathbf{M} \right] \phi_n = \mathbf{0}. \quad (4.6)$$

The nontrivial solutions of this equation are obtained by enforcing

$$\det \left[\mathbf{K} - \omega_0^2 \mathbf{M} \right] = 0. \quad (4.7)$$

This equation is called frequency equation and gives the real and positive roots ω_0^2 . The roots are real and positive if \mathbf{K} and \mathbf{M} are symmetric and positive definite. The positive definiteness is assured by investigating structures which do not make any rigid body movements, which is normally the case in civil engineering [7, p. 407].

The evaluation of the natural modes ϕ_n is possible as soon as the eigenfrequencies are known by inserting in Eq. 4.5. Note that the eigenvalue problem does not give the amplitudes of the modes but rather give the shape of the vector. The vectors are usually normalized¹ in a way that the entries on the main diagonal of the modal mass matrix $\bar{\mathbf{M}}$ are unity [7, p. 410].

It can be shown that the eigenmodes are perpendicular to each other. This property allows the decoupling of the equations and is called *orthogonality of modes*. The orthogonality can be formally written as: choosing two frequencies which are not the same $\omega_n \neq \omega_r$ and pre and post-multiply the stiffness and mass matrix with the corresponding eigenmode. This leads to

$$\phi_n^T \mathbf{K} \phi_r = 0 \quad \text{and} \quad \phi_n^T \mathbf{M} \phi_r = 0. \quad (4.8)$$

The proof of orthogonality can be found, e.g., in [7, p. 409].

To make the further computation more convenient, the eigenvalues and modes are arranged in matrices. These matrices are called modal and spectral matrices. The modal matrix Φ contains the N eigenvectors in column form and is of the following form

$$\Phi = [\phi_{jn}] = \begin{bmatrix} \phi_{11} & \phi_{12} & \cdots & \phi_{1N} \\ \phi_{21} & \phi_{22} & \cdots & \phi_{2N} \\ \vdots & \vdots & \ddots & \vdots \\ \phi_{N1} & \phi_{N2} & \cdots & \phi_{NN} \end{bmatrix}, \quad (4.9)$$

¹Normalization means to modify a vector in a way that for example $\|\mathbf{f}\| \equiv 1$.

where n denotes the natural mode and j the number of the DOF.

The eigenvalues can be expressed in a diagonal matrix. This matrix is the spectral matrix

$$\mathbf{\Omega}^2 = \begin{bmatrix} \omega_1^2 & & & \\ & \omega_2^2 & & \\ & & \ddots & \\ & & & \omega_N^2 \end{bmatrix}. \quad (4.10)$$

The natural frequencies of the equivalent SDOF systems are simply obtained by taking the square root of $\mathbf{\Omega}^2$.

In [7, p. 410], physically motivated interpretations are given. In summary, one implication is that the work done by the n -th mode inertia forces acting on the r -th mode displacements is zero. This means that the modes do not interfere with each other and are decoupled.

With this information the derivation of the decoupled system of equations is continued.

The modal coordinates are inserted in Eq. 4.1a

$$\sum_{n=1}^N \mathbf{M} \phi_n \ddot{q}_n(t) + \sum_{n=1}^N \mathbf{K} \phi_n q_n(t) = \mathbf{f}(t). \quad (4.11)$$

The formal trick to decouple the equations is to premultiply all terms in Eq. 4.11 with the transposed m -th eigenmode which gives

$$\sum_{n=1}^N \phi_m^T \mathbf{M} \phi_n \ddot{q}_n(t) + \sum_{n=1}^N \phi_m^T \mathbf{K} \phi_n q_n(t) = \phi_m^T \mathbf{f}(t). \quad (4.12)$$

Because of the orthogonality of modes, all terms in the summation vanish except the terms where the indices match ($n = m$). Consequently Eq. 4.12 reduces to

$$\left(\phi_n^T \mathbf{M} \phi_n \right) \ddot{q}_n(t) + \left(\phi_n^T \mathbf{K} \phi_n \right) q_n(t) = \phi_n^T \mathbf{f}(t), \quad (4.13)$$

or in slightly different notation

$$M_n \ddot{q}_n(t) + K_n q_n(t) = F_n(t). \quad (4.14)$$

Eq. 4.14 can be interpreted as the equation giving the response $q_n(t)$ of the n th SDOF system obtained by decoupling the MDOF system. As Eq. 4.14 gives the response of the n th modal coordinate, the system of decoupled equations can be written in matrix notation as (with $N \times N$ dimensions)

$$\overline{\mathbf{M}} \ddot{\mathbf{q}}(t) + \overline{\mathbf{K}} \mathbf{q}(t) = \overline{\mathbf{f}}(t), \quad (4.15)$$

with the diagonal matrices $\overline{\mathbf{M}} = \mathbf{\Phi}^T \mathbf{M} \mathbf{\Phi}$ and $\overline{\mathbf{K}} = \mathbf{\Phi}^T \mathbf{K} \mathbf{\Phi}$ and the force vector $\overline{\mathbf{f}}(t) = \mathbf{\Phi}^T \mathbf{f}(t)$. The response \mathbf{q} can be obtained by the procedures described in the following sections. The response in the physical coordinates is then calculated by inserting the response of Eq. 4.15 in Eq. 4.2.

The system of equation which is obtained by investigating a damped system can be handled similarly in case of viscous damping properties as already explained in Section 3.1.2. The damping matrix \mathbf{C} is acquired by superposing \mathbf{K} and \mathbf{M} . As these matrices are symmetric and positive definite, the matrix

\mathbf{C} has the same properties. This fact allows the diagonalization of the damping matrix [7, p. 424]. In the following, the procedure for decoupling the system is given.

The modal coordinates of Eq. 4.2 are inserted into Eq. 4.1b giving

$$\sum_{n=1}^N \mathbf{M}\phi_n \ddot{q}_n(t) + \sum_{n=1}^N \mathbf{C}\phi_n \dot{q}_n(t) + \sum_{n=1}^N \mathbf{K}\phi_n q_n(t) = \mathbf{f}(t). \quad (4.16)$$

Again, the formal trick to decouple the equations is to premultiply all terms in Eq. 4.16 with the transposed m -th eigenmode. This gives

$$\sum_{n=1}^N \phi_m^T \mathbf{M}\phi_n \ddot{q}_n(t) + \sum_{n=1}^N \phi_m^T \mathbf{C}\phi_n \dot{q}_n(t) + \sum_{n=1}^N \phi_m^T \mathbf{K}\phi_n q_n(t) = \phi_m^T \mathbf{f}(t). \quad (4.17)$$

Because of the orthogonality of modes all terms in the summation vanish except the terms where the indices are $n = m$. Eq. 4.17 reduces to

$$\left(\phi_n^T \mathbf{M}\phi_n\right) \ddot{q}_n(t) + \left(\phi_n^T \mathbf{C}\phi_n\right) \dot{q}_n(t) + \left(\phi_n^T \mathbf{K}\phi_n\right) q_n(t) = \phi_n^T \mathbf{f}(t). \quad (4.18)$$

With the same reasons as given above for the undamped system, the decoupled EOM can now be written as

$$\overline{\mathbf{M}}\ddot{\mathbf{q}}(t) + \overline{\mathbf{C}}\dot{\mathbf{q}}(t) + \overline{\mathbf{K}}\mathbf{q}(t) = \overline{\mathbf{F}}(t), \quad (4.19)$$

with the diagonal matrices $\overline{\mathbf{M}} = \mathbf{\Phi}^T \mathbf{M}\mathbf{\Phi}$, $\overline{\mathbf{K}} = \mathbf{\Phi}^T \mathbf{K}\mathbf{\Phi}$ and $\overline{\mathbf{C}} = \mathbf{\Phi}^T \mathbf{C}\mathbf{\Phi}$ and the force vector $\overline{\mathbf{F}}(t) = \mathbf{\Phi}^T \mathbf{f}(t)$.

The initial conditions from Eq. 3.6 need to be transformed into the modal coordinates as well. Following the steps in [7, p. 420], Eq. 4.2 is multiplied with $\phi_n^T \mathbf{M}$ giving

$$q_n = \frac{\phi_n^T \mathbf{M}\mathbf{u}}{\phi_n^T \mathbf{M}\phi_n}. \quad (4.20)$$

Eq. 4.20 is called *modal expansion of displacement* [7, p. 420]. Inserting the initial condition vectors \mathbf{u}_0 and $\dot{\mathbf{u}}_0$ into Eq. 4.20 transforms the initial conditions into modal coordinates.

The modal solution of Eq. 4.19 can be obtained by means of the following sections. The physical and sought response is obtained by inserting the modal response $\mathbf{q}(t)$ into Eq. 4.2.

4.2 Model reduction

As previously mentioned, applications with difficult geometry or loadings are often discretized with a lot of DOFs. Although modern computers can handle these fast and accurate, methods to reduce the model and therefore the calculation time are very useful and introduced next. This chapter gives a short overview of some methods and describes the modal reduction. Various other literature gives further information.

Some model reductions represented in this thesis rely on the projection of the problem to some subspace, e.g. [3]. This subspace is much smaller than the original space which means the problem is

reduced. Other reductions reduce the number of DOFs [13, p. 546]. All approaches reduce the computational effort and the reduction in effort is achieved by the transformation matrix $\mathbf{T} \in \mathbb{R}^{N \times k}$, where N is a very large number (of DOFs). The transformation is defined as

$$\mathbf{u}(t) = \mathbf{T}\mathbf{q}, \quad (4.21)$$

with $\mathbf{q}(t) \in \mathbb{R}^{k \times 1}$ and $k \ll N$.

- **Static reduction**

The static reduction is also called Guyan reduction [14] and reduces the system in a way that the entries of the stiffness matrix associated to the external nodes match with the entries of the stiffness matrix of the full system. Therefore the nodes (or DOFs) are split in master and slave nodes [13, p. 548]. Slave nodes depend on the master nodes. This means that the quantities of the master nodes can be calculated and the quantities of the slave nodes are obtained by the matrix-vector calculation in Eq. 4.22. Slave nodes can, e.g., be chosen as the nodes where no forces act or that the matrices remain their sparsely filled property [13, p. 551].

$$\mathbf{u} = \begin{Bmatrix} \mathbf{u}_M \\ \mathbf{u}_S \end{Bmatrix} \quad \text{and} \quad \mathbf{K} = \begin{bmatrix} \mathbf{K}_{MM} & \mathbf{K}_{MS} \\ \mathbf{K}_{SM} & \mathbf{K}_{SS} \end{bmatrix}, \quad (4.22a)$$

$$\begin{bmatrix} \mathbf{K}_{MM} & \mathbf{K}_{MS} \\ \mathbf{K}_{SM} & \mathbf{K}_{SS} \end{bmatrix} \begin{Bmatrix} \mathbf{u}_M \\ \mathbf{u}_S \end{Bmatrix} = \begin{Bmatrix} \mathbf{f}_M \\ \mathbf{f}_S \end{Bmatrix}, \quad (4.22b)$$

$$\mathbf{u} = \begin{bmatrix} \mathbf{I}_{MM} \\ -\mathbf{K}_{SS}^{-1}\mathbf{K}_{SM} \end{bmatrix} \mathbf{u}_M, \quad (4.22c)$$

$$\mathbf{q} = \mathbf{u}_M \quad \text{and} \quad \mathbf{T}_{\text{stat}} = \begin{bmatrix} \mathbf{I}_{MM} \\ -\mathbf{K}_{SS}^{-1}\mathbf{K}_{SM} \end{bmatrix}. \quad (4.22d)$$

Note that the choice of the master nodes heavily influences the accuracy of the result [13, p. 549].

- **Modern reduction methods** such as Krylov subspace method

The advantage of the Krylov subspace method [3] is that it only needs matrix-vector-operations and there is no need to chose master and sleeve nodes. A possible drawback is that stability is not ensured. Stability means that the calculation is immune to errors in the input and that the solution converges, meaning some predefined error conditions are fulfilled.

- **Modal reduction**

The modal reduction is a method to reduce the system by simply reducing the number of modes which are considered. The transformation matrix \mathbf{T} is defined as

$$\mathbf{T} = [\boldsymbol{\phi}_1 \quad \boldsymbol{\phi}_2 \quad \cdots \quad \boldsymbol{\phi}_k] \equiv \boldsymbol{\Phi}_{\text{red}}, \quad (4.23)$$

with the first k eigenmodes $\boldsymbol{\phi}$ of Eq. 4.6. Gasch proposes in [13, pp. 221-224] three possibilities to choose which modes to include

- Consider DOFs with high generalised loading $\bar{f}_n \gg 1$.
- Consider DOFs with small generalised stiffness $\bar{K}_{nn} \ll 1$.

- Consider modes with natural frequencies which are in the range of big amplitudes of the Fourier transformed load.

In this work the modes associated with the k smallest eigenfrequencies (longwave low eigenmodes [13, p. 553]) are used to reduce the model.

4.3 Solving in the time domain

As already mentioned before, the decoupling of equations enables the use of all (analytical) methods of Chapter 2. In the following the procedure for a numerical solution is described and the specialities in comparison to the full coupled approach is given. The calculation can be summarized by seven steps. The last two steps are optional. The procedure is taken from [13, Fig. 4.3, 4.4] and Newmark's method from Section 3.2.1.

Step one: Solving the eigenvalue problem

$$0 = \det(-\mathbf{M} \cdot \omega^2 + \mathbf{K}). \quad (4.24)$$

This gives the modal matrix $\Phi \in \mathbb{R}^{N \times k}$ and the spectral matrix $\Omega \in \mathbb{R}^{k \times k}$ to continue with step two. N denotes the number of DOFs of the original system and k is the number of considered modes.

Step two: Modal decoupling of the equations by diagonalization of the matrices and load

$$\begin{aligned} \Phi^T \cdot \mathbf{K} \cdot \Phi &= \bar{\mathbf{K}}, \\ \Phi^T \cdot \mathbf{C} \cdot \Phi &= \bar{\mathbf{C}}, \end{aligned} \quad (4.25a)$$

$$\begin{aligned} \Phi^T \cdot \mathbf{M} \cdot \Phi &= \bar{\mathbf{M}}, \\ \Phi^T \cdot \mathbf{f}(t) &= \bar{\mathbf{f}}(t), \end{aligned} \quad (4.25b)$$

where $\bar{\mathbf{K}}, \bar{\mathbf{C}}, \bar{\mathbf{M}} \in \mathbb{R}^{k \times k}$ and $\bar{\mathbf{f}}(t) \in \mathbb{R}^{k \times 1}$.

Step three: Transforming of the initial conditions into modal coordinates

$$\mathbf{q}_0 = \frac{\Phi^T \mathbf{M} \mathbf{u}_0}{\Phi^T \mathbf{M} \Phi} \quad \text{and} \quad \dot{\mathbf{q}}_0 = \frac{\Phi^T \mathbf{M} \dot{\mathbf{u}}_0}{\Phi^T \mathbf{M} \Phi}. \quad (4.26)$$

Step four: Evaluating the modal response using Newmark's method for all time steps

$$\begin{aligned} & (a_0 \bar{\mathbf{M}} + a_1 \bar{\mathbf{C}} + \bar{\mathbf{K}}) \cdot \mathbf{q}_{n+1} = \\ & \bar{\mathbf{f}}_{n+1} + \bar{\mathbf{M}} \cdot (a_0 \mathbf{q}_n + a_2 \dot{\mathbf{q}}_n + a_3 \ddot{\mathbf{q}}_n) + \bar{\mathbf{C}} \cdot (a_1 \mathbf{q}_n - a_4 \dot{\mathbf{q}}_n - a_5 \ddot{\mathbf{q}}_n), \end{aligned} \quad (4.27)$$

where $\mathbf{q}_n \in \mathbb{R}^{k \times 1}$ and the coefficients α_i from Eq. 2.62.

Step five: Transforming the response back into the physical coordinates by inserting in

$$\Phi \cdot \mathbf{q}(t) = \mathbf{u}(t), \quad (4.28)$$

where $\mathbf{u}(t) \in \mathbb{R}^{N \times 1}$.

Step six: Transforming the response into the frequency domain by means of FFT to obtain the frequency spectrum (optional)

$$\mathbf{u}(t) \xrightarrow{\text{FFT}} \mathbf{F}[\mathbf{u}](\omega) \quad (4.29)$$

Step seven: Postprocessing (plotting, evaluation of forces, ...)

The main difference in the calculation of the response in the time domain and in the calculation time is the matrix on the left hand side of Eq. 4.27. This matrix is a diagonal matrix in case of decoupling the equations. Inverting a full matrix compared to a diagonal matrix results in largely different computational effort. Another theoretical advantage of the decoupling is the use of different time steps for each mode. As described in Section 2.3.1, the time step size should be chosen with respect to the highest natural frequency [22, p. 73]. As the modes are decoupled, the time step size can be chosen with respect to the modes' natural frequency. The disadvantage of decoupling the system is that the computation of eigenvalues and modes of large systems requires substantial computational effort.

4.4 Solving in the frequency domain

As already mentioned previously the decoupling of equations enables the use of all (analytical) methods of Chapter 2. Similar to the approach in the time domain, the numerical procedure in the frequency domain is introduced in the following. The procedure is taken from [21, pp. 8-10]. Furthermore the specialities in comparison to the full coupled approach are given. In equivalence to the numerical procedure for the coupled approach, the initial conditions are required to be zero [20, p. 57]. The procedure can be summarized by eight steps. Note that step **one** and **two** need to be made independent of the domain of calculation. The last two steps are again optional.

Step one: Solving the eigenvalue problem

$$0 = \det(-\mathbf{M} \cdot \omega^2 + \mathbf{K}). \quad (4.30)$$

This gives the modal matrix $\Phi \in \mathbb{R}^{N \times k}$ and the spectral matrix $\Omega \in \mathbb{R}^{k \times k}$. N and k are the number of DOFs of the original system and the considered modes respectively.

Step two: Modal decoupling of the equations by diagonalization of the matrices and load

$$\begin{aligned} \Phi^T \cdot \mathbf{K} \cdot \Phi &= \bar{\mathbf{K}}, \\ \Phi^T \cdot \mathbf{C} \cdot \Phi &= \bar{\mathbf{C}}, \end{aligned} \quad (4.31a)$$

$$\begin{aligned} \Phi^T \cdot \mathbf{M} \cdot \Phi &= \bar{\mathbf{M}}, \\ \Phi^T \cdot \mathbf{f}(t) &= \bar{\mathbf{f}}(t), \end{aligned} \quad (4.31b)$$

where $\bar{\mathbf{K}}, \bar{\mathbf{C}}, \bar{\mathbf{M}} \in \mathbb{R}^{k \times k}$ and $\bar{\mathbf{f}}(t) \in \mathbb{R}^{k \times 1}$.

Step three: Fourier transforming the modally decoupled load [8, p. 224] using Fast Fourier transformation

$$\bar{\mathbf{f}}(t) \xrightarrow{\text{FFT}} \mathbf{F}[\bar{\mathbf{f}}](\omega) \quad (4.32)$$

Step four: Evaluation of the frequency response function $\bar{\mathbf{H}}(\omega)$. $\bar{\mathbf{H}}(\omega)$ is evaluated for each discrete frequency value obtained in step three. The function can be evaluated by

$$\bar{\mathbf{H}}^{-1}(\omega) = [1/\bar{H}_{ii}]. \quad (4.33)$$

The frequency response function is in case of decoupling the equations a diagonal matrix thus inverting is trivial and cheap [21, p. 10].

Step five: Obtaining the Fourier transformed modal displacements by the following multiplication

$$\mathbf{F}[\mathbf{q}](\omega) = \bar{\mathbf{H}}(\omega) \cdot \mathbf{F}[\bar{\mathbf{f}}](\omega), \quad (4.34)$$

where $\mathbf{F}[\mathbf{q}](\omega) \in \mathbb{C}^{k \times 1}$.

Step six: Transforming back into the physical coordinates is done by inserting in

$$\Phi \cdot \mathbf{F}[\mathbf{q}](\omega) = \mathbf{F}[\mathbf{u}](\omega), \quad (4.35)$$

where $\mathbf{F}[\mathbf{u}](\omega) \in \mathbb{C}^{N \times 1}$.

Step seven: Transformation of displacements into the time domain by means of inverse fast Fourier transformation (optional)

$$\mathbf{F}[\mathbf{u}](\omega) \xrightarrow{\text{IFFT}} \mathbf{u}(t), \quad (4.36)$$

where $\mathbf{u}(t) \in \mathbb{R}^{N \times 1}$.

Step eight: Postprocessing (plotting, evaluation of forces, ...)

The main difference in the calculation of the response in the frequency domain and in the calculation time is matrix \mathbf{H} . Inverting a fully filled matrix and a diagonal matrix needs different techniques and is more or less expensive. The disadvantage of decoupling the system is that the eigenvalues and modes of large systems need to be acquired.

4.5 Example

In this section the previously introduced example of the multi-story frame is re-considered. The geometry and parameters are identical to Section 3.3.2. The calculation is done in the time and frequency domain. The main focus is the comparison of displacements and calculation time in both, time and frequency domain. The system of equations is decoupled with the methods described above and in order to achieve an improvement of calculation time, the system is reduced taking into account only the first 20 eigenmodes.

4.5.1 Time domain

The methods of Section 4.3 are being used to obtain the solution in the time domain. The solution in the time domain and the comparison with the fully coupled system is given in Fig. 4.1 and Fig. 4.3 for the horizontal and vertical displacements at \mathbf{x}_{SN} , see Fig. 3.12. The displacements match very well graphically. The *absolute* difference ($\Delta u = u_{\text{full}} - u_{\text{reduced}}$) is reasonably small. The jumps in Fig. 4.4 can be explained that the solution obtained by Newmark's method oscillate at the beginning and converging to a solution after some time. The calculation time is reduced from 12.3 seconds to 8.8 seconds resulting in a reduction of roughly one third.

With the information given above it can be stated that a reduction of the system from 8558 to 20 modes is very much useful. The amplitudes and phases are approximated well enough for simple engineering applications. The reduction in calculation time is noticeable and may becomes even bigger for larger systems of equations.

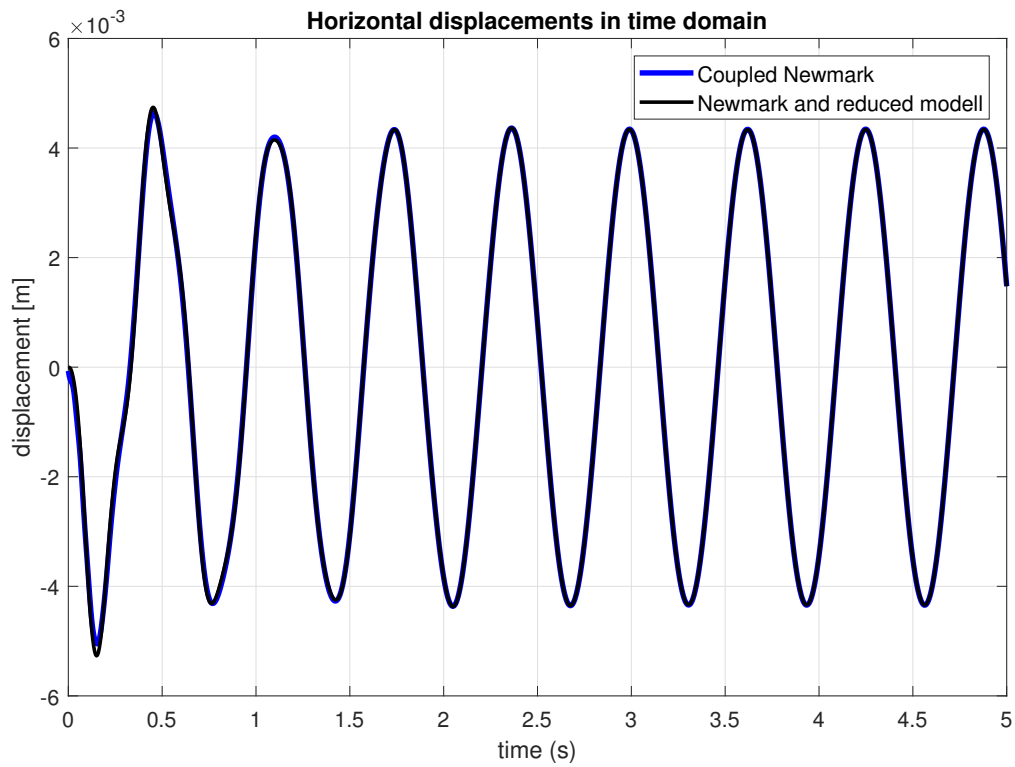


Fig. 4.1: Horizontal displacement in the time domain with reduced system and fully coupled system.

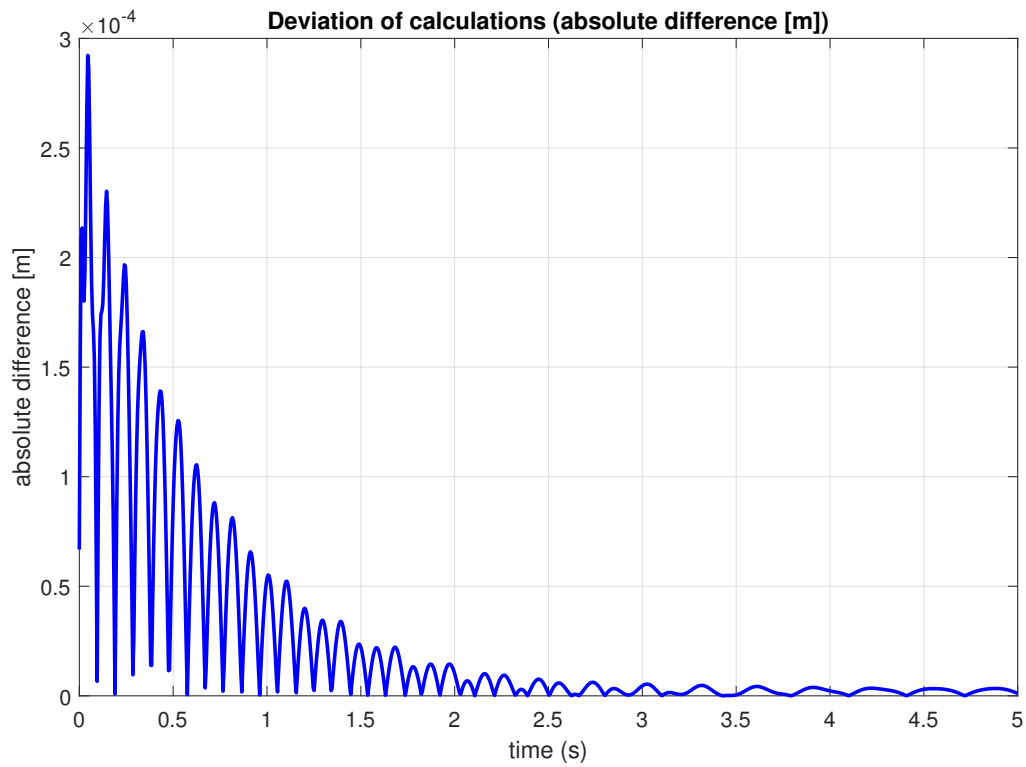


Fig. 4.2: Absolute difference of the calculation types.

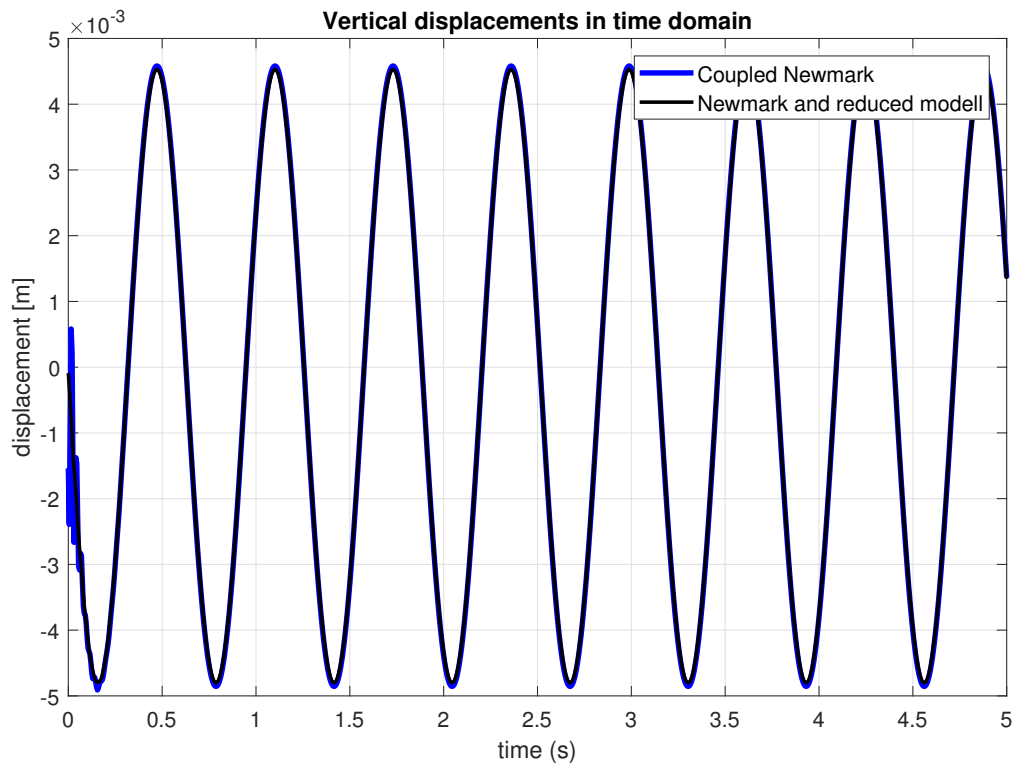


Fig. 4.3: Vertical displacement in the time domain with reduced system and fully coupled system.

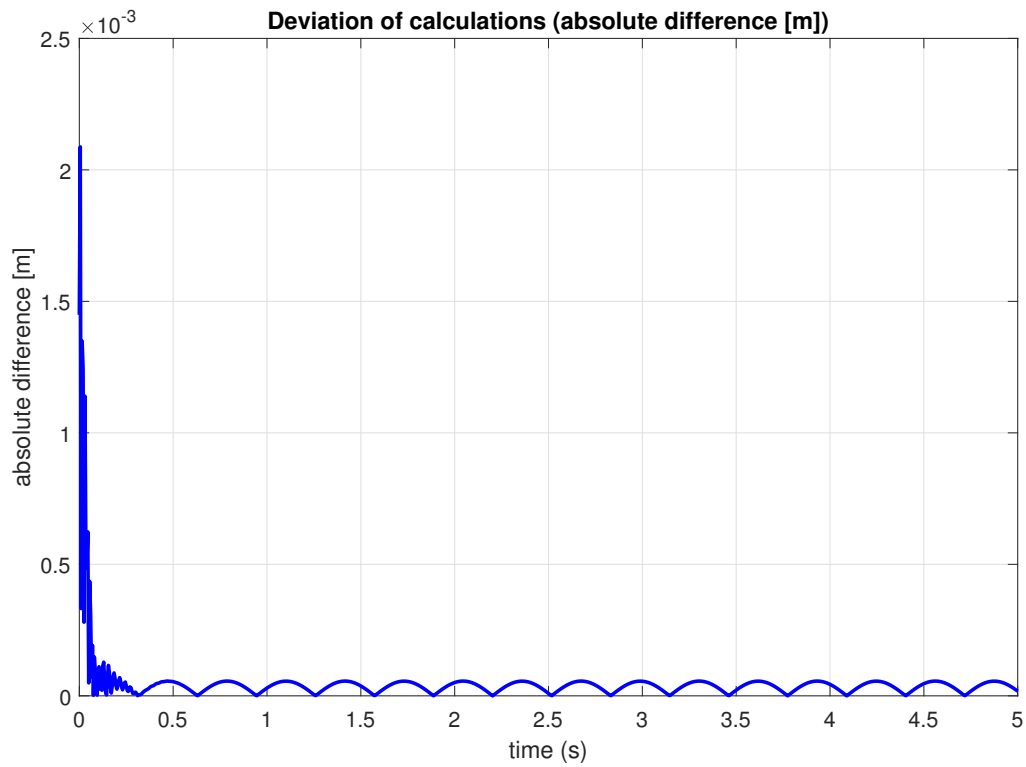


Fig. 4.4: Absolute difference of the calculation types.

4.5.2 Frequency domain

The methods of Section 4.4 are being used to acquire the solution. The solution in the time domain and the comparison with the fully coupled system is given in Fig. 4.5 and Fig. 4.7. The amplitude spectra are given in Fig. 4.6 and Fig. 4.8. The amplitude spectra show dominant peaks at frequency $\omega = 10$ rad/s as expected. The frequency spectra are zero for frequencies $|\omega| > 60$ rad/sec which means the time step is chosen small enough that all important frequencies are covered. The spectra show nicely the dominant frequencies of the oscillation. The vertical oscillation is dominated by the excitation frequency, there is no peak at the natural frequency. The fact that the horizontal oscillation of the frame is partly dominated by the natural frequency is shown nicely.

It can be seen that the amplitudes in the time as well as in the frequency domain are approximated well. The difference is marginal and small enough for simple engineering purposes. The calculation time is dramatically reduced from roughly 17 to one minute resulting in a reduction of 94 %. The reason is that the frequency response function \mathbf{H} is obtained by inverting a small diagonal matrix instead of a large sparsely filled matrix.

It is once again shown that reducing the system to roughly 0.5 % of its original size is very useful in terms of reduced calculation time and obtaining results within engineering precision.

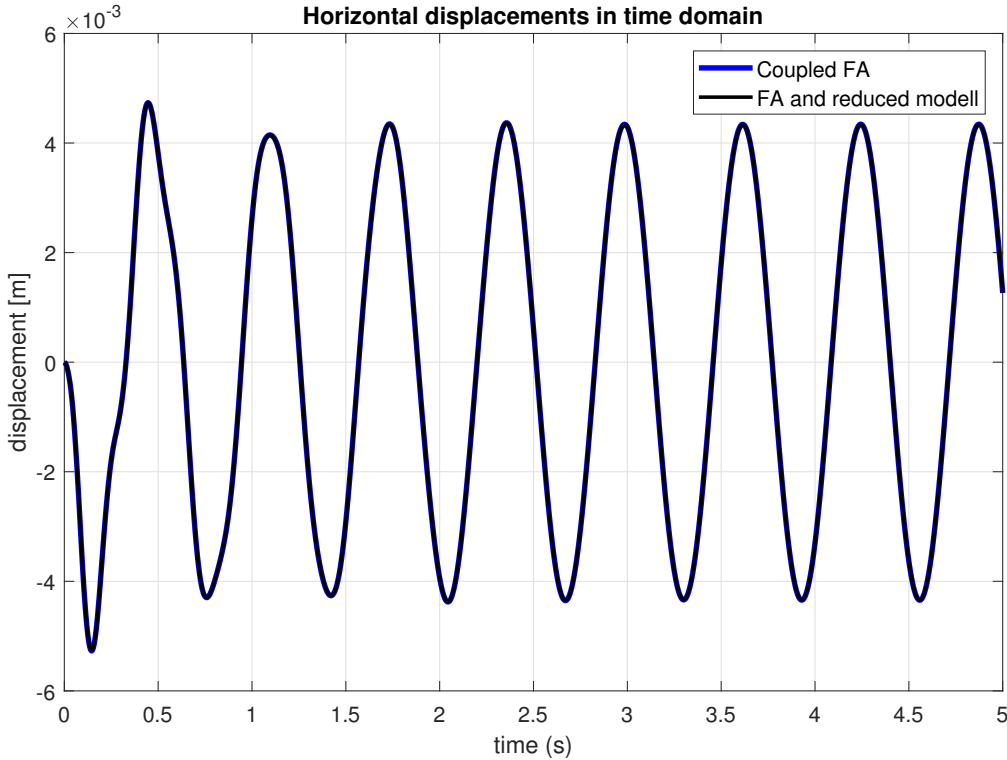


Fig. 4.5: Horizontal displacement in the time domain with reduced system and fully coupled system.

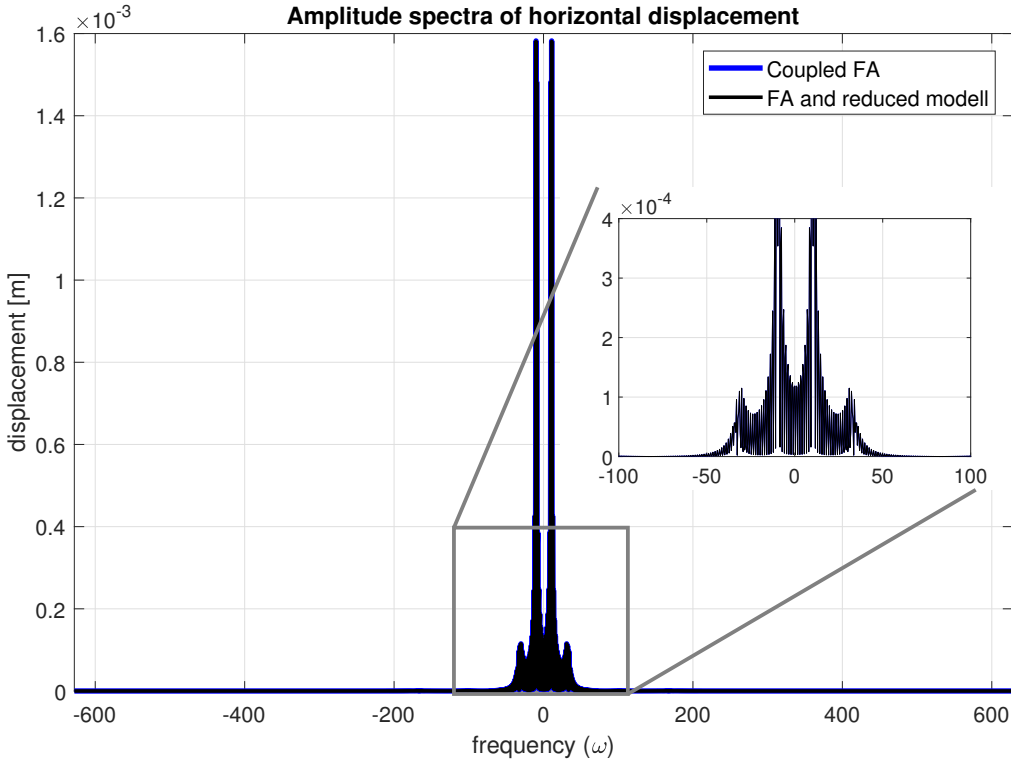


Fig. 4.6: Amplitude spectrum for horizontal displacements with reduced and fully coupled system.

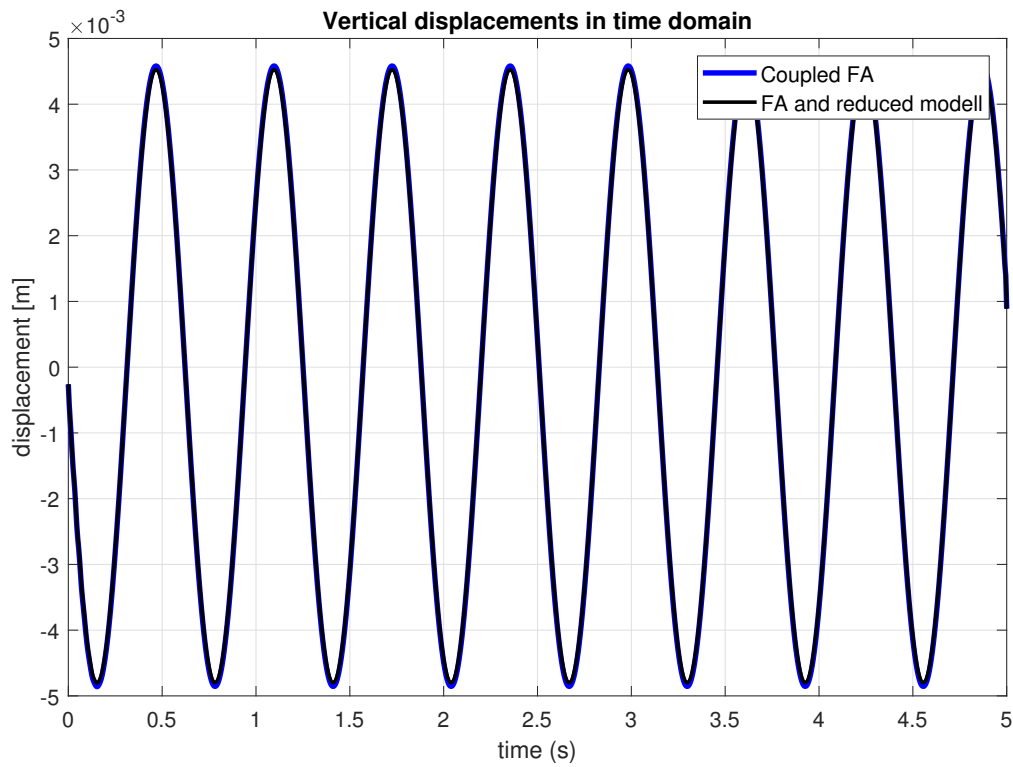


Fig. 4.7: Vertical displacement in the time domain with reduced system and fully coupled system.

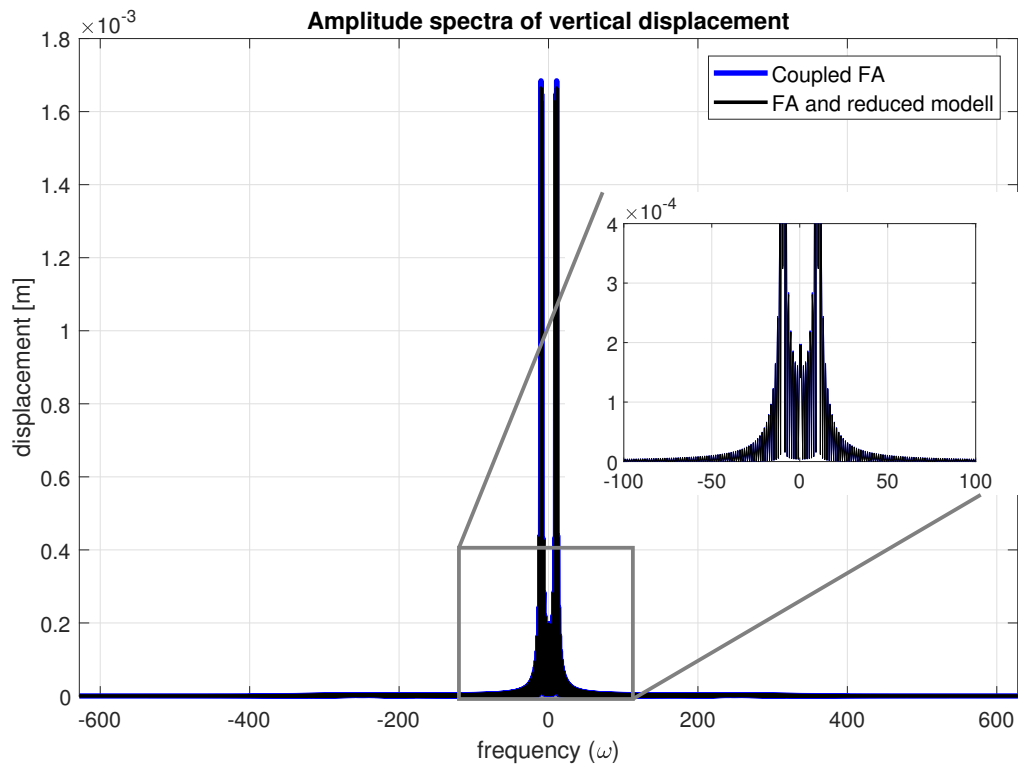


Fig. 4.8: Amplitude spectrum for vertical displacements with reduced and fully coupled system.

4.6 Comparison of approaches

The following chart summarizes the possible approaches to solve a MDOF structural dynamics problem covered in this thesis.

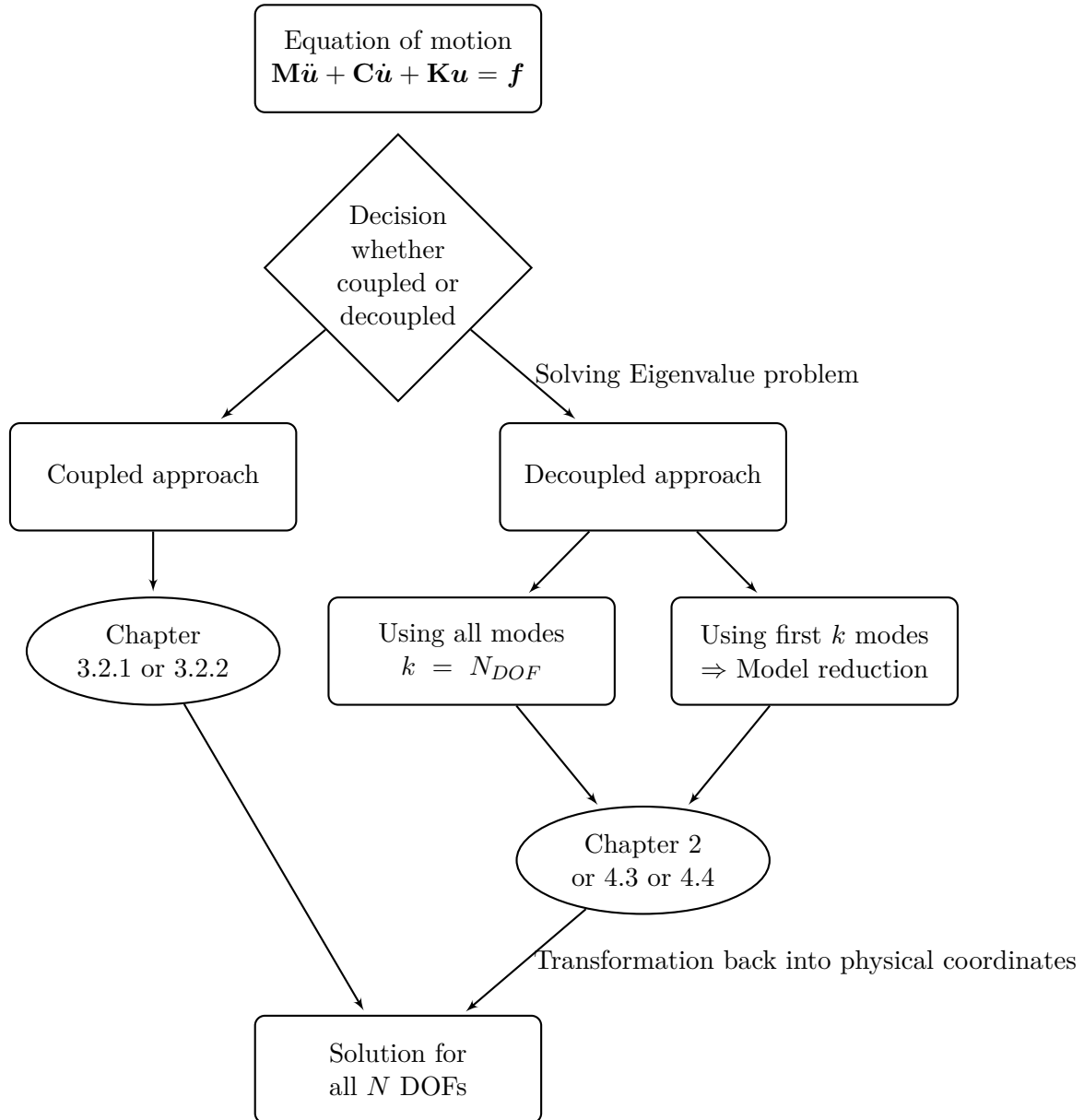


Fig. 4.9: Flow chart of solving MDOF systems.

5 Conclusion

We have investigated calculation methods for physical quantities in both, the time and frequency domain. It can clearly be seen that in both domains equivalent results are achieved. Generally speaking, it can be recommended to use the frequency domain for analytically solving the EOM, while the time domain is the better choice for numerically solving the EOM. The discrepancies can be explained by the fact that round-off errors occur in case of the analytical approach and that the initial value problems (IVP) are not completely identical. In case of numerically computing in the frequency domain, it is implied that the input is periodically continued. In the time domain, no such implication is present. Fig. 5.1 shows the difference graphically. Clearly, both cases may be physically meaningful, so it depends on the desired input function which approach fits better.

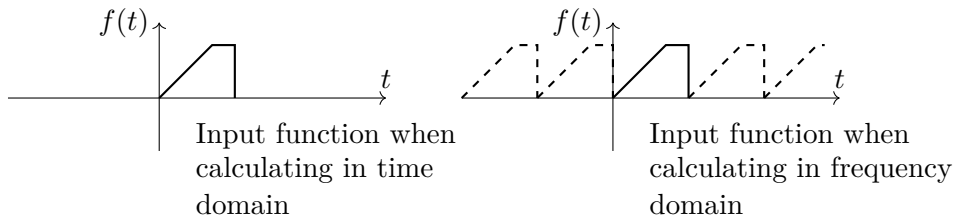


Fig. 5.1: Difference of IVP for numerical computation in both domains.

There are challenges to be faced in both domains when numerically carrying out calculations. In the time domain, a suitable time step size Δt and Newmark parameters β and γ have to be chosen. In the frequency domain, close attention has to be paid to manipulate the input in suitable ways to obtain accurate and viable results (zero-padding, windowing, calculation time).

Furthermore, model reduction was considered and consequences investigated. It was shown that reducing the model to roughly 0.5 % of its original size still leads to good results. The reduction in calculation time depends on the concrete application and on the fact whether calculations are performed in the time or frequency domain. The reduction in the frequency domain was enormous ($\sim 94\%$) while it was less obvious in the time domain using Newmark's method ($\sim 33\%$).

This leads to the conclusion that both domains are very well suitable to perform calculations in structural dynamics. The most important advantage of the calculation in the frequency domain is that frequency-dependent properties can be easily considered. The challenges of choosing the right parameters for calculations are outlined in this thesis. It is thus seen that the aim of this work, to compare calculations obtained in various different ways, has been achieved. The final decision which domain (time or frequency) is more suitable for calculations largely depends on the application and the type of loading and is still up to the preferences of the individual user.

List of Figures

1.1	Cartesian coordinate system.	2
1.2	Definition of period T	5
1.3	Example of a sawtooth function.	5
1.4	Approximation of sawtooth function with (a) $k = 3$ and (b) $k = 30$ terms.	6
1.5	Frequency spectra of approximated sawtooth function with (a) $k = 3$ and (b) $k = 30$ terms.	7
1.6	Example of a step function.	8
1.7	Frequency spectra of step function (a) $\text{Re}(F[f](\omega))$ and (b) $\text{Im}(F[f](\omega))$	8
1.8	Amplitude spectrum of step function $\text{Abs}(F(\omega))$	9
1.9	Implied periodicity of the DFT.	10
1.10	Series of Fourier coefficients obtained by DFT.	10
1.11	Visualization of Butterfly-Scheme.	11
1.12	Scheme of FFT-Algorithm for $N = 4$	12
2.1	Idealized SDOF system: (left) physical system; (right) free body diagram.	16
2.2	Flow chart of obtaining the analytical solution in the frequency domain.	28
2.3	Flow chart of analytically solving the equation of motion.	29
2.4	Flow chart of numerically solving the EOM with Newmark's method.	32
2.5	Flow chart of numerically solving the EOM in the frequency domain.	33
2.6	Influence of the time t_f on the results obtained by using the FFT in frequency analysis, taken from [7, p. 900]	34
2.7	Flow chart of numerically solving EOM in both domains	35
2.8	Geometrical configuration of a cantilever beam with load on end.	36
2.9	Example of a (a) harmonic load and (b) periodic load.	36
2.10	Example of a (a) non-periodic load and (b) arbitrary load.	37
2.11	Displacement in the time domain with harmonic load obtained in time domain.	40
2.12	Displacement in the time domain with harmonic load obtained in frequency domain.	40
2.13	Amplitude spectrum of response with harmonic load obtained in frequency domain.	41
2.14	Comparison of displacements due to harmonic load in the time and frequency domain.	41
2.15	Displacement in the time domain with periodic load obtained in time domain.	44
2.16	Displacement in the time domain with periodic load obtained in frequency domain.	44
2.17	Amplitude spectrum of response with periodic load obtained in frequency domain.	45
2.18	Comparison of displacements due to periodic load in the time and frequency domain.	45
2.19	Displacement in the time domain with periodic load obtained with Newmark's method.	46
2.20	Displacement in the time domain with nonperiodic load obtained in time domain.	49
2.21	Displacement in the time domain with nonperiodic load obtained in frequency domain.	49
2.22	Amplitude spectrum of response with nonperiodic load obtained in frequency domain.	50
2.23	Comparison of displacements due to nonperiodic load in the time and frequency domain.	50
2.24	Comparison of displacements due to arbitrary load in the time and frequency domain.	52

2.25	Relative difference of displacements in the time and frequency domain.	52
3.1	(left) Geometry and (right) force coefficients of example frame.	55
3.2	Stiffness coefficients of example frame.	56
3.3	Damping coefficients of example frame.	56
3.4	Inertia coefficients of example frame.	57
3.5	Relationship between damping ratio and frequency.	61
3.6	Geometrical configuration of the cantilever beam.	64
3.7	Mesh and boundary conditions of the cantilever beam.	65
3.8	Comparison of the horizontal displacement in the time domain.	66
3.9	Relative difference of the two calculation methods.	66
3.10	Comparison of the vertical displacement in the time domain.	67
3.11	Relative difference of the two calculation methods.	67
3.12	Geometrical configuration of the multi-story frame.	68
3.13	Mesh and boundary conditions of the multi-story frame.	69
3.14	Comparison of the horizontal displacement in the time domain.	71
3.15	Absolute difference of the two calculation methods.	71
3.16	Comparison of the vertical displacement in the time domain.	72
3.17	Absolute difference of the two calculation methods.	72
4.1	Horizontal displacement in the time domain with reduced system and fully coupled system.	82
4.2	Absolute difference of the calculation types.	82
4.3	Vertical displacement in the time domain with reduced system and fully coupled system.	83
4.4	Absolute difference of the calculation types.	83
4.5	Horizontal displacement in the time domain with reduced system and fully coupled system.	85
4.6	Amplitude spectrum for horizontal displacements with reduced and fully coupled system.	85
4.7	Vertical displacement in the time domain with reduced system and fully coupled system.	86
4.8	Amplitude spectrum for vertical displacements with reduced and fully coupled system.	86
4.9	Flow chart of solving MDOF systems.	87
5.1	Difference of IVP for numerical computation in both domains.	88

All figures without a explicit note of source in the caption are made by the author of this thesis with tikzpicture in L^AT_EX or with Matlab[1].

List of Tables

1.1	List of intervals of the spectra for different Fourier transformations.	15
2.1	List of damping ratios from [23].	19
2.2	List of Ansätze for particular solution.	20
3.1	Comparison of the calculation in time and frequency domain - Cantilever beam.	65
3.2	Comparison of the calculation in time and frequency domain - Multi-story frame.	70

Further acknowledgement

The used \LaTeX -template is from DI Daniel Schöllhammer, BSc (Institute of Structural Analysis at Graz University of Technology) and is updated by DI Michael Kaiser, BSc (Institute of Structural Analysis at Graz University of Technology).

The template for the flow chart figures is from DI Michael Kaiser, BSc and modified by the author of this thesis.

Bibliography

- [1] URL: <https://de.mathworks.com/>.
- [2] H. Altenbach. *Kontinuumsmechanik: Einführung in die materialunabhängigen und materialabhängigen Gleichungen*. 4th ed. Berlin-Heidelberg: Springer Vieweg, 2018.
- [3] Z. Bai. “Krylov subspace techniques for reduced-order modeling of large-scale dynamical systems”. In: *Applied Numerical Mathematics* 43.1 (2002). 19th Dundee Biennial Conference on Numerical Analysis, pp. 9–44. ISSN: 0168-9274.
- [4] R. Brigola. *Fourier-Analysis und Distributionen: Eine Einführung mit Anwendungen*. 4th ed. Nürnberg: edition swk, 2019.
- [5] I.N. Bronshtein et al. *Handbook of Mathematics*. 6th ed. Springer-Verlag Heidelberg New York Dordrecht London, 2015.
- [6] T. Butz. *Fouriertransformation für Fußgänger*. 6th ed. Wiesbaden: Vieweg+Teubner Verlag, 2009.
- [7] A.K. Chopra. *Dynamics of Structures: Theory and Applications to Earthquake Engineering*. 4th ed. Always Learning. Pearson Education, 2012.
- [8] R.W. Clough and J. Penzien. *Dynamics of Structures*. 3rd ed. CSI Computers and Structures, Inc., 2003.
- [9] J. Cooley and J. Tukey. “An Algorithm for the Machine Calculation of Complex Fourier Series”. In: *Mathematics of Computation* 19.90 (1965), pp. 297–301.
- [10] C. Dünser. *Structural Dynamics*. TU Graz, unpublished.
- [11] T.-P. Fries. *EduFEM- a finite element method educational software*. TU Graz, 2020.
- [12] T.-P. Fries. *FEM I and II*. TU Graz, unpublished.
- [13] R. Gasch, K. Knothe, and R. Liebich. *Strukturodynamik: Diskrete Systeme und Kontinua*. 2nd ed. Berlin-Heidelberg: Springer Vieweg, 2012.
- [14] R. Guyan. “Reduction of stiffness and mass matrices”. In: *AIAA Journal* 3 (1965), pp. 380–380.
- [15] F.J. Harris. “On the use of windows for harmonic analysis with the discrete Fourier transform”. In: *Proceedings of the IEEE* 66.1 (1978), pp. 51–83.
- [16] N. Henze and G. Last. *Mathematik für Wirtschaftsingenieure und naturwissenschaftlich-technische Studiengänge: Band 2 Analysis im \mathbb{R}^n , Lineare Algebra, Hilberträume, Fourieranalyse, Differentialgleichungen, Stochastik*. 2nd ed. Mathematik für Wirtschaftsingenieure und für naturwissenschaftlich-technische Studiengänge Bd. 2. Wiesbaden: Vieweg+Teubner Verlag, 2010.
- [17] T.J.R. Hughes. *The Finite Element Method: Linear Static and Dynamic Finite Element Analysis*. Dover Civil and Mechanical Engineering. New York: Dover Publications, 2000.

-
- [18] M. Jung and U. Langer. *Methode der finiten Elemente für Ingenieure: Eine Einführung in die numerischen Grundlagen und Computersimulation*. 2nd ed. Wiesbaden: Springer Fachmedien, 2013.
- [19] R.G. Lerner and G.L. Trigg. *Encyclopedia of Physics*. 3rd ed., completely rev. and enl. Weinheim: Wiley-VCH, 2005.
- [20] Li Li et al. “Dynamics of structural systems with various frequency-dependent damping models”. In: *Frontiers of Mechanical Engineering* 10 (Mar. 2015), pp. 48–63.
- [21] M. Möser (Ed.) and E. Sarradj. *Modalanalyse*. Fachwissen Technische Akustik. Springer Vieweg, 2020.
- [22] N. Newmark. “A Method of Computation for Structural Dynamics”. In: *Proceedings of the American Society of Civil Engineers, Journal of the Engineering Mechanics Division* 85 (1959), pp. 67–94.
- [23] N. Newmark and W. Hall. *Earthquake Spectra and Design (Engineering monographs on earthquake criteria, structural design, and strong motion records)*. Earthquake Engineering Research Institute, 1982.
- [24] L. Papula. *Mathematische Formelsammlung: Für Ingenieure und Naturwissenschaftler*. 12th ed. Wiesbaden: Springer Fachmedien, 2017.
- [25] C. Petersen and H. Werkle. *Dynamik der Baukonstruktionen*. 2nd ed. Wiesbaden: Springer Vieweg, 2017.
- [26] J. Pöschel. *Noch mehr Analysis: Mehrdimensionale Integration, Fouriertheorie, Funktionentheorie*. 1st ed. Wiesbaden: Springer Spektrum, 2015.